UNIVERSITY OF CALIFORNIA, SAN DIEGO

Microscale habitats and activities of bacteria and their ecological and biogeochemical significance in the ocean

A dissertation submitted in partial satisfaction of the requirements for the degree Doctor of Philosophy

in

Marine Biology

by

Ty James Samo

Committee in charge:

Professor Farooq Azam, Chair
Professor Eric E. Allen
Professor Lihini I. Aluwihare
Professor Peter J.S. Franks
Professor Brian Palenik
Professor Kit Pogliano

2012

The Dissertation of Ty James Samo is approved, and it is acceptable in quality and form for publication on microfilm and electronically:

Chair

University of California, San Diego

2012

DEDICATION

To my family and friends. Thank you for your love and support.

.

EPIGRAPH

There are the rushing waves
Mountains of molecules
Each stupidly minding its own business
Trillions apart
Yet forming white surf in unison.
-Richard P. Feynman

TABLE OF CONTENTS

LIST OF FIGURES

LIST OF TABLES

ACKNOWLEDGEMENTS

I would like to acknowledge my advisor, Professor Farooq Azam, for his acute insights and unwavering support as the chair of my committee. Special thanks are also given to my dissertation committee: Drs. Eric Allen, Lihini Aluwihare, Peter Franks, Brian Palenik, and Kit Pogliano. I greatly appreciate the comments, suggestions, and assistance they provided throughout my forays into the work described in this dissertation.

I would also like to acknowledge past and current members and visitors of the Azam laboratory for countless, helpful, and friendly discussions. These people are Francesca Malfatti, Xavier Mayali, Steve Smriga, Maura Manganelli, Johnny Nguyen, Jessica Ward, Melissa Garren, Krystal Rypien, Anne-Claire Baudoux, and Byron Pedler.

To my parents, Ron and Georgia Samo, and sister, Haley, thank you for your unconditional love and respect. I appreciate this so much, and it speaks volumes to each of your amazing qualities as caring, devoted, curious, and fun individuals. Many thanks go to my extended family as well for their never-ending love and interest.

All of my closest friends have provided countless discussions, laughs, and memories. As a result, I have been able to experience a balanced, fun, and intellectually stimulating life. Thank you to Eric Ball, Katie Barott, Tristan Carland, Santos Cordon, Cheryl Estoesta-Smith, Zac Hays, Jeff Locke, Bret Loughridge, Francesca Malfatti, Kristen Marhaver, Dan Mark, Xavier Mayali, Byron Pedler, Ryan Pepin, Matt Read, Danny Richter, Chris Ritchie, Kevin Smith, Sarah Smith, Steve Smriga, and Tali Vardi.

Chapter 2 appears as a reprint of the version in the journal Aquatic Microbial Ecology. Samo T.J., Malfatti F., and Azam F. (2008) A new class of transparent organic particles in seawater visualized by a novel fluorescence approach. *Aquatic Microbial*

Ecology, **53**, 307-321. The dissertation author was the primary investigator and author of this material.

Chapter 3 is a reprint of the version published in the Journal of Plankton Research. Samo T.J., Pedler B.E., Ball G.I., Pasulka A.L., Taylor A.G., Aluwihare L.I., Azam F., Goericke R., Landry M.R. (2012) Microbial distribution and activity across a water mass frontal zone in the California Current Ecosystem. *Journal of Plankton Research* doi:10.1093/plankt/fbs048. The dissertation author was the primary investigator and author of this paper.

Chapter 4, in part, is prepared for submission to the International Society for Microbial Ecology Journal. The dissertation author was the primary investigator and author of this paper.

VITA

2002	Associate of Art, Liberal Studies, Solano Community College
2002	Associate of Art, General Science, Solano Community College
2004	Bachelor of Science, Cell Biology & Biochemistry, University of California, San Diego
2004-2005	Staff Research Associate, Scripps Institution of Oceanography, University of California, San Diego
2005-2012	Graduate Student Researcher, Scripps Institution of Oceanography, University of California, San Diego
2010	Master of Science, Marine Biology, Scripps Institution of Oceanography, University of California, San Diego
2012	Doctor of Philosophy, Marine Biology, Scripps Institution of Oceanography, University of California, San Diego

PUBLICATIONS

Samo TJ, Malfatti F, Azam F (2008) A new class of transparent organic particles in seawater visualized by a novel fluorescence approach. Aquatic Microbial Ecology 53:307-321

Manganelli M, Malfatti F, Samo TJ, Mitchell BG, Wang H, Azam F (2009) Major Role of Microbes in Carbon Fluxes during Austral Winter in the Southern Drake Passage. PLoS ONE 4:e6941

Malfatti F, Samo TJ, Azam F (2010) High-resolution imaging of pelagic bacteria by Atomic Force Microscopy and implications for carbon cycling. ISME Journal 4:427-439

Stukel MR, Landry MR, Ohman MD, Goericke R, Samo T, Benitez-Nelson CR (2012) Do inverse ecosystem models accurately reconstruct plankton trophic flows? Comparing two solution methods using field data from the California Current. Journal of Marine Systems 91:20-33

Samo TJ, Pedler BE, Ball GI, Pasulka AL, Taylor AG, Aluwihare LI, Azam F, Goericke R, Landry MR (2012) Microbial distribution and activity across a water mass frontal zone in the California Current Ecosystem. Journal of Plankton Research 34:802-814

SUBMITTED PUBLICATIONS

Samo TJ, Smriga SP, Malfatti F, Azam F (2012) Single-cell protein synthesis and growth rates in marine bacteria using the methionine analog homopropargylglycine. ISME Journal. In preparation.

ABSTRACT OF THE DISSERTATION

Microscale habitats and activities of bacteria and their ecological and biogeochemical significance in the ocean

by

Ty James Samo

Doctor of Philosophy in Marine Biology

University of California, San Diego, 2012

Professor Farooq Azam, Chair

The focus of this dissertation is to observe and quantify the contribution of bacteria and their habitats to the nutrient cycling in marine environments. As a result of the complex exchanges between ocean physics, chemistry, and biology, the formation and distribution of microbial communities, their metabolisms, and their microenvironments is invariably influenced. Current research is beginning to reveal the heterogeneity of microbial growth, community/species composition, and habitats in the natural marine environment. However, little is currently know about how the mechanisms and interactions of these parameters influence each other. These topics were addressed

through the application of microscopy and various fluorescence staining techniques, and following several oceanographic research cruises.

After developing a staining protocol of seawater derived microbes and organic matter concentrated on a polycarbonate filter, it was found that an abundant and unclassified type of transparent organic particle exists in coastal and open ocean environments. These structures were termed filter fluorescing particles (FFP) based on their staining characteristics. In addition to their small size of a few to hundreds of micrometers in length, the particles are occasionally associated with heterotrophic bacteria, cyanobacteria, and phytoplankton. Several oceanographic research cruises confirmed the widespread presence of these particles, and suggest that these particles are relatively more abundant in oligotrophic waters containing enhanced concentrations of refractory organic matter. The discovery of these particles adds to our current knowledge of transparent exopolymer particles (TEP), DAPI yellow particles (DYP), and Coomassie stained particles (CSP).

The spatial characteristics and dynamics of a deep-water oceanic frontal zone made it possible to study the influence of submesoscale processes on the microscale responses of microbes and organic matter. The strong gradient created at this site created distinct zones of microbial activity, abundance, and size characterized by elevated primary and secondary production at the front. Further, the non-living material comprising the particulate and dissolved organic mater pools was enhanced as well due to elevated the production of the phyto- and bacterioplankton. The abundance and size of FFP and TEP were also monitored, and found to coincide with water mass features as well, presumably due to the physical-biological interactions acting at the front.

Lastly, a method was established to simultaneously visualize and quantify the protein synthesis rates of single heterotrophic bacterial cells in order to identify growth ranges and relative biogeochemical contributions in natural populations. This approach relied on the bioorthogonal amino acid homopropargylglycine (HPG), a methionine analog functionalized with an alkyne group. After incubation of natural seawater with HPG followed by fixation and cell immobilization on a filter, the HPG incorporated into the cellular protein of active cells was fluorescently labeled with Alexa Fluor 488® via click chemistry. A conversion factor to measure single-cell protein synthesis was generated from laboratory culture grown in natural seawater. Applying this factor to labeled cells from the Scripps Pier revealed a large range of rates, and highlighted the sensitivity of the method to measure very low activity cells, growth of cells attached to particles, and the continuum of activities that characterize natural heterotrophic bacterial assemblages.

CHAPTER 1

Introduction

Over the past 30 years, the field of microbial oceanography and ecology has made progress in elucidating some of the microbial influences on marine biogeochemistry and climate. On the global scale, phytoplankton and cyanobacteria account for approximately ~0.2% of the photosynthetic biomass on Earth yet they are responsible for one half of the net primary production that converts inorganic carbon, nitrogen, and phosphorus compounds in biologically available organic molecules. The vastness of the ocean and ubiquity of phytoplankton and photosynthetically derived material are major contributors to oceanic nutrient budgets and cycling (Falkowski et al. 1998). Early studies found that organic matter released by phytoplankton enables the growth and subsistence of heterotrophic marine bacteria (Fuhrman et al. 1980, Mague et al. 1980), and that up to 50% of this primary production was consumed by bacteria through secondary production (Fuhrman & Azam 1982). In the process, bacteria perform the reverse reaction of photosynthesis, that is, respiration of organic components back to their inorganic state (del Giorgio & Cole 1998). In doing so, bacteria remineralize these elements to be used again by primary producers, thereby maintaining these pools in microbial food webs and potentially moving them up higher trophic levels as bactivorous grazers are then consumed by larger metazoans and then fish (Azam 1986, Cho & Azam 1988). This general premise of the microbial loop (Azam et al. 1983) has been continually expanded upon to more completely account for the role of organic matter in structuring marine ecosystems and biogeochemical fluxes. However, the relevance of spatial and observational scales in determining how these mechanisms affect marine elemental cycles is only beginning to be addressed. This dissertation focuses on the importance of the microscale (defined here as sub-millimeter ecology and biogeochmistry) as the major

conduit through which individual microbes influence meso- and larger scale trophic and biogeochemical dynamics in the ocean.

Bacterial incorporation and metabolism of organic matter is largely dictated by the source, quality, and type of constituents available (Azam 1998, Jiao et al. 2010). As obligate osmotrophs, bacteria largely rely on the organic matter (OM) released from phytoplankton to generate energy through catabolism that enables growth and biochemical functions via anabolism. Organic matter exists as a continuum of sizes and compositions (Verdugo et al. 2004), and unlike many marine organisms, bacteria utilize it as both sustenance and habitat (Malfatti & Azam 2009). This duality has important implications for not only elemental cycling in marine systems, but climate as well. Depending on the availability of nutrients, phytoplankton fix atmospheric-based CO_2 into biomass, and transform this greenhouse gas into dissolved and particulate organic matter (DOM and POM) phases that sink or mix into the deep ocean (Eppley & Peterson 1979). This process significantly influences global CO_2 concentrations as sinking particles potentially sequester the atmosphere-derived carbon on very long timescales (Martin et al. 1987, Raven & Falkowski 1999).

Bacteria are intimately involved with this process as their continuous enzymatic processing of DOM and POM solubilizes the material for incorporation and metabolism (Smith et al. 1992). The monomerization of peptides to amino acids by bacterial ectoenzymes was found to be a significant factor in coupling between hydrolysis and uptake of organic matter (Hoppe et al. 1988). This concept was expanded to include POC, specifically marine snow, where high bacterial enzyme activities were responsible for rapid dissolution, yet did not support enhanced bacterial production (Smith et al. 1992).

Later, the behavior of bacteria on and near organic particles was noted to be a potentially significant force in structuring organic material distributions and microbial communities (Kiørboe & Jackson 2001). Using models of flow and concentration fields, the authors found that solute release from the particles likely supported unattached motile bacteria in the surrounding water. Taking the model a step further, Azam & Long (2001) suggested several ecological and climatic scenarios for this phenomena. Not only does enzymatic hydrolysis create solute plumes, it enables bacterial daughter cells of particle-attached bacteria to be released into the nutrient rich environment, thus evading low temperatures and high pressures for an overall benefit. Fast growing cells (released daughter cells and unattached motile cells) in the plume are more likely to exhibit enhanced growth efficiency, thereby releasing less CO_2 through respiration and contributing to heterogeneity of microbial activity in the ocean.

It is not surprising, then, that marine microorganisms exist in a matrix of colloids, polymers, enzymes, and particles (Alldredge & Silver 1988, Wells & Goldberg 1991, Martinez et al. 1996, Santschi et al. 1998). While these features of the marine microenvironment have been known for many years, their spatiotemporal distributions, patterns, and role in structuring microbial communities have been relatively less studied. To assist with identifying the origin and composition of the organic matter continuum, several classifications of DOM and POM have been created for points of reference and comparison. The descriptions have brought about a better understanding of not only the patterns and dynamics of OM, but also their relationship with marine microbes and potential influence on global biogeochemistry. Traditionally, DOM and POM are operationally divided as material that can pass through a 0.45 μm pore size filter (DOM)

and the retentate (POM). DOM has been found to be composed of a wide range of polysaccharide, lipid, and amino acid compounds, and is further subdivided into labile, semi-labile, and refractory pools that determine the turnover time and thus accumulation in the ocean (Hedges 2002, Hansell et al. 2009; and references therein). Although DOM cannot directly participate in the biological pump through sinking, it is capable of transport below the euphotic zone and throughout the world ocean through the physical processes of wind-induced mixing and meridional overturn (Hansell & Carlson 2001, Carlson et al. 2010).

Under certain physical and chemical conditions, DOM precursors may assemble and aggregate into larger structures and eventually particles (Chin et al. 1998, Passow 2000, Burd & Jackson 2009). Among the overarching implications for this transformation is the enhanced transport of carbon to the deep ocean via particles, the potential to provide food to particle consumers at higher trophic levels (Passow & Alldredge 1999), and the creation of discrete microhabitats with active and communicating bacteria (Verdugo et al. 2004, Hmelo & Van Mooy 2009). Furthermore, some of these particles display specific staining characteristics when exposed to histological and fluorescent dyes. For example, Alldredge *et al.* (1993) first described a class of microscopic and transparent particles in the ocean using the polysaccharide dye Alcian Blue. Distinct from the macroscopic marine snow described previously, these transparent exopolymer particles (TEP) are ubiquitous in the ocean, colonized by bacteria, and associated with phytoplankton. Later, the usefulness of the DNA stain 4',6-diamidino-2-phenylindole (DAPI) was expanded when it was found to also enable observation of DAPI yellow particles (DYP; Mostajir et al. 1995). Like TEP, the particles were found in many

different environments, and while the small sized examples did not exhibit bacterial colonization, the larger ones occasionally did. In a similar approach to Alldredge *et al.*, Long and Azam (1996) used the histological protein stain Coomassie Blue to visualize proteinaceous transparent structures, or Coomassie stained particles (CSP). As with the other particles, this class was ubiquitous and occasionally colonized by bacteria, confirming the importance of these features in microbial food webs.

In considering the interplay between microbes and their non-living, organic microenvironment, it is also necessary to understand microbial physiology in the context of the microenvironment and the downstream effects on nutrient cycling in the marine ecosystem. Approaches have been developed to quantitatively or semi-quantitatively ascertain growth responses of cells in order to determine and constrain their role in marine geochemical cycles and food web dynamics. The groundwork for this approach was established by Brock in studies that showed the usefulness and sensitivity autoradiography as a tool to understand microbial assimilation and processing of radiolabeled compounds in nature (Brock & Brock 1966). Interestingly, the method was used to determine the location of bacteria attached to diatoms and red algae in order to demonstrate colocalizaion of active cells within concentrated cell masses, and to show that the algae support higher percentages of bacterial cells incorporating thymidine to enable rapid DNA replication and cell division. Radioisotope labeled amino acids and sugars were later used to study natural marine bacteria and their influence on carbon cycling (Azam & Holm-Hansen 1973, Azam & Hodson 1977). Subsequent experimental and field results using visual/microautoradiographic-based approaches concluded that marine bacteria were an active and dynamic part of the marine food web (Fuhrman et al.

1980, Hollibaugh et al. 1980). These studies eventually led to bulk/seawater radiotracer-based measurements of natural communities incorporating tritiated thymidine or leucine to determine the total amounts of each compound assimilated into the whole bacterial community (Fuhrman & Azam 1982, Kirchman et al. 1985). Later, carbon cycling potential and growth rates were assigned to these measurements by determining the average amount of thymidine or leucine in marine bacteria, normalizing this to the amount of carbon in the cell, and calculating how quickly bulk communities incorporated the radiolabels into biomass (Simon & Azam 1989, Ducklow 2000).

As imaging technology improves along with the availability of new stains and dyes, so does our ability to observe and quantify the particles, interactions, activities, and eventually the mechanisms underlying the contributions of marine microbial ecology to biogeochemistry and nutrient cycling. Real-time visualization of microbes in the field or laboratory is allowing researchers to quantify distributions and activity with minimal disturbance and bias (Franks & Jaffe 2008, Seymour et al. 2008). These studies underscore the importance of spatial and temporal scales in structuring microbial ecosystems and effects on biogeochemistry.

This aspect of scale requires consideration throughout the scientific process. Many oceanographic cruises observing the distributions of elements and plankton activity and abundance have done so across wide swaths of the ocean, including gyres and basins, and employed large spatial samplings in lieu of observing temporal dynamics in a more confined area (Kirchman et al. 1995, Hansell & Waterhouse 1997, Zubkov et al. 1998, Kähler & Koeve 2001, Hoppe et al. 2002). In providing an informative overview of a large region, the approach makes it difficult to document potentially important short-term

processes. More magnified studies have investigated meso- and submesoscale (kilometer to meters) features on chemical and biological parameters to enable detailed views of phenomena with shorter timescales (Ducklow & Hill 1985, Morán et al. 2001, Van Wambeke et al. 2004, Ewart et al. 2008). By looking at the downstream effects of frontal zones and eddies on production and distribution of organic matter and marine microbes, these authors explored how such dynamics fluctuated in space and time since both microbial growth and water mass movements occur on the range of hours to days (these phenomena can vary from weeks to months as well). As a result, we are gaining a clearer picture of how these physical-chemical-biological interactions enhance or diminish microbial activity and thus structure food webs and higher trophic levels. Yet, the microscale is the most relevant mode of observation to characterize microbial consortia and eventually obtain a better mechanistic and predictive understanding of the communities' effects on elemental cycling and climate (Azam & Smith 1991, Azam 1998). Microbes and the myriad environments with which they interact are, for the most part, allocated heterogeneously in the water column (Mitchell et al. 1985, Long & Azam 2001, Prairie et al. 2010). Influenced by the physicohemical characteristics of the water column, non-living dissolved and particulate organic matter shape microbial activities and abundances through control of elemental distributions and concentrations (Jackson & Burd 1998). Knowledge of the extent to which such microenvironmental characteristics alter individual cell activity is currently lacking. However, strategies are being developed to sample, observe, and quantify the patchy continuum of microbial habitats and activities to address the contribution of these components in marine ecosystems.

This dissertation aims to study microbial processes on different scales using several experimental approaches in order to further characterize microbial contribution to marine carbon cycling and identify effective approaches to forecast these activities and their implications.

Chapter 2 explains a method used to observe a class of transparent organic particles in seawater and characterize them as microscale components that act as hotspots of microbial activity, thus augmenting the currently known classes of transparent particles (Koike particles, TEP, DYP, CSP). Initially observed at Scripps Pier, they were later observed in Antarctic waters and the California Current Ecosystem (CCE). Both bacteria and phytoplankton were associated with FFP. The internal structure was probed with fluorescently labeled lectins to show that some of the particles contained an architecture of glucose/mannose and galactose containing molecules, but not N-acetyl-glucosamine (the major unit of bacterial cell walls and monomer of chitin).

Chapter 3 details the results from an oceanographic research cruise that measured several microbial parameters across a rapidly sampled deep-water frontal zone in the California Current Ecosystem. This mesoscale feature was characterized by nitrate injection from deeper waters into the surface that elicited rapid growth responses from phytoplankton (high chlorophyll concentration) and very high production rates of bacteria in comparison to the adjacent oligotrophic and mesotrophic masses (Li et al. 2012, Taylor et al. 2012). Additionally, bacterial mortality was likely controlled more by viruses than nanoflagellate grazers that were being consumed by microflagellate predators. The front also displayed maxima of bacterial cell-specific biovolume, POC and PON, and sizes of transparent particles. These observations may have biogeochemical implications for the

broader CCE region since the frontal jet velocity approached 0.3 m s^{-1}, enabling the jet to rapidly transport the elevated organic matter and active microbes to influence elemental cycling in different water masses further away. This work contributed new knowledge of how marine microbes respond to sharply defined frontal zones, and constrained how the microbial food web can influence elemental cycling in the CCE.

Chapter 4 details the establishment of a protocol to observe and quantify protein synthesis, carbon production, and growth rates of single bacterial cells using the methionine analog homopropargylglycine. Subsequent microbial ecological experiments using the method investigated spatiotemporal activity dynamics with time-series incubations and comparisons between unattached versus particle-attached cells. One of the novel quantitative measurements from this research include power law distributions of single-cell activity, as opposed to the Gaussian allocation generally assumed and applied in bulk measurements of heterotrophic bacterial activity. It was also observed that particle-attached cells did not exhibit enhanced protein production rates relative to unattached cells when comparing average values of the fastest growing cells.

Chapter 5 integrates the background, results, and implications of chapters 2 – 4 to provide an assessment for how the current state of single-cell marine microbiology in concert with the evolution of multi-scale approaches may represent powerful tools for identifying how microbial activities and interactions impact marine ecology and elemental cycling.

References

Alldredge AL, Passow U, Logan BE (1993) The abundance and significance of a class of large, transparent organic particles in the ocean. Deep-Sea Research Part I: Oceanographic Research Papers 40:1131-1140

Alldredge AL, Silver MW (1988) Characteristics, Dynamics and Significance of Marine Snow. Progress in Oceanography 20:41-82

Azam F (1986) Nutrient cycling and food web dynamics in the Southern California Bight: The microbial food web. In: Eppley RW (ed) Plankton Dynamics of the Southern California Bight. Springer-Verlag, Berlin, West German; New York, N.Y., U.S.A

Azam F (1998) Microbial control of oceanic carbon flux: The plot thickens. Science 280:694-696

Azam F, Fenchel T, Field JG, Gray JS, Meyer-Reil LA, Thingstad F (1983) The ecological role of water-column microbes in the sea. Marine Ecology Progress Series 10:257-263

Azam F, Hodson RE (1977) Size Distribution and Activity of Marine Microheterotrophs. Limnology and Oceanography 22:492-501

Azam F, Holm-Hansen O (1973) Use of tritiated substrates in the study of heterotrophy in seawater. Marine Biology 23:191-196

Azam F, Long RA (2001) Oceanography - Sea snow microcosms. Nature 414:495-498

Azam F, Smith DC (1991) Bacterial influence on the variability in the ocean's biogeochemical state: A mechanistic view. In: Demers S (ed) Particle analysis in oceanography, Book 27. Springer-Verlag, Berlin; New York

Brock TD, Brock ML (1966) Autoradiography as a tool in microbial ecology. Nature 209:734-&

Burd AB, Jackson GA (2009) Particle aggregation. Annual Review of Marine Science 1:65-90

Carlson CA, Hansell DA, Nelson NB, Siegel DA, Smethie WM, Khatiwala S, Meyers MM, Halewood E (2010) Dissolved organic carbon export and subsequent remineralization in the mesopelagic and bathypelagic realms of the North Atlantic basin. Deep-Sea Research Part II-Topical Studies in Oceanography 57:1433-1445

Chin WC, Orellana MV, Verdugo P (1998) Spontaneous assembly of marine dissolved organic matter into polymer gels. Nature 391:568-572

Cho BC, Azam F (1988) Major Role of Bacteria in Biogeochemical Fluxes in the Oceans Interior. Nature 332:441-443

del Giorgio PA, Cole JJ (1998) Bacterial growth efficiency in natural aquatic systems. Annual Review of Ecology and Systematics 29:503-541

Ducklow HW (2000) Bacterial production and biomass in the oceans. In: Kirchman DL (ed) Microbial Ecology of the Oceans. Wiley-Blackwell, Hoboken, New Jersey, USA

Ducklow HW, Hill SM (1985) Tritiated-thymidine incorporation and the growth of heterotrophic bacteria in warm core rings. Limnology and Oceanography 30:260-272

Eppley RW, Peterson BJ (1979) Particulate organic matter flux and planktonic new production in the deep ocean. Nature 282:677-680

Ewart CS, Meyers MK, Wallner ER, McGillicuddy Jr DJ, Carlson CA (2008) Microbial dynamics in cyclonic and anticyclonic mode-water eddies in the northwestern Sargasso Sea. Deep-Sea Research Part II: Topical Studies in Oceanography 55:1334-1347

Falkowski PG, Barber RT, Smetacek V (1998) Biogeochemical controls and feedbacks on ocean primary production. Science 281:200-206

Franks PJS, Jaffe JS (2008) Microscale variability in the distributions of large fluorescent particles observed in situ with a planar laser imaging fluorometer. Journal of Marine Systems 69:254-270

Fuhrman JA, Ammerman JW, Azam F (1980) Bacterioplankton in the coastal euphotic zone - Distribution, activity and possible relationships with phytoplankton. Marine Biology 60:201-207

Fuhrman JA, Azam F (1982) Thymidine Incorporation as a Measure of Heterotrophic Bacterioplankton Production in Marine Surface Waters - Evaluation and Field Results. Marine Biology 66:109-120

Hansell DA, Carlson CA (2001) Biogeochemistry of total organic carbon and nitrogen in the Sargasso Sea: control by convective overturn. Deep-Sea Research Part II 48:1649-1667

Hansell DA, Carlson CA, Repeta DJ, Schlitzer R (2009) Dissolved Organic Matter in the Ocean: A Controversy Stimulates New Insights. Oceanography 22:202-211

Hansell DA, Waterhouse TY (1997) Controls on the distributions of organic carbon and nitrogen in the eastern Pacific Ocean. Deep-Sea Research Part I-Oceanographic Research Papers 44:843-857

Hedges JI (2002) Why dissolved organics matter. In: Hansell DA, Carlson CA (eds) Biogeochemistry of Marine Dissolved Organic Matter Academic Press, San Diego

Hmelo LR, Van Mooy BAS (2009) Kinetic constraints on acylated homoserine lactone-based quorum sensing in marine environments. Aquatic Microbial Ecology 54:127-133

Hollibaugh JT, Fuhrman JA, Azam F (1980) Radioactively labeling of natural assemblages of bacterioplankton for use in trophic studies. Limnology and Oceanography 25:172-181

Hoppe H-G, Kim S-J, Gocke K (1988) Microbial Decomposition in Aquatic Environments: Combined Process of Extracellular Enzyme Activity and Substrate Uptake. Applied and Environmental Microbiology 54:784-790

Hoppe HG, Gocke K, Koppe R, Begler C (2002) Bacterial growth and primary production along a north-south transect of the Atlantic Ocean. Nature 416:168-171

Jackson GA, Burd AB (1998) Aggregation in the marine environment. Environmental Science & Technology 32:2805-2814

Jiao N, Herndl GJ, Hansell DA, Benner R, Kattner G, Wilhelm SW, Kirchman DL, Weinbauer MG, Luo TW, Chen F, Azam F (2010) Microbial production of recalcitrant dissolved organic matter: long-term carbon storage in the global ocean. Nature Reviews Microbiology 8:593-599

Kirchman D, K'Nees E, Hodson R (1985) Leucine incorporation and its potential as a measure of protein synthesis by bacteria in natural aquatic systems. Applied and Environmental Microbiology 49:599-607

Kirchman DL, Rich JH, Barber RT (1995) Biomass and biomass production of heterotrophic bacteria along 140W in the equatorial Pacific: Effect of temperature on the microbial loop. Deep-Sea Research Part II-Topical Studies in Oceanography 42:603-619

Kiørboe T, Jackson GA (2001) Marine snow, organic solute plumes, and optimal chemosensory behavior of bacteria. Limnology and Oceanography 46:1309-1318

Kähler P, Koeve W (2001) Marine dissolved organic matter: can its C : N ratio explain carbon overconsumption? Deep-Sea Research Part I-Oceanographic Research Papers 48:49-62

Li QP, Franks PJS, Ohman MD, Landry MR (2012) Enhanced nitrate fluxes and biological processes at a frontal zone in the southern California current system. Journal of Plankton Research 34:790-801

Long RA, Azam F (1996) Abundant protein-containing particles in the sea. Aquatic Microbial Ecology 10:213-221

Long RA, Azam F (2001) Microscale patchiness of bacterioplankton assemblage richness in seawater. Aquatic Microbial Ecology 26:103-113

Mague TH, Friberg E, Hughes DJ, Morris I (1980) Extracellular release of carbon by marine phytoplankton; a physiological approach. Limnology and Oceanography 25:262-279

Malfatti F, Azam F (2009) Atomic force microscopy reveals microscale networks and possible symbioses among pelagic marine bacteria. Aquatic Microbial Ecology 58:1-14

Martin JH, Knauer GA, Karl DM, Broenkow WW (1987) VERTEX: carbon cycling in the northeast Pacific. Deep-Sea Research Part A - Oceanographic Research Papers 34:267-285

Martinez J, Smith DC, Steward GF, Azam F (1996) Variability in ectohydrolytic enzyme activities of pelagic marine bacteria and its significance for substrate processing in the sea. Aquatic Microbial Ecology 10:223-230

Mitchell JG, Okubo A, Fuhrman JA (1985) Microzones Surrounding Phytoplankton Form the Basis for a Stratified Marine Microbial Ecosystem. Nature 316:58-59

Morán XAG, Taupier-Letage I, Vázquez-Domínguez E, Ruiz S, Arin L, Raimbault P, Estrada M (2001) Physical-biological coupling in the Algerian Basin (SW Mediterranean): Influence of mesoscale instabilities on the biomass and production of phytoplankton and bacterioplankton. Deep-Sea Research Part I-Oceanographic Research Papers 48:405-437

Mostajir B, Dolan JR, Rassoulzadegan F (1995) A simple method for the quantification of a class of labile marine pico- and nano-sized detritus: DAPI Yellow Particles (DYP). Aquatic Microbial Ecology 9:259-266

Passow U (2000) Formation of transparent exopolymer particles, TEP, from dissolved precursor material. Marine Ecology-Progress Series 192:1-11

Passow U, Alldredge AL (1999) Do transparent exopolymer particles (TEP) inhibit grazing by the euphausiid Euphausia pacifica? Journal of Plankton Research 21:2203-2217

Prairie JC, Franks PJS, Jaffe JS (2010) Cryptic peaks: Invisible vertical structure in fluorescent particles revealed using a planar laser imaging fluorometer. Limnology and Oceanography 55:1943-1958

Raven JA, Falkowski PG (1999) Oceanic sinks for atmospheric CO_2. Plant, Cell & Environment 22:741-755

Santschi PH, Balnois E, Wilkinson KJ, Zhang JW, Buffle J, Guo LD (1998) Fibrillar polysaccharides in marine macromolecular organic matter as imaged by atomic force microscopy and transmission electron microscopy. Limnology and Oceanography 43:896-908

Seymour JR, Ahmed T, Marcos, Stocker R (2008) A microfluidic chemotaxis assay to study microbial behavior in diffusing nutrient patches. Limnology and Oceanography-Methods 6:477-488

Simon M, Azam F (1989) Protein content and protein synthesis rates of planktonic marine bacteria. Marine Ecology Progress Series 51:201-213

Smith DC, Simon M, Alldredge AL, Azam F (1992) Intense hydrolytic enzyme activity on marine aggregates and implications for rapid particle dissolution. Nature 359:139-142

Taylor AG, Goericke R, Landry MR, Selph KE, Wick DA, Roadman MJ (2012) Sharp gradients in phytoplankton community structure across a frontal zone in the California Current Ecosystem. Journal of Plankton Research 34:778-789

Van Wambeke F, Lefèvre D, Prieur L, Sempéré R, Bianchi M, Oubelkheir K, Bruyant F (2004) Distribution of microbial biomass, production, respiration, dissolved organic carbon and factors controlling bacterial production across a geostrophic front (Almeria-Oran, SW Mediterranean Sea). Marine Ecology-Progress Series 269:1-15

Verdugo P, Alldredge AL, Azam F, Kirchman DL, Passow U, Santschi PH (2004) The oceanic gel phase: a bridge in the DOM-POM continuum. Marine Chemistry 92:67-85

Wells ML, Goldberg ED (1991) Occurrence of small colloids in sea water. Nature 353:342-344

Zubkov MV, Sleigh MA, Tarran GA, Burkill PH, Leakey RJG (1998) Picoplanktonic community structure on an Atlantic transect from 50 degrees N to 50 degrees S. Deep-Sea Research Part I-Oceanographic Research Papers 45:1339-1355

Chapter 2

A new class of transparent organic particles in seawater visualized by a novel fluorescence approach

Vol. 53: 307–321, 2008
doi: 10.3354/ame01251

AQUATIC MICROBIAL ECOLOGY
Aquat Microb Ecol

Printed December 2008
Published online December 11, 2008

A new class of transparent organic particles in seawater visualized by a novel fluorescence approach

Ty J. Samo*, Francesca Malfatti, Farooq Azam

Marine Biology Research Division, Scripps Institution of Oceanography, University of California San Diego, La Jolla, California 92093, USA

ABSTRACT: A method for visualizing transparent material in seawater, described here, has led to the discovery of novel particles. The protocol is based on Alcian Blue and SYBR Gold staining of seawater samples on polycarbonate filters. While the particles detected by our method may have some overlap with previously described transparent exopolymer particles and Coomassie stained particles, these particles largely comprise a previously undetected class. We propose that the particles are detected because they cause spatially explicit inhibition of Alcian Blue quenching of SYBR Gold fluorescence of the filter. Samples collected from various locations (Ellen Browning Scripps Memorial Pier, California, the Palmer Peninsula, Antarctica, and Point Conception, California) revealed particles with abundances on the order of 10 and 10^5 l^{-1} and ranging in size from 10 to 10^5 μm^2. The particles varied in the types of organisms attached, the internal structure and probable biological sources. Field observations and laboratory experimental manipulations suggest varied sources and mechanisms of formation. These particles are potential hot spots of organic matter, microbial diversity and interactions, and, depending on their size and sinking rates, serve as conduits for carbon export to the ocean's interior.

KEY WORDS: Transparent organic particles · Seawater · Alcian Blue · SYBR Gold fluorescence-based visualization

INTRODUCTION

A challenging goal of microbial oceanography is to understand the role of organic matter and its interactions with microorganisms in the functioning of marine ecosystems. Marine organic matter exhibits great variations in its sources and characteristics, such as biodegradability, charge, chemical composition, microbial colonization, density, molecular weight, optical characteristics, size, shape, stickiness and viscosity. Further, the organic matter can undergo biological, chemical and physical transformations while also participating in oceanic biogeochemical processes (Isao et al. 1990, Passow & Alldredge 1994, Aluwihare et al. 1997, Chin et al. 1998, Azam & Worden 2004, Orellana et al. 2007). These processes include the cycling of carbon, nutrients and trace metals, carbon flux to the deep ocean, bloom dynamics, and the formation and dissolution of organic matter mediated by microbial activities.

Marine organic matter is often divided operationally between dissolved organic matter (DOM) and particulate organic matter (POM) on the basis of filterability through 0.45 to 1.7 µm pore size filters. The POM components have been characterized by microscopic observations and the binding specificity of several stains (Mostajir et al. 1995, Long & Azam 1996, Johnsen et al. 2000). For example, the production of transparent exopolymer particles (TEP) has been attributed to phytoplankton, notably diatoms. TEP may be chemically complex, have a wide range of sizes and morphologies and may be created and modified by a myriad of biological, chemical and physical interactions (Alldredge et al. 1993). TEP may also be colonized by bacteria, presumably serving as a niche for them, but it may also be modified by bacterial activities (Verdugo et al. 2004, Azam & Malfatti 2007). Bacteria–organic matter interactions at nanometer to millimeter scales may play a role in microbial loop dynam-

*Email: tsamo@ucsd.edu

Aquat Microb Ecol 53: 307–321, 2008

ics, affect carbon fluxes and the biological pump and influence ecosystem functioning (Azam & Long 2001, Long & Azam 2001, Simon et al. 2002, DeLong & Karl 2005). Microbiological studies have yielded insights on the relationship between organic matter and the roles microbes play in structuring the organic matter in their microenvironments through release, uptake and degradation of organic matter (Smith et al. 1995, Aluwihare & Repeta 1999, Radic et al. 2006). It is, therefore, important to know the *in situ* microscale characteristics of organic matter and the mechanisms of its formation and degradation, as context for understanding how the biochemical interactions of bacteria with organic matter influence their ecology and the functioning of marine ecosystems.

Imaging of bacteria and the organic matter in their microenvironment is becoming tractable with the advent of sensitive labeling and optical techniques. Thus, the proverbial drop of seawater may soon be observed from the microbial point of view. Just as the use of fluorescent DNA stains enabled visualization of marine bacteria, so too have certain dyes been applied to seawater to attain glimpses of their microscale environments. TEP is made visible by staining with Alcian Blue (Alldredge et al. 1993) and proteinaceous particles in seawater are visualized with Coomassie Blue (Coomassie stained particles [CSP]; Long & Azam 1996). The current techniques, in conjunction with 4′-6-diamidino-2-phenylindole (DAPI) to stain microbes, suggest that transparent polymeric and suprapolymeric loci of organic matter represent environments in which viruses, prokaryotes and eukaryotes are brought into close contact (Proctor & Fuhrman 1991). These observations have led to the concept that organic matter in seawater occurs as a heterogeneous continuum ranging in size from nanometers to millimeters (Azam et al. 1993, Verdugo et al. 2004), and the proposal that such environmental heterogeneity is important in microbial ecology, diversity and biogeochemistry (Long & Azam 2001, Kiørboe et al. 2003, Grossart et al. 2006, Azam & Malfatti 2007).

The current staining methods, however, do not stain lipid, cationic or uncharged polysaccharide, DNA or humic acids, materials that may also be important components of the transparent particle field. Further, some particles may be too small to be discerned by optical microscopy. Using transmission electron microscopy Wells & Goldberg (1991) discovered highly abundant (10^8 to 10^9 ml^{-1}) colloids from 20 nm to hundreds of nanometers in size. We made a number of unsuccessful attempts to constrain the hypothesis that the currently visualized organic matter is but a minor fraction of the organic matter continuum. Based on the results of positive controls, we hypothesized that many components of transparent organic matter are too dilute to visualize by the current protocols. We found that a protocol combining prolonged staining with Alcian Blue followed by staining with SYBR Gold revealed a new population of particles not seen by previous methods. On the basis of their general appearance and proposed mechanism of visualization, we have named them filter fluorescing particles (FFP). These particles provide new insights into our view of the microbial world and microbial biogeochemical functions.

MATERIALS AND METHODS

Sampling and staining. Seawater was sampled with a polycarbonate flask from Ellen Browning Scripps Memorial Pier (Scripps Pier), La Jolla, California (32° 52.02′ N, 117° 15.43′ W), USA, at ~1 m depth. Water was also collected during cruises via deployment of a CTD rosette at depths up to 750 m. Samples were processed within 10 to 120 min, or stored at *in situ* temperature until used, and fixed with formaldehyde (2% final concentration) unless otherwise noted. Samples, 2 to 120 ml in volume, were filtered through white 0.22 or 1 µm pore size polycarbonate filters (at ≤20 kPa) until no liquid remained, then stained with 0.5 ml of 1× Alcian Blue for 30 s. Suction was re-applied to filter the stain. Alcian Blue was prepared as an aqueous solution containing 0.04% Alcian Blue (w/v) plus 0.12% acetic acid (v/v) in Milli-Q water and diluted 2× and filtered (0.22 µm) before use. The filter was then placed on 80 µl of 1× or 5× SYBR Gold (Invitrogen) that was first prepared and filtered (0.22 µm) with Millli-Q water or seawater. Staining times ranged from 3 to 20 min. Filters were then dried on paper towels and mounted on glass slides with Resolve® immersion oil.

Visualization. Samples were examined with an Olympus IX-71 inverted microscope at 200×, 600×, and 1000× magnifications using transmitted light or epifluorescence illumination (excitation: 488 nm; emission: long pass filter). Depending on sample location, seconds to minutes were needed to find a fluorescing particle. Cyto-Clear slides (GE Osmonics) were placed on top of the sample slides to allow visualization in transmitted light. Images were recorded with an Olympus Microfire digital camera using PictureFrame software. Additionally, some filters were observed at 1000× magnification with a Nikon laser scanning confocal microscope. Images were obtained using using EZCI software coupled to 488 and 543 nm excitation lasers with broad green and red emission filters.

Counting and sizing. Abundance and size of the particles were determined at 600× magnification. Forty random fields were visualized on each filter and the particles in a 10 × 10 ocular grid or the entire field of view were counted and sized (with the ocular grid).

Samples with very low abundance of particles were counted in transects across one-half or a whole filter. Areas were calculated by measuring length and width to the nearest one-quarter ocular grid square.

Blanks. Negative controls were prepared to determine the potential for SYBR Gold-mediated aggregation of ambient dissolved macromolecules. These controls included the standard Alcian Blue and SYBR Gold staining of the following 10 ml samples: (1) freshly prepared and sterilized ZoBell media diluted to 1/1000 and 1/10 000 concentrations; (2) supernatant taken from 13 ml of whole seawater centrifuged at 16 000 × *g* for 10 min; and (3) filtrate from whole seawater passed through a 0.22 µm filter. To mirror the treatment of natural samples, formaldehyde was added to each control to a final concentration of 2%. Finally, 10 ml of unmanipulated, whole seawater used for the filtrate and centrifugation blanks was fixed and stained.

Additional manipulations and staining protocols were developed to fully illustrate that these structures did not result from an interaction between SYBR Gold and molecules in natural seawater samples. We collected four 10 ml seawater samples from the Scripps Pier. These were 0.2 µm filtered and fixed with 0.02 µm filtered formaldehyde (2% final concentration). Approximately 450 ml of extra 0.2 µm filtered seawater was then cycled through a 100 kDa tangential flow filtration column until 300 ml was collected. This volume provided four 10 ml samples, which were subsequently fixed. From each filtration, 2 samples were filtered and stained with the standard protocol. The remaining 4 samples were incubated at room temperature with 1× SYBR Gold for 15 min, filtered, stained with Alcian Blue and counted. The role of temperature in the formation of FFP was also investigated by performing the standard staining protocol at room temperature or at 4°C. Counts were performed at room temperature and 4°C through the use of a cooling stage connected to the microscope.

Fixed versus unfixed samples. We prepared triplicate seawater samples with or without formaldehyde fixation, but otherwise used the standard protocol described for the samples.

Cell lysis artifacts. We considered that filtration might have lysed delicate phytoplankton and that separating the phytoplankton from the particles with gentle centrifugation might minimize cell lysis. Seawater samples were centrifuged slowly (100 × *g*), and abundance and size compared between supernatant and pellet. Conical 15 ml tubes, each containing 10 ml seawater, were centrifuged for 5 min. The top 7 ml and bottom 3 ml were filtered and stained.

Phytoplankton artifacts. Non-axenic, stationary phase phytoplankton cultures of *Thalassiosira weissflogii*, *Cylindrotheca*, *fusiformis*, *Chaetoceros gracilis* and *Lingulodinium polyedrum* were diluted 1:100 in 0.22 µm filtered seawater, which had been autoclaved. Aliquots of 1 ml were filtered on 1 µm polycarbonate membranes and the membrane was stained with Alcian Blue and SYBR Gold, as described previously.

Preparations of stains, filters and samples. To understand why and how our protocol enabled visualization of FFP, several variations of the protocol were tested:

(1) Filter seawater; stain with SYBR Gold (0.5 ml, 1×, 30 s); stain with Alcian Blue (15 min); while membrane stays on the filter base.

(2) Pre-stain the filter 2× with Alcian Blue on the filter base (1 ml, 1 min), filter, then place the filter on a drop of SYBR Gold.

(3) Pre-stain the filter 5× with 0.5 ml Alcian Blue, filter, then stain with SYBR Gold.

(4) Add SYBR Gold to seawater (1× final), incubate (10 min) then filter.

(5) Stain samples where indicated by the standard SYBR Green protocol of Noble & Fuhrman (1998).

(6) Test different filter types and pore sizes to see whether they provide better visualization: 0.45 µm white cellulose filter (Micron Separations), 0.02 µm white AlO_2 filters (Whatman), and 0.2 µm white or black polycarbonate filters (Whatman).

(7) Test several other histological stains to see whether they help visualize additional features: Ruthenium Red (0.001 and 0.02%), Crystal Violet (0.1%), and Coomassie Blue (0.04%). Filter-retained samples were stained with 0.5 ml for 30 s, followed by standard SYBR Gold protocol.

(8) Test whether the stained FFP could be resuspended. Filter-retained samples (vacuum or gravity filtered) were stained with Alcian Blue, placed on a drop of SYBR Gold for 10 min, then placed in a Petri dish and vigorously rinsed (using a pipette) 10 times with 2 ml autoclaved 0.22 µm filtered seawater. The suspension was filtered and stained once again. Controls were prepared by omitting the seawater rinse.

(9) Subject seawater samples to several treatments prior to filtration and compare with controls: (1) 50 mM (final) EDTA was added to see whether disrupting divalent cation cross-linking would disperse the FFP organic matter; (2) Triton X-100 (1% final) was added to seawater, which was then sonicated (full power, 1 min; Sonic Dismembrator, Fisher Scientific), stained and visualized; (3) after filtering samples, the filters were dried (60°C, 30 min in a hybridization oven).

Characterization. We attempted to produce particles that might mimic the FFP by adding varying concentrations of several types of macromolecules (DNA, lipid, protein) and hydrolytic enzymes to the filters. Samples were then filtered and stained as in our protocol.

(1) Herring sperm DNA (D181B, Promega) was diluted in the following solutions: de-ionized water

Aquat Microb Ecol 53: 307–321, 2008

(Milli-Q) to 1 mg ml^{-1}, 100 µg ml^{-1}, 10 µg ml^{-1} and 1 µg ml^{-1}; 10% bovine serum albumin (BSA) in Milli-Q water; 1% agarose in autoclaved 0.22 µm filtered seawater. The solutions were spotted once on the filters, stained and visualized.

(2) BSA was added to an aliquot of agarose at 10% final concentration and DNA was prepared similarly in agarose at 10 µg ml^{-1}. The agarose, BSA, agarose + BSA and agarose + DNA was then spotted on the filter and prepared for visualization.

(3) A spotting experiment with 2 different solutions of phosphatidylcholine: 5 mg ml^{-1} in 100% ethanol then diluted to 2.5 mg ml^{-1} or 50 µg ml^{-1} in autoclaved filtered seawater. Then 100 µl of 5 mg ml^{-1} phosphatidylcholine in ethanol was subjected to evaporation to remove the alcohol. A 1 mg ml^{-1} phosphatidylcholine solution was prepared by adding 500 µl of autoclaved and filtered seawater to the remaining lipid residue. Solutions were spotted on filters, stained and visualized. Ethanol spots served as control.

(4) Treatments with hydrolytic enzymes were done to infer macromolecular composition of FFP and determine whether the enzymes would cause FFP to disintegrate into smaller particles: DNase (80 U ml^{-1}, 30 min), lipase (10 U ml^{-1}, 20 min), pronase (5 U ml^{-1}, 20 min) and β-glucosidase (10 U ml^{-1}, 20 min). Samples were filtered and stained, and the FFP were counted, sized and compared with untreated samples.

Staining with fluorescently labeled lectins. Tetramethylrhodamine labeled peanut agglutinin and concanavalin A were used to target the D-galactose and both D-glucose and D-mannose residues, respectively, in the FFP. Seawater was filtered and stained with Alcian Blue as per the protocol, but then were stained for 3 min with 1× SYBR Gold. The filter was placed back on the filter base and suctioned to dryness, then transferred to a Petri dish and 100 µl of each lectin (5 µg ml^{-1} final concentration) was added on top. Samples were incubated in the dark for 20 min.

Nitrogen and phosphorous amendment. We considered that the nutrient status of seawater could highlight links between the sources of FFP and microbial physiology and metabolism. Since phytoplankton release large amounts of marine organic carbon and their health is affected by inorganic nutrient availability, we hypothesized that a measurable FFP response would be observed following a pulse of limiting nutrients. We added KH_2PO or NH_4Cl and KH_2PO at 1 µM final concentrations to 1 l seawater in duplicate polycarbonate bottles and incubated at 14°C on a shaker at 70 rpm. Unamended seawater was stained and analyzed for FFP abundance and dimensions. After 10 d, a subsample was taken from each bottle, stained and analyzed for FFP abundance and dimensions.

RESULTS AND DISCUSSION

Initial observations

Appearance and distribution

Seawater samples filtered on 1 µm polycarbonate membranes and stained with Alcian Blue followed by SYBR Gold ('standard protocol') showed bright regions of yellow-green fluorescence. At 600× and 1000× magnification they appear as fluorescent groupings of filter pores occasionally connected by mucus-like material. (Fig. 1A,B). We first observed them (July 2005) during a *Lingulodinium polyedrum* bloom while testing whether bacterial colonization of TEP previously seen by double staining with Alcian Blue plus DAPI (Alldredge et al. 1993) might be better visualized with Alcian Blue plus SYBR Gold. We have subsequently detected FFP in samples from Scripps Pier as well as from nearshore and offshore stations in the Drake Passage and Bransfield Strait, Antarctica, in August 2006 and waters off of Point Conception, California, during April 2007 (Table 1). An excellent fluorescence signal from the microbes was obtained in some but not all areas of the filter, and in other regions brightly fluorescing shapes were present and occasionally showed an association with bacteria and protozoa.

While FFP were observed in geographically separate and distinct locations, both similarities and differences in FFP appearance were observed. Samples were visualized with confocal microscopy to better observe these subtle characteristics (Fig. 2). The side view of the particles suggested that the filter pore fluorescence does not extend upward and out from the surface, supporting an indirect staining mechanism that does not rely on binding of the stain to the particle. Inspection of the side views from several samples suggests that the extension of the fluorescing pores is variable, anywhere from 4 to 13 µm deep. This led to the observation that all of the filter pores actually display a small amount of SYBR Gold fluorescence and can be clearly seen by increasing the gain function of the confocal microscope. Most of these 'quenched' pores decrease in intensity and become undetectable below 6 µm into the filter pores. In some cases it was apparent that the SYBR Gold did attach to some portion of the particle and resulted in a protrusion of a bright yellow-green structure. Samples from Scripps Pier could be characterized by brightly fluorescing material and chlorophyll exhibiting a FFP signal while also sometimes associating with various phytoplankton, protozoa, and bacteria (Fig. 2A). These types of FFP signals could also be described as fairly 'robust', i.e. the fluorescence was intense and confined to a discrete area. Initial observations would suggest that FFP from the Califor-

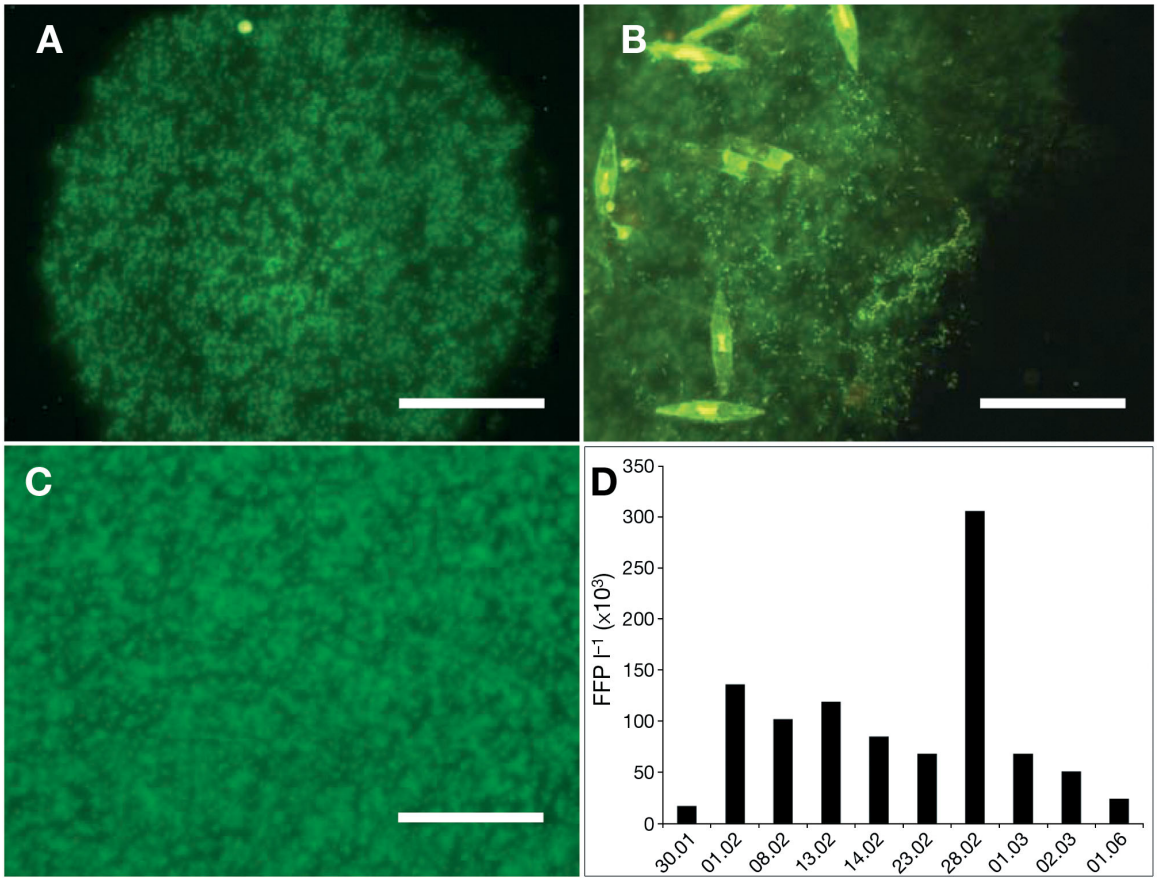

Fig. 1. (A–C) Filter fluorescing particles (FFP) in Scripps Pier seawater filtered onto 1 µm pore size polycarbonate filters and visualized by the staining protocol described in the text. Each fluorescing spot is a single 1 µm diameter pore that emits a bright green SYBR Gold fluorescence signal. In addition to the roughly circular shape in (A) a wide range of shapes were observed, e.g. (B), which is a FFP associated with high concentrations of bacteria and diatoms. (C) Image of a filter prepared without Alcian Blue. (D) Abundances of FFP determined in waters off Scripps Pier periodically during January to June 2006 (dates given as DD.MM). Magnification = 600×, scale bars = 50 µm

nia Current were similar to those from Scripps Pier. Microbial attachment and connections to other fluorescent structures were again seen, but periodically showed dissimilar morphologies and associations. For example, a coat of hazy fluorescence was seen around seemingly random FFP regions and when the focal plane was adjusted farther into the sample, the fluorescing filter pores could then be easily discerned (Fig. 2D). Antarctic FFP were rarely colonized by microbes and were not usually seen near or containing fluorescing material. The pore fluorescence varied from a 'typical' signal observed in all samples to bright pores localizing with a relatively bright filter surface (e.g. Fig. 2G) to dim pores that seemed to become brighter farther within. It remains unclear whether these differences were a result of SYBR Gold

Table 1. Sampling site locations and environmental types, and collection dates

Location	Coordinates	Environment	Collection date
Scripps Pier	32° 52.02′ N, 117° 15.43′ W	Coastal	28 Feb 2006
Palmer Peninsula, Antarctica	62° 11.93′ S, 58° 8.28′ W	Coastal	7 Jul 2006
	60° 37.00′ S, 54° 37.48′ W	Open ocean	21 Jul 2006
California Current, near Point Conception	34° 16.30′ N, 121° 9.95′ W	Near shore	8 Apr 2007
	33° 20.48′ N, 123° 32.07′ W	Offshore	12 Apr 2007

Aquat Microb Ecol 53: 307–321, 2008

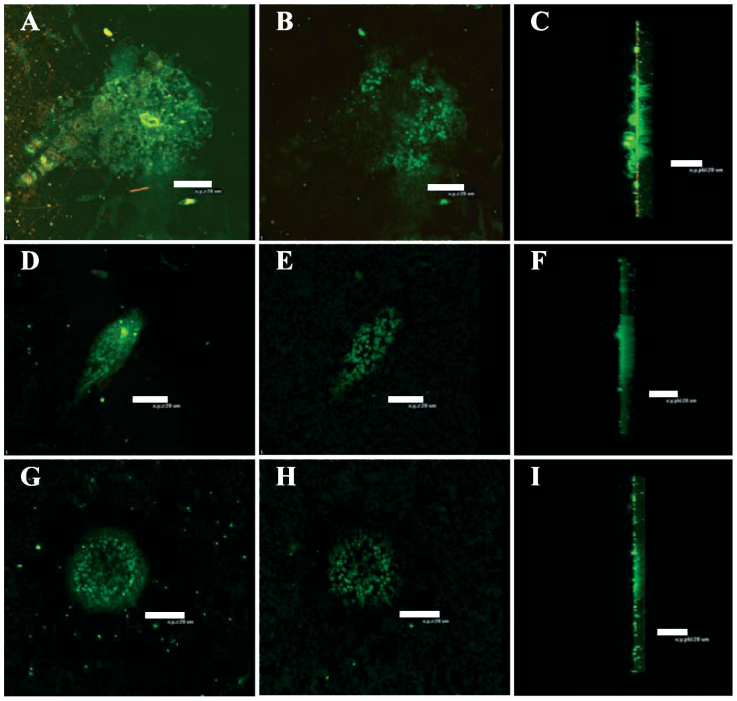

Fig. 2. Confocal images of FFP in seawater from (A–C) Scripps Pier, (D–F) the California Current and (G–I) Antarctica. (A,D,G) Images are scans of the surface of the particles and represent what would be seen if observing with regular epifluorescence microscopy. (B,E,H) Image slices taken approximately 3 µm below the surface. (C,F,I) Side view images of the particles obtained from a 3D rendering of the confocal scan. Scale bars = 20 µm

binding to an organic surface film or whether the properties of the particle caused some alteration in the emitted light. A combination of these explanations may also be plausible since the green light emitted from SYBR Gold stainable substances shows 2 nm differences in emission spectra (data not shown). Thus, for the FFP to be visualized, the binding target of the stain may be as important as the environment on the filter in which it occurs. Additional observations and experiments are required for further elucidation of the mechanism of visualization.

Abundance and dimensions

Abundances from the sampled locations ranged from 10 to 5×10^5 l^{-1}. Abundance in the water from Scripps Pier exhibited nearly 10× variability on timescales of days, weeks and months (Fig. 1D). FFP on the same filter and among filters were dispersed randomly and differed in brightness and hue of the fluorescence. These differences could be due to variation in SYBR Gold staining of filters or the composition of FFP. The particles occasionally harbored attached microbes, including bacteria and cyanobacteria, diatoms, dinoflagellates and other protists. However, an approximately equal number showed no association with microbes. Associations with other components of the particulate organic matter, e.g. SYBR Gold stained material as well as TEP, was also seen.

The samples collected during cruises in the California Current and Antarctica Peninsula generally showed decreasing trends in abundance with depth. In some samples, however, abundances reached a maximum that tends to coincide with both chlorophyll increases and decreases in light transmission (Fig. 3). In these environments we hypothesize that the densities of seawater and FFP may result in concentrated patches due to settling on isopycnal surfaces. These may be sites of enhanced remineralization by bacteria as well as influential locales of carbon export brought about by abrupt changes in stratification. Cursory assessments provide support for this notion, but additional and more precise samplings are needed.

A variety of shapes and sizes were observed at 100×, 200×, 600× and 1000× magnifications. Circular, elongated and irregular shapes were present in all samples, with irregular-shaped material dominating most samples. Areas ranged from 1 to 10^5 μm^2. However, it is probable that filtration or mounting on slides altered the shapes. A method is needed to image them in 3D as they occur in seawater.

Control experiments

SYBR Gold is part of a family of positively charged, asymmetrical cyanine dyes that bind to double and single stranded DNA and RNA targets through base pair intercalation as well as attachment to the minor groove and phosphate backbone via ionic binding (Zipper et al. 2004). We considered that the hydrophobicity of SYBR Gold for intercalation reaction potentially caused aggregation of molecules at the filter surface. However, the results of negative controls did not support this possibility. The 0.22 µm filtered seawater blanks did not exhibit any FFP, suggesting that the particles were not due to SYBR Gold medi-

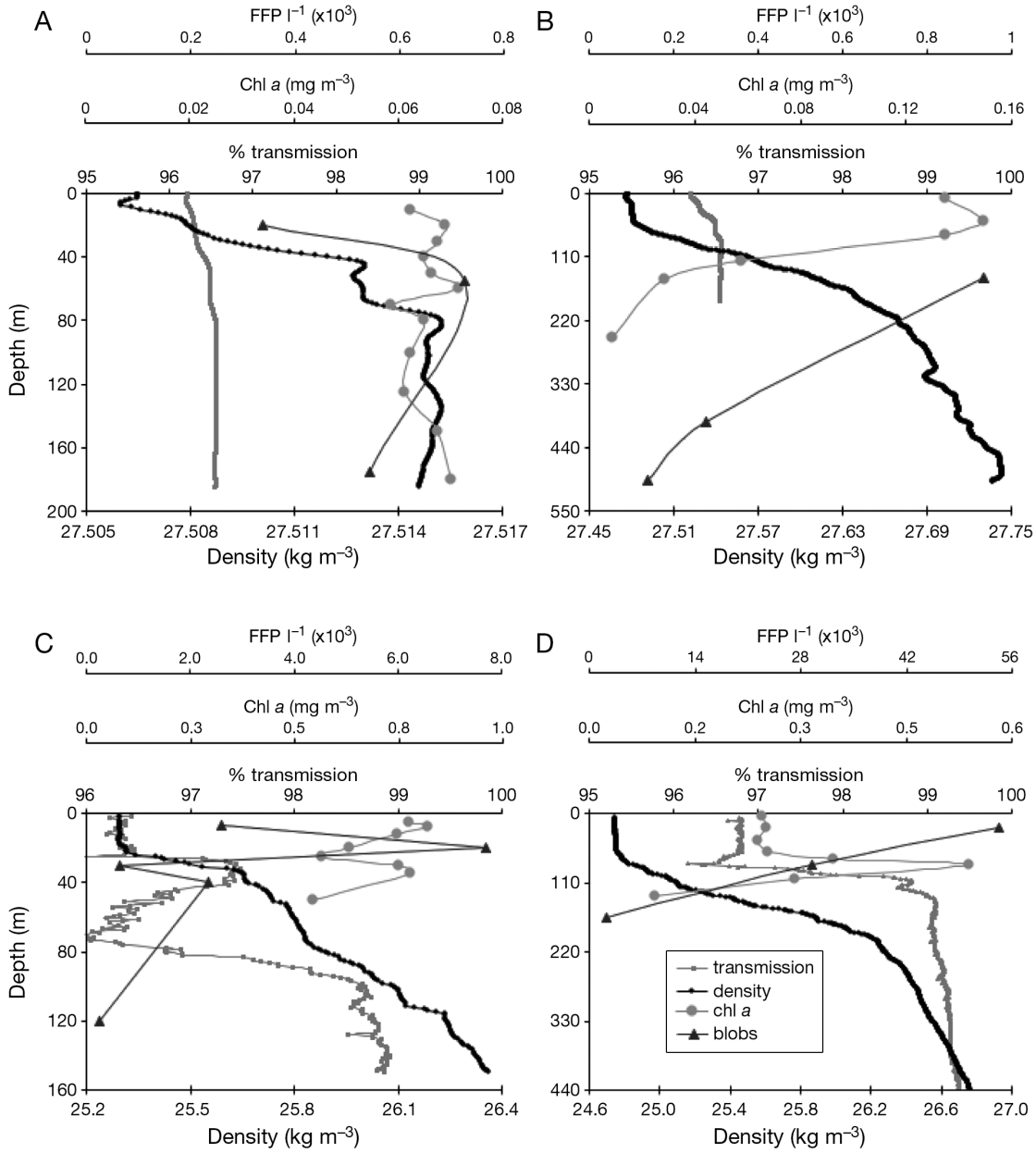

Fig. 3. Seawater density, percent light transmission, chl *a* and FFP abundance versus depth for the (A) Antarctica shelf and (B) open ocean stations, and the California Current (C) nearshore and (D) offshore stations

ated coalescing of <0.22 µm material. This was also the case for the Z/1000 and Z/10 000 samples intended to accentuate the potential for DOM aggregation and represents an important observation since dissolved carbon concentrations in these solutions were increased by ca. 6 and 0.6 µg ml^{-1}, respectively. The centrifuged sample showed FFP counts of 8.0×10^2 l^{-1} while the whole seawater sample contained 1.8×10^4 l^{-1}.

Addition of hydrophobic exopolymer substances (EPS) isolated from a bacterial culture induces assembly of amphipathic DOM into small gels (~4 µm diameter) in a temperature dependent fashion (Ding et al. 2008). The results from the 0.2 µm, tangential flow

filtration (TFF) and temperature controlled samples suggested that the molecular interactions described by Ding et al. (2008) did not cause formation of FFP via networking of DOM by SYBR Gold. Particles could not be detected in the 0.2 µm or TFF preparations, in clear contrast to the 4.8×10^5 l^{-1} found in the natural seawater. The induction of gel formation by EPS was inhibited at 4°C in the study of Ding et al. (2008), but we saw no decrease in FFP at this temperature. FFP concentrations were 1.3×10^4 and 6.0×10^4 l^{-1} for room temperature and 4°C treatments, respectively.

Potential experimental artifacts

Cell lysis in natural seawater

We considered that FFP might be produced as artifacts of sample processing, e.g. due to cell lysis or sloughing off of cell mucus during filtration. Fig. 4 shows that FFP abundance exhibited slight differences between live and fixed samples. Fixed samples had fewer small FFP, but the abundance of large ones was similar in the fixed and unfixed samples.

We did further tests to rule out protozoan lysis as a source. We centrifuged seawater at low speed and then stained the pellet and supernatant with the standard protocol. FFP were present in the supernatant that was essentially free of larger phytoplankton, so it is unlikely that they are produced from larger phytoplankton owing to sample treatment. The abundance of large and intermediate sized material in the pellet was much greater than in the supernatant, but the abundance of small size classes was not significantly different (data not shown). The pellet contained many pigmented cells and protozoa that stained with the standard protocol, and the supernatant contained some picoeukaryotes and many bacteria.

Phytoplankton lysis in cultures

Unfixed phytoplankton cultures were stained to see whether some species release cell contents due to staining and slide preparation. Only lightly fluorescent objects were seen and these did not resemble FFP. Furthermore, these objects and phytoplankton were not seen to be associated with one another, e.g. we did not see fluorescing material oozing out of phytoplankton cells. This was also true for *Lingulodinium polyedrum*, which is notable because *L. polyedrum* is delicate and highly susceptible to shear forces and osmolarity changes (Lewis & Hallett 1997). Such a delicate organism might lyse readily when exposed to suction and low osmolarity stain solutions. We could not rule out the possible scenario that cell lysis occurs, but the released organic matter can either remain dissolved — thus, it is not retained on the filter — or forms gels and particles that are retained and visualized with our

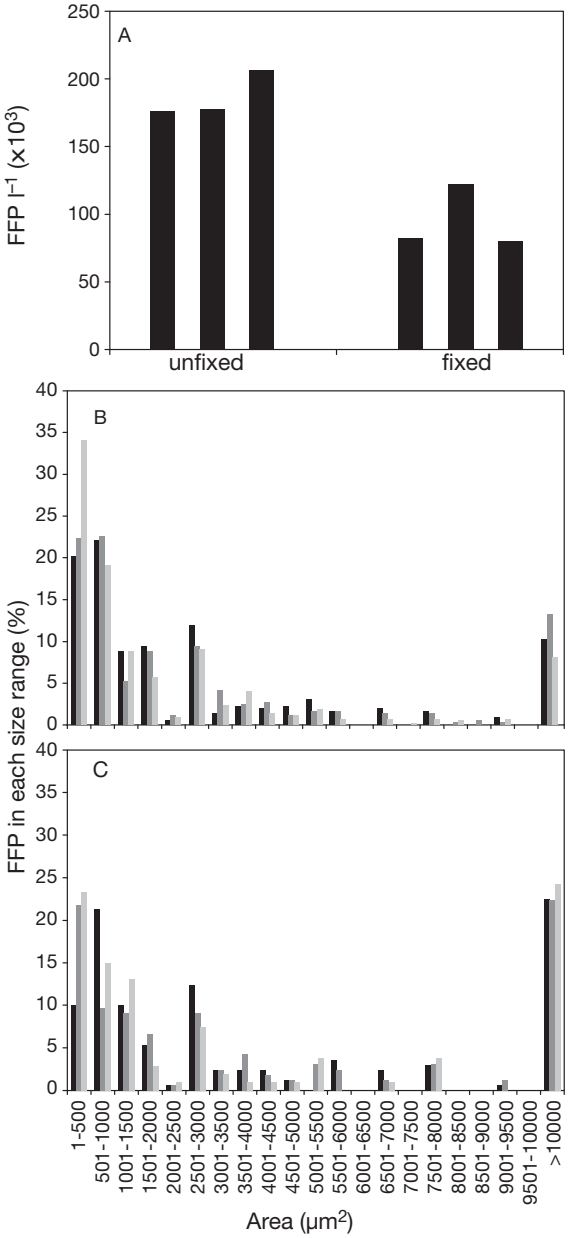

Fig. 4. (A) Abundances of FFP in unfixed and fixed seawater samples. Size frequencies of FFP in (B) unfixed and (C) 2% formaldehyde fixed seawater samples. Bars in (B) and (C) are shaded for ease of viewing, with black corresponding to the first replicate, grey to the second and light grey to the third

staining protocol. Chin et al. (2004) showed that *Phaeocystis globosa* secrete condensed polysaccharide particles that swell up and form gels when released into seawater.

Support for *in situ* occurrence

Several lines of evidence support the view that FFP exist in seawater and are not experimental artifacts. FFP were occasionally and to varying degrees colonized by bacteria. It is highly unlikely that bacteria migrated to lysed contents of a cell during or immediately after filtration. Close associations between FFP and non-bacteria/archaea microorganisms were also observed. Individuals of *Akashiwo* sp. were seen alone and in association with bacteria or FFP within the same sample. The *Akashiwo* sp. cells associated with FFP appeared intact and unlysed in unfixed and 2% formaldehyde fixed seawater. Intriguingly, chains of cyanobacteria occasionally co-localized with FFP (Fig. 5), but these were not randomly distributed on the filter. Lastly, TEP often appeared to border FFP and, thus, may be previously unseen extensions of the transparent particle field.

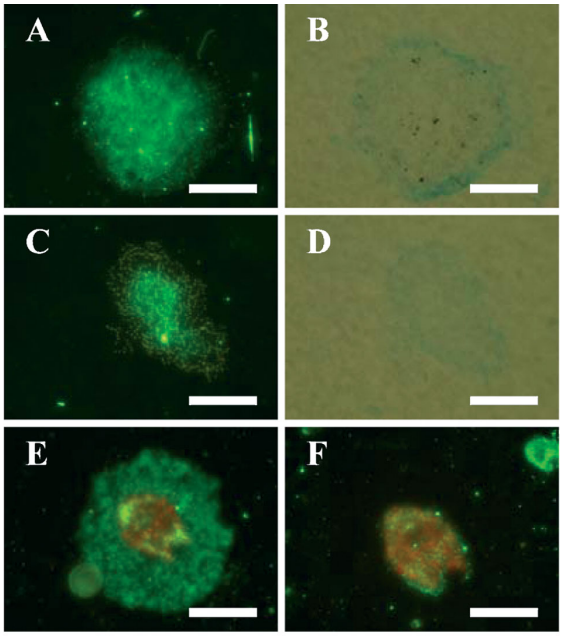

Fig. 5. Epifluorescent micrographs of FFP with extensive populations of associated (A) bacteria, (C) cyanobacteria and (E) *Akashiwo* sp. Panel (F) shows a *Akashiwo* cell not surrounded by an FFP signal. Panels (B) and (D) are transmitted light micrographs of (A) and (C), respectively, showing TEP signals along the particle periphery. Scale bars = 50 µm

Mechanism of visualization

Interactions of stains

All tested combinations of Alcian Blue plus SYBR Gold yielded positive staining for FFP. Visualization was optimal when we filtered seawater, stained the retained material with Alcian Blue and placed the filter on a drop of SYBR Gold. Omitting Alcian Blue caused the entire filter to fluoresce brightly and identically to the FFP (Fig. 1C). We think that Alcian Blue quenches the SYBR Gold induced filter background, except where the FFP are located. Crystal Violet and Ruthenium Red provided similar staining results as Alcian Blue although the images were not as bright or distinct. Chemical quenching by Alcian Blue seemed unlikely since the copper center and complex ring structure of Alcian Blue is unlike both the carbon centered triphenylmethane structure of Crystal Violet and the ruthenium center and amine side chains of Ruthenium Red. However, all these stains caused apparent fluorescence quenching of the filter. FFP were the regions of high SYBR Gold background. What is visualized then are the brightly fluorescing pores of the polycarbonate filter in the region of the FFP. Thus, we hypothesized that FFP were regions on the filter where transparent particles landed and prevented Alcian Blue from quenching SYBR Gold induced fluorescence by an as yet unknown mechanism. Visualization of transparent organic matter by our protocol is, thus, due to inhibition of fluorescence quenching.

Particle–filter interactions

Our tests suggested that FFP could be observed because the transparent particles deposited on filters prevented Alcian Blue from interacting with the filter to quench SYBR Gold fluorescence. We attempted to dislodge the transparent particles from the filter with the prediction that this would allow Alcian Blue to quench SYBR Gold fluorescence and eliminate FFP signals. This prediction was supported. We filtered seawater by gravity and then rinsed the filter with filtered seawater to try to dislodge the FFP. This manipulation did nearly eliminate FFP while many microbes and a few positive signals remained. However, the FFP were not removed if the seawater sample (not the water used for dislodging the FFP) had been vacuum filtered at 20 kPa, possibly because the material became pulled into the filter pores and firmly adsorbed. This entrainment of material into the pores may be required for Alcian Blue inhibition of SYBR

Gold fluorescence; it would coat the pores and therefore prevent Alcian Blue interaction with the SYBR Gold-stained filter surface and pores. This result is consistent with our hypothesis that FFP are visualized due the inhibition of fluorescence quenching.

Influence of filters

To test whether fluorescence quenching was only applicable to polycarbonate filters, we tried other filter materials as well. FFP were also seen with white 0.22 µm polycarbonate and 0.45 µm nitrocellulose filters and 0.02 µm aluminum oxide filters without Alcian Blue treatment. The 0.02 µm filters were not amenable to Alcian Blue staining and produced indiscernible images. The black 0.22 µm polycarbonate membranes were negative for FFP, presumably due to the black color reducing background fluorescence required for visualization by fluorescence quenching. Alternatively, the black filter might have interfered with interaction of the stains on the filter. Despite positive results with several filter types, the 1 µm polycarbonate filter gave images that were best in definition and brightness. With the focal plane on the surface of the filter, the fluorescing edges of the pores contrasted well with the non- or slightly fluorescent interior. The pores of 1 µm polycarbonate filters permit resolution of SYBR Gold stained microbes attached to the fluorescing FFP; 0.22 µm pore size polycarbonate filter fluorescence is so intense that it overwhelms the fluorescence signal of the SYBR Gold stained organisms.

Seawater and filter manipulation

Gel properties

With evidence to support that filter fluorescing particles were present in seawater, we asked whether they display gel or gel-like characteristics. Preliminary experiments (results not shown) indicated that EDTA reduced FFP abundance but not their size distributions, suggesting that cationic bridges bind FFP polymers, and their disruption caused some particles to disperse. Other FFP may have lost some, although not all, material, but maintained their definitions. Recent findings show that the integrity of marine gels is influenced by cationic bridges in a polymer matrix, and that the gels are dispersed by EDTA (Verdugo et al. 2004). The effect of EDTA shows that FFP may be created and maintained in a similar fashion to that of other marine gel particles. They may be intermediate in a stepwise formation of POM from some of the sources of organic matter, going from colloid to gel to filter fluorescing particle to marine snow. We considered that if the FFP material is gel-like it would be highly hydrated, so desiccation might alter its gel characteristics and allow Alcian Blue to contact the filter surface and quench fluorescence. However, attempts to dehydrate the material on the filter actually increased FFP abundance. In addition, the size distribution of FFP increased with an increase in abundance of FFP from 5500 to >10 000 µm^2 in one experiment. We cannot explain this result, but speculate that dehydration changed the properties of some other types of transparent particles to confer on them the ability to cause inhibition of fluorescence quenching similar to the action of FFP. Alternatively, the initial entrapment of material within the filter pores before dehydration may have provided a source of molecules that, after dehydration, were capable of the inhibitory effect.

Triton X-100 addition followed by sonication decreased the abundance of total as well as large FFP. One interpretation would be that FFP are amphipathic, with hydrophobic regions holding an aggregate together while the hydrophilic areas are exposed to water. Alternatively, FFP may be sensitive to turbulence and shear.

Macromolecular characterization

In an attempt to constrain the composition, we tested how known macromolecules added to the samples would appear in the standard protocol. We tested DNA, carbohydrate, protein and lipid since they are among the major organic matter pools in marine biomass and DOM. Positive staining was seen with DNA at concentrations of 100 and 1 mg ml^{-1}. Also, BSA and DNA mixed in agarose were prepared as mimics of natural gels. They produced fluorescence similar to FFP. Phosphatidylcholine, as a model for lipids, also yielded FFP-like images. Natural marine gels and particles are probably mixtures of diverse macromolecules (Long & Azam 1996) so our results show that FFP images may be due to a variety of macromolecular types. Further, the requirement for quite high macromolecular concentrations suggests the possibility that we are still missing some transparent gels because they contain macromolecules at concentrations too low to cause detectable inhibition of fluorescence quenching.

Specific hydrolytic enzymes helped further characterize the macromolecular makeup of FFP by their breakdown or solubilization. β-glucosidase caused the most apparent decrease in abundances, reducing numbers to 65% of their total and eliminating most of the large size classes. DNase and pronase treatments

did not seem to appreciably alter size frequencies and resulted in abundances of 96 and 94% of the total, respectively. Interestingly, lipase resulted in a slight increase in abundance (104%), but no change in size frequency distribution. One possibility is that lipid hydrolysis reduced hydrophobic sites and permitted agglomeration of materials at exposed hydrophilic and polar surfaces (Fig. 6).

Assessing the presence of sugar moieties within the FFP via fluorescently labeled lectins provided intriguing chemical and structural information. Positive signals from concavalin A indicated the presence of glucose and/or mannose. The absence of signal co-localization with peanut agglutinin fluorescence suggested that galactose residues were either absent in the FFP or below detection. Sugar-binding moieties displayed a striking interior structure of strings and strands that varied among FFP (Fig. 7). The fact that glucose is a significant fraction of organic matter in FFP would make them a good source of energy for the colonizing bacteria. It is noteworthy that lectin signals always remained within the boundaries of the SYBR Gold fluorescence image, but in many cases did not uniformly occur over the entire FFP. Other organic polymers may occupy the lectin-negative areas.

Nitrogen and phosphorous amendment

We examined the relationship of FFP with nutrient status of the phytoplankton. Nutrient limited phytoplankton may release gels, so one could predict that phytoplankton will be found associated with FFP. In support of this hypothesis, we consistently noticed that phytoplankton occurred within FFP and occasionally bacteria also colonized the FFP. We considered that if nutrient limited phytoplankton produced mucus that generated the FFP, then high rates of nutrient remineralization within the FFP, due to high concentrations of

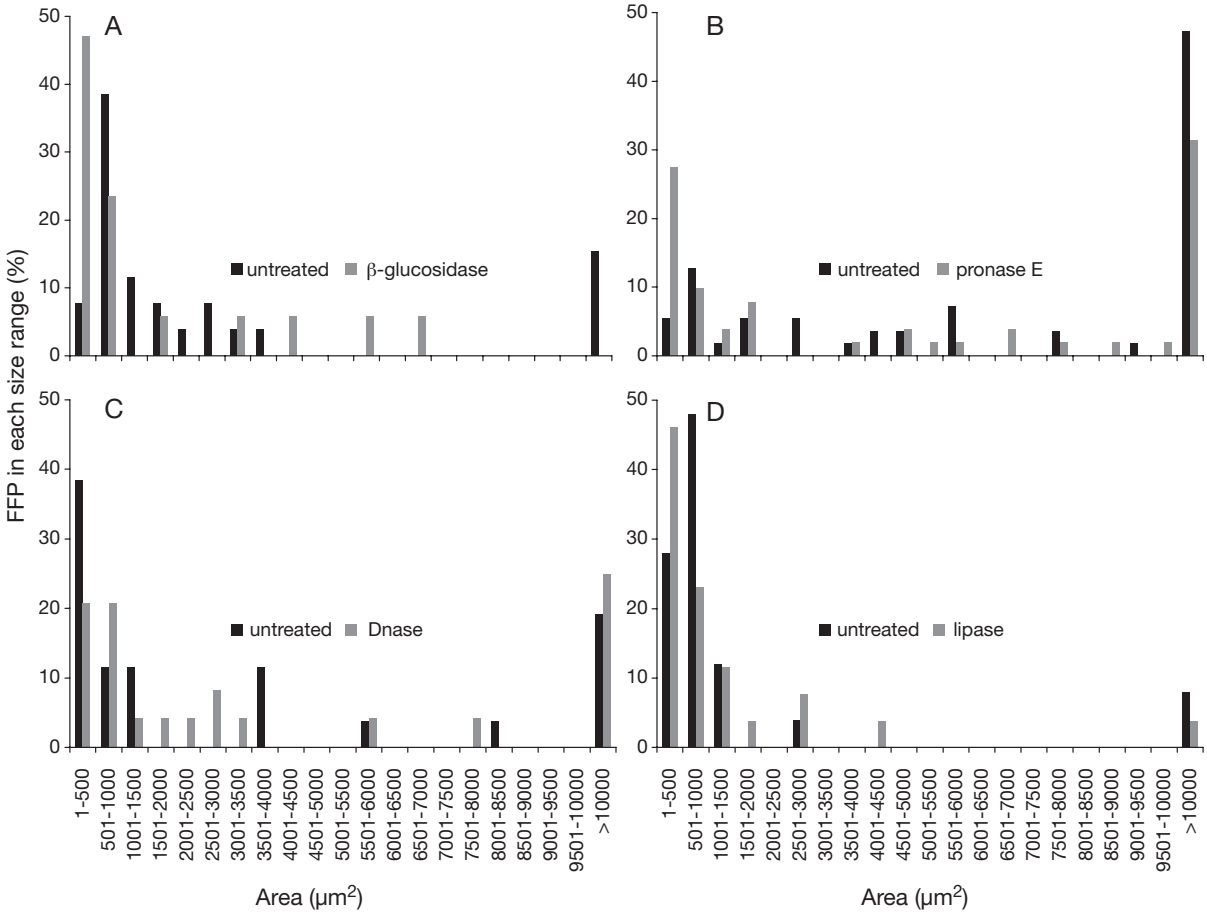

Fig. 6. Size frequency charts following treatment with (A) β-glucosidase, (B) pronase, (C) DNase and (D) lipase

Aquat Microb Ecol 53: 307–321, 2008

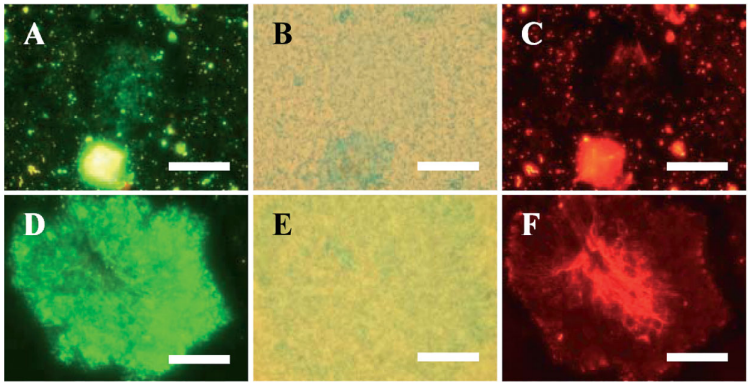

Fig. 7. Each horizontal row of images shows a single FFP visualized with: (A,D) 488 nm excitation, long pass emission to observe SYBR Gold, (B,E) transmitted light to observe acidic mucopolysaccharide material stained by Alcian Blue, and (C,F) 540 nm excitation, long pass emission to observe concanavalin A lectin localization. Scale bars = 50 µm

bacteria and phytoplankton, might have a negative feedback on mucus production. Increased exudation of organic matter by phytoplankton with high C:N ratios occurs during periods of nutrient deprivation. Various explanations for enhanced exudation include (1) reductant overflow and (2) adaptive strategy of the phytoplankton cell to improve the nutrient status of its microenvironment (Azam & Smith 1991, Borsheim et al. 2005). Exudates of nutrient stressed phytoplankton are rich in carbohydrates, low in nitrogen, probably sticky and subsequently consumed by bacteria. Azam & Malfatti (2007) proposed that bacteria hydrolyze and metabolize the exuded polymers and DOM adsorbed onto the 'phycosphere' such that N, P and Fe in the phytoplankton cell microenvironment becomes available at high concentrations.

The water off Scripps Pier is typically P-replete but N-limited for phytoplankton growth. We added 1 µM ammonium nitrate to try to overcome N limitation with the prediction that this would reduce FFP production. Rather than lowering the FFP abundance, it actually increased it. Smaller particle size classes increased, but did not resemble the particles in unenriched samples (Fig. 8). Larger size FFP also showed a small increase. Even though the water off Scripps Pier is generally rich in P (typically 0.3 to 1 µM), P enrichments decreased FFP abundance and did not change the size range. Bacteria were found attached to FFP in both N and P treatments, but attachment in the N-replete samples was particularly noticeable due to the large number of FFP present. The observed increase in the N-replete treatment might be due to enhanced phytoplankton production and its processing by grazers, which lead to spills of stainable polymers into seawater. The N-replete conditions may also have changed the chemical composition of the released polymer pool and, thus, its stainability. We conclude that the nutrient status of seawater can affect FFP dynamics, and also influence the associated microbial community. However, this preliminary experiment does not address the mechanism regulating FFP formation.

CONCLUSIONS

Our discovery extends the types of transparent particles known to be present in seawater. As has been proposed for the ecological role of TEP, DAPI yellow particles (DYP) and CSP, these FFP may also provide microenvironments of high microbial activity (Alldredge et al. 1993, Mostajir et al. 1995, Long & Azam 1996). Their chemical and physical diversity may lead to great microbial diversity and assorted biogeochemical transformations.

It is critical to rule out that the particles seen are not due to artifacts and indeed are present in seawater. This challenge has been faced by oceanographers from the discoveries of Bathybius (Huxley 1868), TEP, CSP, Koike particles (Isao et al. 1990), gels and colloids (Wells & Goldberg 1991, Chin et al. 1998), as well as the FFP here. Ideally one would want to image particles as they exist in seawater, without physically sampling them. The technology to do so may become available in the future (Franks & Jaffe 2001, Gonzalez-Quiros & Checkley 2006). At present, to rule out artifacts while at the same time learn more about the chemical and physical characteristics of the particles, multiple constraints can be applied, as we have done in this study. The potential sources of FFP and other transparent particles are probably diverse. Many microorganisms release polymers by exudation, exocytosis or programmed cell death (PCD). However, identifying the type of transparent particles and relating them to their sources is confounded by the diversity of particles as well as microorganisms and their *in situ* physiologies. Berman-Frank et al. (2007) found that cultures of the cyanobacterium *Trichodesmium* increased TEP production following PCD in response to nutrient and/or oxidative stress. Notably, iron limitation was correlated with PCD and the highest pools of TEP and particulate organic carbon. Whether the same would be true for FFP was not tested. The diverse sources and production mechanisms are probably reflected in their chemical composition (Long & Azam

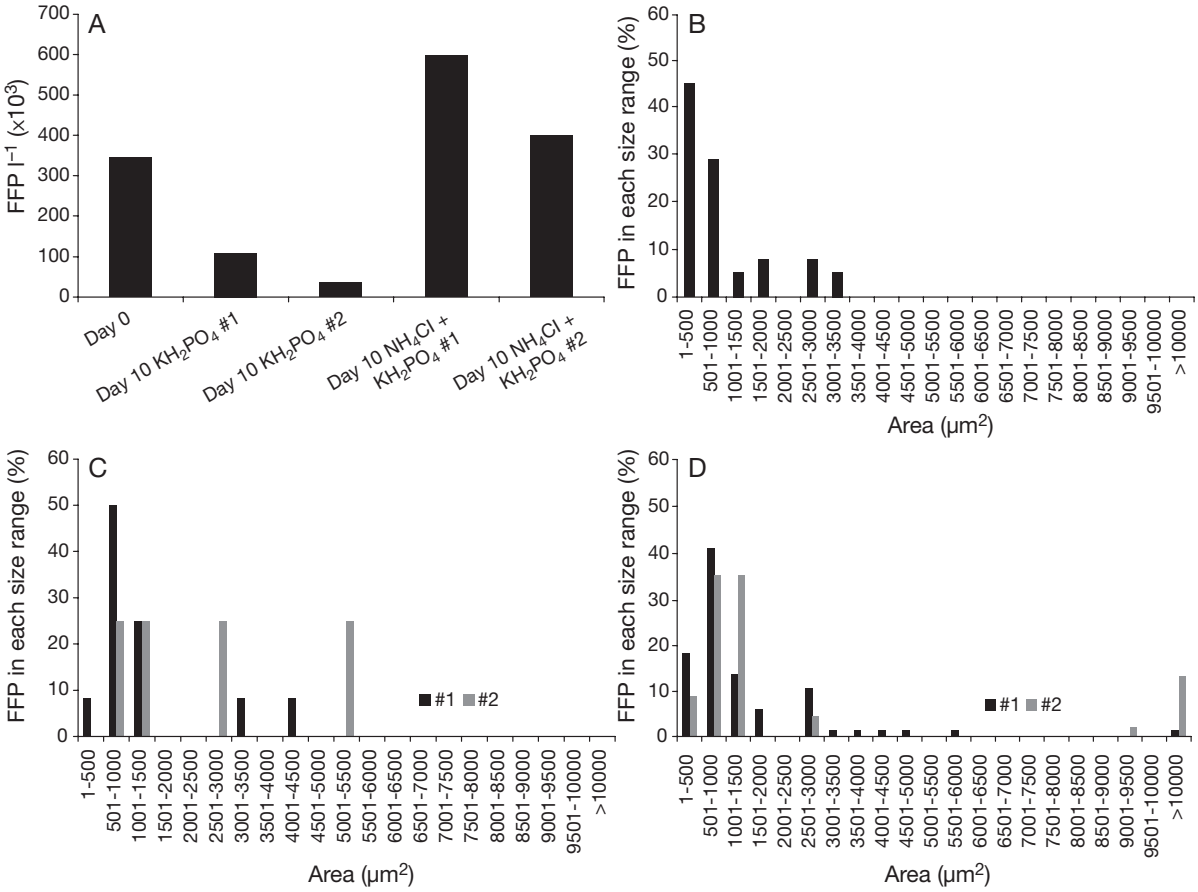

Fig. 8. (A) Abundances at Days 0 and 10 with and without amendments. Size frequencies of FFP at (B) Day 0, (C) Day 10 following amendment with phosphorus and (D) Day 10 following amendment with nitrogen plus phosphorus. Black and gray bars in (C) and (D) display the first and second replicates, respectively

1996, Passow 2002, Verdugo et al. 2004). Our results indicate that a variety of macromolecules — carbohydrates, DNA, lipids and proteins — can elicit positive signals in our protocol. It would be of interest to see whether the standard Alcian Blue/SYBR Gold protocol may also be applied to staining for other types of transparent particles and sources.

If we consider that FFP and other transparent particles behave in a fashion similar to polymer gels, then local changes in the chemistry of seawater will result in shrinking and swelling of the material. The effects of pressure, temperature and pollutants may cause a gel to become a highly compact and dense structure, capable of excluding or entrapping anything less than 500 Da (Chin et al. 1998). Alcian Blue has an atomic weight of approximately 1200 Da, and it may follow that the use of histological stains greater than 1200 Da will permit staining of more diffuse and/or porous particles. Observing this material and associated microbes may aid in linking microbial physiology and diversity to the state of the organic matter field in seawater. This may be especially important in understanding carbon export and the fates of organic particles.

Whether some dissolved polymers, colloids and gels might sink out of the euphotic zone will depend on many factors, such as the speed and degree of substrate hydrolysis, the chemical composition and stickiness of the material, the consortia of organisms present and the local physical and chemical characteristics of the water column, and whether respiration will convert most of the fixed carbon back to its oxidized state. A common theme among these parameters is the phenomenon of aggregation and its relation to export flux, with implications for global climate. As a particle is hydrolyzed and colonized by the microbial community and comes into contact with other particles and molecules, the resulting changes in density may have direct

connections to carbon export. However, it is currently unclear whether the net biological, chemical and physical effects enable carbon drawdown. These processes are not necessarily limited to microscale environments, as a variety of metazoans may also significantly affect the particulate carbon pool. The copepod *Calanus pacficus* consumes significant amounts of TEP under starved and diatom-replete conditions (Ling & Alldredge 2003). FFP may represent another pathway by which higher trophic levels are able to consume viruses, prokaryotes and small eukaryotes located on or within the organic matrix. Further characterization of marine organic matter, its interactions with marine microbes and its behavior in a microecological framework would advance our knowledge of the mechanisms operating at the microscale that contribute to oceanic biogeochemical cycles.

Acknowledgements. This research was supported by grants from the US-NSF (OCE04-28900 and ANT04-44134) and the Gordon and Betty Moore Foundation to F.A. Additional support was provided by US-NSF funding for the California Current Ecosystem Long Term Ecological Research (CCE-LTER) to Dr. M. D. Ohman (OCE04-17616). We thank the Captains and crews of the RV/IB 'Nathaniel B. Palmer and R/V Thomas G. Thompson' for excellent shipboard support. We appreciate the assistance of J. V. Nguyen and Drs. M. Manganelli and J. R. Ward in sample collection.

LITERATURE CITED

Alldredge AL, Passow U, Logan BE (1993) The abundance and significance of a class of large, transparent organic particles in the ocean. Deep-Sea Res I 40:1131–1140

Aluwihare LI, Repeta DJ (1999) A comparison of the chemical characteristics of oceanic DOM and extracellular DOM produced by marine algae. Mar Ecol Prog Ser 186:105–117

Aluwihare LI, Repeta DJ, Chen RF (1997) A major biopolymeric component to dissolved organic carbon in surface sea water. Nature 387:166–169

Azam F, Long RA (2001) Oceanography: sea snow microcosms. Nature 414:495–498

Azam F, Malfatti F (2007) Microbial structuring of marine ecosystems. Nat Rev Microbiol 5:782–791

Azam F, Smith DC (1991) Bacterial influence on the variability in the ocean's biogeochemical state: a mechanistic view. In: Demers S (ed) Particle analysis in oceanography, Vol 27. Springer-Verlag, Berlin, p 213–236

Azam F, Worden AZ (2004) Microbes, molecules, and marine ecosystems. Science 303:1622–1624

Azam F, Martinez J, Smith DC (1993) Bacteria-organic matter coupling on marine aggregates. In: Guerrero R, Pedrós-Alió C (eds) Trends in microbial ecology. Spanish Society for Microbiology, Barcelona, p 410–414

Berman-Frank I, Rosenberg G, Levitan O, Haramaty L, Mari X (2007) Coupling between autocatalytic cell death and transparent exopolymeric particle production in the marine cyanobacterium *Trichodesmium*. Environ Microbiol 9:1415–1422

Borsheim KY, Vadstein O, Myklestad SM, Reinertsen H, Kirkvold S, Olsen Y (2005) Photosynthetic algal production, accumulation and release of phytoplankton storage carbohydrates and bacterial production in a gradient in daily nutrient supply. J Plankton Res 27:743–755

Chin WC, Orellana MV, Verdugo P (1998) Spontaneous assembly of marine dissolved organic matter into polymer gels. Nature 391:568–572

Chin WC, Orellana MV, Quesada I, Verdugo P (2004) Secretion in unicellular marine phytoplankton: demonstration of regulated exocytosis in *Phaeocystis globosa*. Plant Cell Physiol 45:535–542

DeLong EF, Karl DM (2005) Genomic perspectives in microbial oceanography. Nature 437:336–342

Ding YX, Chin WC, Rodriguez A, Hung CC, Santschi PH, Verdugo P (2008) Amphiphilic exopolymers from *Sagittula stellata* induce DOM self-assembly and formation of marine microgels. Mar Chem 112:11–19

Franks PJS, Jaffe JS (2001) Microscale distributions of phytoplankton: initial results from a two-dimensional imaging fluorometer, OSST. Mar Ecol Prog Ser 220:59–72

Gonzalez-Quiros R, Checkley DM (2006) Occurrence of fragile particles inferred from optical plankton counters used in situ and to analyze net samples collected simultaneously. J Geophys Res-Oceans 111:C05S06

Grossart HP, Kiorboe T, Tang KW, Allgaier M, Yam EM, Ploug H (2006) Interactions between marine snow and heterotrophic bacteria: aggregate formation and microbial dynamics. Aquat Microb Ecol 42:19–26

Huxley TH (1868) On some organisms living at great depths in the North Atlantic Ocean. Q J Microsc Sci 8:203–212

Isao K, Hara S, Terauchi K, Kogure K (1990) Role of submicrometre particles in the ocean. Nature 345:242–244

Johnsen AR, Hausner M, Schnell A, Wuertz S (2000) Evaluation of fluorescently labeled lectins for noninvasive localization of extracellular polymeric substances in Sphingomonas biofilms. Appl Environ Microbiol 66: 3487–3491

Kiørboe T, Tang K, Grossart HP, Ploug H (2003) Dynamics of microbial communities on marine snow aggregates: colonization, growth, detachment, and grazing mortality of attached bacteria. Appl Environ Microbiol 69: 3036–3047

Lewis J, Hallett R (1997) *Lingulodinium polyedrum* a blooming dinoflagellate. In: Ansell AD, Gibson RN, Barnes M (eds) Oceanography and marine biology: an annual review, Vol 35. UCL Press, London, p 97–161

Ling SC, Alldredge AL (2003) Does the marine copepod *Calanus pacificus* consume transparent exopolymer particles (TEP)? J Plankton Res 25:507–515

Long RA, Azam F (1996) Abundant protein-containing particles in the sea. Aquat Microb Ecol 10:213–221

Long RA, Azam F (2001) Microscale patchiness of bacterioplankton assemblage richness in seawater. Aquat Microb Ecol 26:103–113

Mostajir B, Dolan JR, Rassoulzadegan F (1995) Seasonal variations of pico- and nano-detrital particles (DAPI Yellow Particles, DYP) in the Ligurian Sea (NW Mediterranean). Aquat Microb Ecol 9:267–277

Noble RT, Fuhrman JA (1998) Use of SYBR Green I for rapid epifluorescence counts of marine viruses and bacteria. Aquat Microb Ecol 14:113–118

Orellana MV, Petersen TW, Diercks AH, Donohoe S, Verdugo P, van den Engh G (2007) Marine microgels: optical and proteomic fingerprints. Mar Chem 105:229–239

Passow U (2002) Production of transparent exopolymer particles (TEP) by phyto- and bacterioplankton. Mar Ecol Prog Ser 236:1–12

Passow U, Alldredge AL (1994) Distribution, size and bacter-

ial-colonization of transparent exopolymer particles (TEP) in the Ocean. Mar Ecol Prog Ser 113: 185–198

Proctor LM, Fuhrman JA (1991) Roles of viral infection in organic particle flux. Mar Ecol Prog Ser 69:133–142

Radic T, Ivancic I, Fuks D, Radic J (2006) Marine bacterioplankton production of polysaccharidic and proteinaceous particles under different nutrient regimes. FEMS Microbiol Ecol 58:333–342

Simon M, Grossart HP, Schweitzer B, Ploug H (2002) Microbial ecology of organic aggregates in aquatic ecosystems. Aquat Microb Ecol 28:175–211

Smith DC, Steward GF, Long RA, Azam F (1995) Bacterial mediation of carbon fluxes during a diatom bloom in a mesocosm. Deep-Sea Res II 42:75–97

Verdugo P, Alldredge AL, Azam F, Kirchman DL, Passow U, Santschi PH (2004) The oceanic gel phase: a bridge in the DOM–POM continuum. Mar Chem 92:67–85

Wells ML, Goldberg ED (1991) Occurrence of small colloids in sea-water. Nature 353:342–344

Zipper H, Brunner H, Bernhagen J, Vitzthum F (2004) Investigations on DNA intercalation and surface binding by SYBR Green I, its structure determination and methodological implications. Nucleic Acids Res 32:e103, doi:10.1093/nar/gnh101

Editorial responsibility: Craig Carlson, Santa Barbara, California, USA

Submitted: March 4, 2008; Accepted: September 23, 2008
Proofs received from author(s): December 12, 2008

Chapter 3

Microbial distribution and activity across a water mass frontal zone in the California Current Ecosystem

Microbial distribution and activity across a water mass frontal zone in the California Current Ecosystem

TY J. SAMO*, BYRON E. PEDLER, GREGORY I. BALL, ALEXIS L. PASULKA, ANDREW G. TAYLOR, LIHINI I. ALUWIHARE, FAROOQ AZAM, RALF GOERICKE AND MICHAEL R. LANDRY

SCRIPPS INSTITUTION OF OCEANOGRAPHY, UNIVERSITY OF CALIFORNIA, SAN DIEGO, LA JOLLA, CA 92093-0202, USA

*CORRESPONDING AUTHOR: tsamo@ucsd.edu

Received November 4, 2011; accepted in principle May 24, 2012; accepted for publication June 2, 2012

Corresponding editor: John Dolan

Ocean fronts with accumulated biomass and organic matter may be significant sites of enhanced microbial activity. We sampled a frontal region (the A-Front) separating oligotrophic and mesotrophic water masses within the California Current Ecosystem (CCE) to assess the influence of frontal hydrography on several microbial parameters. Samples for heterotrophic bacterial, viral and flagellate abundance, dissolved and particulate carbon and nitrogen, transparent particles and bacterial carbon production were collected at 6 depths from the surface to 100 m with 5–9 conductivity/temperature/depth casts along a 26-km northerly transect across the front. Relative to adjacent oligotrophic and mesotrophic waters, the frontal transition displayed peaks in the mean estimates of cell-specific bacterial carbon and bulk bacterial production, particulate organic carbon and particulate organic nitrogen concentrations, and the abundance and size of transparent particles. Bacterial carbon production increased ~5-fold northward from oligotrophic waters to the frontal zone, in agreement with an increase in the frequency of dividing cells, but bacterial abundance was lower than at adjacent stations. This may be partially explained by high chlorophyll, elevated virus:bacteria ratios and low nanoflagellate grazer abundance at the front. Our data suggest that CCE fronts can facilitate intense biological transformation and physical transport of organic matter, in sharp contrast to adjacent low productivity waters, and harbor dynamic microbial populations that influence nutrient cycling.

KEYWORDS: bacteria flagellates; viruses; organic matter biogeochemistry; A-Front California Current

INTRODUCTION

The California Current Ecosystem (CCE) is a seasonally dynamic region that contains oligotrophic offshore and highly productive coastal environments. Eastern boundary currents and wind-driven upwelling events combine with the current divergence near Point Conception, California, creating distinct water masses that extend southward (Bray *et al.*, 1999; Rykaczewski and Checkley, 2008). As these cold, mesotrophic water parcels contact warmer oligotrophic waters offshore of the Southern California Bight, frontal zones with sharp gradients and filaments of sea surface temperature (SST) and chlorophyll often form at the junction, exhibiting variable spatiotemporal frequencies controlled by

doi:10.1093/plankt/fbs048, available online at www.plankt.oxfordjournals.org. Advance Access publication June 29, 2012

local forcings and temperature gradients (Kahru *et al.*, 2012).

Driven by primary and secondary circulation from geostrophic and ageostrophic processes (Franks, 1992; Claustre *et al.*, 1994), the confluence of water masses at fronts can result in fertilization and horizontal advection. This can lead to the growth and accumulation of plankton at fronts or within frontal jets. Responses of microbial communities can vary, underscoring the importance of physical features in biological processes. Studies in the southwestern Mediterranean Sea examined the effects of the Almeria-Oran geostrophic front in the eastern Alboran Sea (Prieur and Sournia, 1994). Frontal zones were characterized by elevated primary production rates and diatom-dominated communities (Fiala *et al.*, 1994), enhanced bacterial carbon production (BCP) (Fernández *et al.*, 1994) and increases in particle export (Peinert and Miquel, 1994). In the subtropical convergence zone of the Sargasso Sea, enhanced nutrient fluxes across the transition zone led to increased chlorophyll *a* (chl *a*), though without a concomitant heterotrophic bacterial response (Riemann *et al.*, 2011). Mesoscale blooms of phytoplankton have also been attributed to upwelling at fronts in the northern CCE (Pallàs-Sanz *et al.*, 2010). Others have examined the influence of cyclonic and anticyclonic eddies on primary and secondary production (Ducklow and Hill, 1985; Falkowski *et al.*, 1991; Ewart *et al.*, 2008). Consistently, the injection of inorganic nutrients stimulated phytoplankton growth, resulting in biomass and organic matter accumulation relative to adjacent waters.

Dissolved organic matter (DOM) produced by phytoplankton and other microorganisms is important in marine biogeochemical cycles and climate regulation (Aluwihare and Repeta, 1999; Raven and Falkowski, 1999; Azam and Malfatti, 2007). The biogeochemical fate of DOM is largely regulated by the heterotrophic activity of marine prokaryotes (bacteria and archaea, here collectively called "bacteria") (Hagström *et al.*, 1984). The efficiency with which bacteria utilize the DOM of varied quality to create new biomass or, alternatively, respire carbon, ultimately determines the relative partitioning of carbon into labile, semi-labile and refractory organic matter classes, influencing global ocean–atmosphere carbon dioxide (CO_2) exchange and carbon export (del Giorgio and Cole, 1998). These processes influence carbon export via the biological pump operating through the microbial loop (Azam *et al.*, 1983; Martin *et al.*, 1994; Karl *et al.*, 1998).

Studies on the roles of microbes in carbon cycling at oceanic fronts have shed light on the role of hydrography in regulating the metabolism and growth of photoautotrophic and heterotrophic microbes. Nutrient injections in frontal zones, as well as meso- and submesoscale instabilities, often support enhanced bacterial production due to increased primary production by larger phytoplankton (Videau *et al.*, 1994; Morán *et al.*, 2001), but the mechanisms are not clear. Alternatively, fronts can support a food web characterized by abundant picophytoplankton where elevated bacterial production may be due at least in part to the release of top-down grazer control modulated by flagellates (Heinänen *et al.*, 1995). Such variability in bottom-up versus top-down control of marine bacterial populations at frontal zones has also been observed at the Almeria-Oran front (Van Wambeke *et al.*, 2004), and the relative contributions of these two mechanisms to microbial ecological dynamics in the Mediterranean region was found to differ between oligotrophic, frontal and gyre systems. Such interactions between hydrodynamics and biological responses are likely to determine the extent to which bacteria, phytoplankton and organic matter impact local food webs as well as the CO_2 exchange with the atmosphere (Sempéré *et al.*, 2003).

The microbial influences on carbon cycling at frontal zones have not been well studied in the CCE, nor has a baseline of microbial activities or abundance within these features been established in this region. As a component of the California Current Ecosystem—Long Term Ecological Research (CCE-LTER) site, we investigated a frontal boundary, designated the A-Front, between abutting oligotrophic and mesotrophic water masses to assess patterns, gradients and implications of microbially mediated carbon cycling. The results are discussed within the comprehensive ecosystem context of this CCE-LTER study.

METHOD

We sampled a 26-km transect of nine stations across a deep water front (Landry, Ohman *et al.*, 2012; Ohman *et al.*, 2012) located 350 km west of San Diego in the southern CCE (Fig. 1). All samples were collected during 24–25 October 2008 over a 9 h period at night (21:30–05:00, local time) with Niskin bottles on a conductivity/temperature/depth (CTD) rosette. Based on satellite images of the SST and chl *a*, hydrography, nutrients and biological parameters, stations 1–3 were located on the oligotrophic side of the front, stations 4 and 5 were designated frontal and stations 6–9 were on the mesotrophic side. Unless otherwise noted, microbial variables were measured from 0 to 100 m depths at stations 1, 3, 5, 7 and 9. Data for temperature, salinity and density were

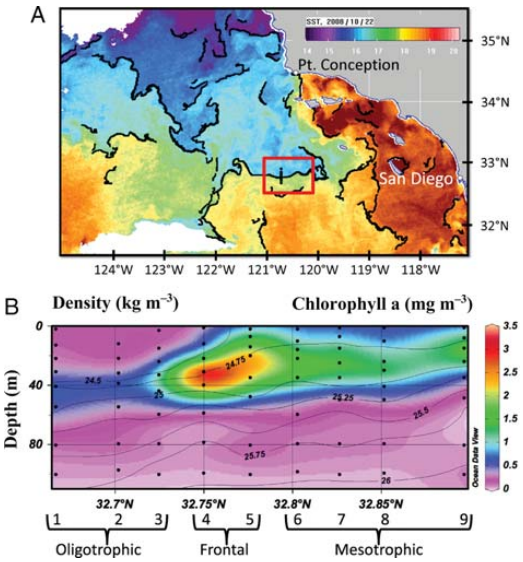

Fig. 1. Satellite images of the sea surface temperature (**A**) with the study area indicated by the red box. The section plot of chlorophyll *a* concentration across the front with density contours (**B**).

obtained from the shipboard CTD package (Sea-Bird Electronics, Inc., Bellevue, WA, USA).

Bacterial abundance, biomass and frequency of dividing cells

Water samples (3 mL) were fixed with 2% (final) formaldehyde, filtered on white 0.2-μm pore size 25-mm diameter polycarbonate filters (Nuclepore, GE Whatman, Piscataway, NJ, USA), dried at room temperature and stored at −20°C. Each filter was mounted and stained with VECTASHIELD containing 1.5 μg mL^{-1} of 4′, 6-diamidino-2-phenylindole (DAPI, Vector Laboratories, Burlingame, CA, USA), and imaged at 1000× magnification on a Nikon TE2000-U inverted epifluorescence microscope using a CoolSnapHQ CCD camera connected to NIS-Elements 3.2 software. Ten image fields per filter were processed to measure cell abundance, length and width using the signal thresholding and binary layer functions of the software. Cyanobacteria were excluded from the total bacterial counts by manual removal from the DAPI channel identified as autofluorescent cells in the TRITC channel (excitation 555 ± 14 nm, emission 617 ± 37 nm). An area cutoff of 0.1–2 μm^2 was used to exclude viral-like particles (VLP) and protists from the analyses. The average cell number per field was converted to abundance, and the dimensions of the cells were used to calculate biovolumes (μm^3 $cell^{-1}$) based on the equation $V = (\pi/4) \times W^2 \times (L - W/3)$ (Bratbak, 1985). Biovolumes were converted to per cell protein content (fg $cell^{-1}$) using the power law function $P=88.6*V^{0.59}$, and multiplied by 0.86 to calculate cell-specific carbon (fg C $cell^{-1}$) (Simon and Azam, 1989). DAPI-based biovolume estimates were found to be acceptable in a previous calibration study using atomic force microscopy (Malfatti *et al.*, 2010). Cell carbon values for each depth were averaged, then multiplied by the cell abundance to calculate the bacterial carbon (BC) concentration (μg C L^{-1}).

The frequency of dividing cells (FDC) was calculated according to Hagström *et al.* (Hagström *et al.*, 1979). Septated cells were counted from the same fields used for the total cell abundance and divided by the total number of bacteria from each field. The numbers were arcsine transformed to ensure normality of the data and correct averaging of percentages, and then back-transformed to obtain a percentage for each depth.

Heterotrophic bacteria were also enumerated by flow cytometry (FCM) from stations 1–9 and depths from the surface down to 80 m. Two milliliter samples were preserved (0.5% paraformaldehyde; final) and then flash frozen in liquid nitrogen. Onshore, the samples were stored at −80°C until shipment to the University of Hawaii FCM facility (SOEST Flow Cytometry Facility, www.soest.hawaii.edu/sfcf). Samples were thawed and stained with Hoechst 33342 (1 μg mL^{-1} final concentration) (Monger and Landry, 1993). A Beckman-Coulter Altra flow cytometer was mated to a Harvard Apparatus syringe pump for quantitative analyses, and equipped with two argon ion lasers tuned to UV (200 mW) and 488 nm (1 W) excitation (Coherent, Inc., Santa Clara, CA, USA). Scatter (side and forward) and fluorescence signals were collected. Fluorescence signals were normalized to 0.5 and 1.0-μm yellow–green polystyrene beads (Polysciences, Inc., Warrington, PA, USA). Data generated as listmode files (FCS 2.0 format) were acquired from the flow cytometer using Expo32 software (Beckman-Coulter). FlowJo software was used to assign population designations from the data based on scatter and fluorescence signals (Tree Star, Inc., www.flowjo.com). Autotrophic bacteria, *Prochlorococcus* and *Synechococcus*, identified, respectively, by their chl *a* and phycoerythrin autofluorescences, were excluded from FCM estimates of total (heterotrophic) bacteria.

Microscopy-based counts (MIC) from every other station were not well resolved between stations or with depths from 40 to 100 m. To compensate for unsampled stations and depths, two regression plots (intercepts set to 0) were made between MIC- and

FCM-based measurements. One showed a strong relationship in MIC versus FCM-derived cell counts (MIC = 0.850*FCM; $R^2 = 0.958$, $P < 0.0001$; Supplementary data, Fig. S1A); the other examined MIC-based carbon biomass (BC, $\mu g\ C\ L^{-1}$) versus the product of FCM-derived cell counts and FCM-derived normalized, mean DNA fluorescence (BC = 8.122 FCM*DNA; $R^2 = 0.644$, $P < 0.0001$; Supplementary data, Fig. S1B). We used the slopes of these regressions to estimate BC at stations 2, 4, 6 and 8 and for bacterial abundances at stations 1–3 and 7–9, both to a depth of 80 m. Microscope counts were used for 100 m and surface samples at the front station and mesotrophic stations due to consistent deviations in MIC–FCM regressions for those samples.

Viral abundance and virus:bacteria ratios

Viral abundance was determined for 0–80-m depths at stations 4, 5 and 6. Samples were fixed with 0.5% (final) EM-grade glutaraldehyde, flash frozen in liquid nitrogen and stored at −80°C (Brussaard, 2004). After thawing, 500 μL was filtered (≤25 cm Hg) onto 0.02-μm pore size aluminum oxide filters (Anodisc 25, GE Whatman, Piscataway, NJ, USA), stained with SYBR Gold (Invitrogen, Carlsbad, CA, USA; 0.25% final concentration of original stock) and mounted onto glass slides with anti-fade solution (0.1% *p*-phenylenediamine in phosphate-buffered saline:glycerol at 1:1 concentration). At least 200 viruses per sample were counted on an Olympus BX51 microscope at 1000× magnification using wide-field excitation centered at 470–490 nm with a long pass emission filter (Patel *et al.*, 2007). Bacterial counts were made on the same filters to calculate the virus:bacteria ratios.

Nano- and microflagellate enumeration

Heterotrophic nano- and microflagellates were counted in 50 and 500 mL samples, respectively. Samples were preserved sequentially with alkaline Lugol's solution, formalin and sodium thiosulfate, stained with proflavin and DAPI, concentrated onto 25-mm diameter 0.8- and 8-μm black polycarbonate filters (for nano- and microflagellates, respectively), and mounted on slides. Samples were digitally imaged at 630× (nano) or 200× (micro) using a Zeiss Axiovert 200 M inverted compound epifluorescence microscope. Images were processed with Image Pro software. Nano- and microheterotrophs were distinguished by the cell length (2–20 versus 20–200 μm) and lack of chloroplasts or significant red chlorophyll fluorescence. Details are described in an accompanying paper by Taylor *et al.* (Taylor *et al.*, 2012).

Chlorophyll *a* concentration

Chlorophyll *a* was measured by high-performance liquid chromatography (HPLC). Seawater volumes (2.2 or 4.4 L) were filtered onto Whatman GF/F filters, stored in liquid nitrogen, extracted in acetone and analyzed by HPLC (Goericke, 2002) and described by Taylor *et al.* (Taylor *et al.*, 2012).

Bacterial carbon production

The leucine incorporation method was used to estimate the rates of BCP. Samples (2 mL) were incubated with 20 nM of L-[4,5-^{3}H] leucine in the dark for 1 h at *in situ* temperature in triplicate with duplicate 5% TCA-killed controls (Kirchman *et al.*, 1985; Smith and Azam, 1992). Samples were then filtered on either 0.2-μm or 1-μm pore size polycarbonate filters (total or >1-μm BCP). Three successive additions of 1 mL 5% TCA were made and left without suction for 30 s. This approach was used in the response to measurements on a previous cruise and laboratory experiments that revealed anomalously wide-ranging values on filters when the sample was first fixed with formaldehyde or TCA. We assumed that negligible amounts of labeled proteins passed through the filter prior to TCA precipitation. Each filter was dried in a glass scintillation vial at room temperature. Onshore, EcoLite scintillation cocktail was added to each vial and analyzed in a Beckman LS6000A liquid scintillation counter. Conversion of leucine incorporation to estimate the carbon production rate was performed assuming 3.1 kg C mol^{-1} leucine (2× isotope dilution) and 24 h day^{-1} (Simon and Azam, 1989).

Organic and inorganic nutrients

Seawater samples (40 mL) from stations 1–9 were acidified with hydrochloric acid to pH∼2 for total organic carbon (TOC) and total nitrogen (TN) analyses on a Shimadzu 500 V-CSN/TNM-1 TOC. Quantification used seven-point C and N standard curves in conjunction with consensus reference material (RSMAS, University of Miami) interspersed between samples. The consensus reference material routinely measured values in the range 41 and 45 μM C. Filtration was not done prior to TOC determination to minimize contamination. Although particulate organic carbon (POC) values were available (below), the dissolved organic carbon (DOC) was not computed as the difference between the TOC and the POC because the determinations were made on different volumes (100 μL injections versus 2 L filtrations) and because the DOC was

typically higher than the POC by an order of magnitude. So, the TOC can be assumed to be mostly composed of the DOC. Total organic nitrogen (TON) concentrations, on the other hand, may be strongly influenced by particulate organic nitrogen (PON) as their values can be similar during phytoplankton bloom conditions.

Samples for analyses of ammonium (NH_4^+), nitrate (NO_3^-) and nitrite (NO_2^-) were taken from the same depths and Niskin bottles as those for TOC and TN. Nitrate concentrations determined during California Cooperative Oceanic Fisheries Investigations (CalCOFI) survey cruise 0810, located in the same area during 14 and 30 October 2008, were also used (below). Dissolved inorganic nitrogen (DIN; nitrate plus nitrite, in this case) must be subtracted from TN to calculate TON. In this study, TON concentrations were calculated for all depths <60 m. Below these depths DIN and TN were too similar to allow for accurate TON determination. Nitrate concentrations were available from the A-Front cruise. However, when nitrate and phosphate concentrations and ratios in water masses with similar densities were compared between A-Front and CalCOFI 0810 it was apparent that A-Front nitrate samples may have been compromised. Therefore, nitrate concentrations measured during CalCOFI 0810, in water masses with similar density and phosphate concentration characteristics to those sampled for TN during A-Front, were used to compute the TON. This assumed that phosphate concentrations did not change independently of nitrate in a particular water mass of the same density between the two cruises.

Two liters of seawater were filtered onto 25 mm precombusted (450°C, 6 h) Whatman GF/F filters for POC and PON determinations. Filters were exposed to concentrated HCl vapors to remove inorganic carbon, oven-dried overnight and one-half of each filter was analyzed for C and N at the Scripps Institution of Oceanography's Analytical Facility using a Costech Elemental Analyzer (Costech Analytical Technologies, Valencia, CA, USA) according to standard protocols.

Transparent particles

Following fixation with 2% formaldehyde (final), 20 mL seawater samples were filtered on 1-μm pore size polycarbonate membranes. With vacuum released, 500 μL of Alcian blue (0.2-μm filter-sterilized solution of 0.02% Alcian blue + 0.06% acetic acid in milli-Q water) was then added on the filter and allowed to stain for 30 s, after which vacuum was reapplied and the filter was dried at room temperature and stored at −20°C for analysis onshore (Alldredge *et al.*, 1993). In the laboratory, the filters were placed on 100 μL drops of 1× SYBR Gold, incubated for 15 min, then removed and allowed to fully dry on absorbent paper and mounted onto microscope slides using Resolve immersion oil (Richard Allan Scientific, Kalamazoo, MI, USA). Filter fluorescing particles (FFP) were counted at ×600 magnification on an Olympus BX51 epifluorescence microscope using wide field excitation centered at 470–490 nm with a long pass emission filter. Counts were made from 20 haphazardly selected fields on each slide, and the area of each particle was estimated using the ocular grid of the microscope (Samo *et al.*, 2008). Transparent exopolymer particles (TEP) were quantified on the same preparations using sub-stage illumination that was diffused through a Cytoclear slide (Sterlitech Corp, Kent, WA, USA) placed below the slide holding the mounted filter (Alldredge *et al.*, 1993; Samo *et al.*, 2008).

Contour and section plots

Data collected along the transect was heterogeneous and unevenly spaced in both the horizontal and vertical axes. The contouring and shading of the DIVA gridding algorithm in Ocean Data View was therefore used to create all section and contour plots (Schlitzer, 2008).

RESULTS

Distributions of chlorophyll *a* and bacterial abundance and biomass

The maximum chl *a* concentration among all stations and depths was found at ∼30 m from the frontal station 4, coinciding with the $\sigma_\theta = 24.75$ isopycnal (3.20 μg L^{-1}). Frontal station 5 also exhibited a chlorophyll maximum of 2.46 μg L^{-1} at the $\sigma_\theta = 24.75$ isopycnal (Fig. 1B). Integrated chlorophyll was maximal at stations 4 and 5, and station 5 also exhibited the highest integrated BCP (Table I). The nitracline, defined as the depth where nitrate concentration exceeds 1 μM, was located at 42 m at the southernmost station 1 in oligotrophic waters and shoaled to 21 m at the northernmost mesotrophic station 9 (Table I). The detailed depth profile data collected at the transect stations are provided in Supplementary data, Table S1.

Bacterial abundance in the southern, oligotrophic surface waters was typically 10^9 L^{-1}, decreasing to 10^8 cells L^{-1} below 40 m (Fig. 2A). The depth profile at the front was slightly different, with lower abundance at the surface and a greater variability in abundance with depth, which ranged from $\sim 5 \times 10^8$ to 10^9 cells L^{-1}.

Table I: Summary values of the nitracline depth and integrated stocks of chlorophyll, bacterial carbon, bacterial carbon production and calculated bacterial growth rate

Station	Latitude (°N)	Longitude (°W)	Nitracline depth (m)	Integrated chl a′	Integrated BC (mg C m^{-2})	Integrated BCP (mg C m^{-2} day^{-1})	Bacterial growth rate (day^{-1})
1	32.6667	120.7098	42	30.1	1770	153	0.0863
2	32.7018	120.7085	39	25.3	983		
3	32.7247	120.7075	31	33.9	1230	159	0.129
4	32.7498	120.7088	36	94.4	1420		
5	32.7762	120.7077	32	98.1	1520	698	0.459
6	32.8027	120.7097	28	66.3	2190		
7	32.8263	120.7097	29	56.4	2190	406	0.185
8	32.8515	120.7105	25	51.7	2560		
9	32.8965	120.7082	21	45.8	3240	301	0.0929

Depth integrated values were calculated from the surface to 100 m.

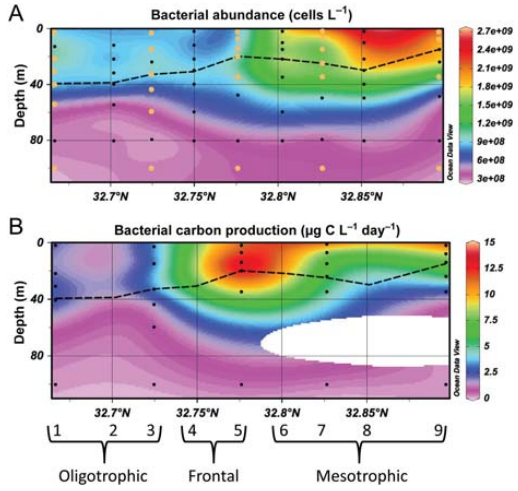

Fig. 2. Bacterial abundance (**A**) and bacterial production (**B**) along the A-Front transect. Stations are identified by numbers with water masses bracketed. Beige circles within each plot denote microscopy-based data when flow cytometry was used to augment the abundance and total carbon datasets. The dashed line denotes the depth of maximum chlorophyll concentrations.

Abundances in the northern, mesotrophic waters were substantially higher, ranging $1.50-2.25 \times 10^9$ cells L^{-1}. Comparison of the BCP and BC (Fig. 2B; Supplementary data, Fig. S2B) with chlorophyll (Fig. 1B) revealed these measurements to be effectively bounded by the depth of the chlorophyll maximum. The depth of maximum BCP at station 5 was coincident with the depth of maximum chlorophyll.

Cell-specific BC was highest at the southernmost (oligotrophic; 27 fg C $cell^{-1}$) and northernmost (mesotrophic; 28 fg C $cell^{-1}$) stations compared with adjacent stations (14–20 fg C $cell^{-1}$; Supplementary data, Fig. S2A), and a relatively high value was also found at the surface of the front (29 fg C $cell^{-1}$). Profiles of BC followed a pattern similar to cell abundance, with highest values at the northernmost station, and thus appeared to be driven by this parameter and not cell-specific carbon.

Bacterial carbon production

BCP strongly reflected the frontal boundary. Maxima of 11–13 µg C L^{-1} day^{-1} were measured from the surface to ~40 m at the front, with enhanced production shoaling to the surface on the northern, mesotrophic side (Fig. 2A). Bacterial production in southern, oligotrophic waters was low, averaging a quarter of that at the front (~3 µg C L^{-1} day^{-1}). These patterns were corroborated by nearly identical profiles of >1-µm fractionated carbon production values (data not shown) and the FDC at each depth, both of which exhibited shallow, subsurface maxima at the front (Supplementary data, Fig. S2C). Furthermore, growth rates calculated by dividing depth-integrated BCP by depth-integrated BC (e.g. Ducklow, 2000) exhibited the highest value (0.46 day^{-1}) at the front, decreasing to 0.1 day^{-1} north and south of the front (Table I).

Viral abundance and virus:bacteria ratios

Viral abundance at the surface of the front was $1.5-2 \times 10^{10}$ VLP L^{-1}, and decreased to 5×10^9 VLP L^{-1} <50 m (Supplementary data, Fig. S3A). The mesotrophic station showed a similar trend, but elevated viral abundance extended deeper than 30 m. The oligotrophic station exhibited viral abundances of $1-1.5 \times 10^{10}$ particles L^{-1} from the surface to a depth of 40 m.

Bacterial abundances at station 5 calculated from Anodisc filters using the BX51 Olympus microscope were not significantly different from those measured on

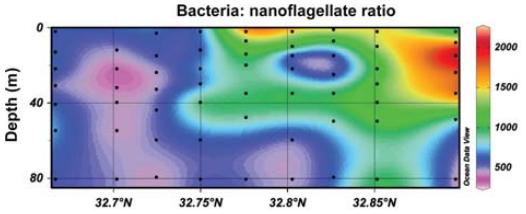

Fig. 3. Bacteria:nanoflagellate ratios across the front. In comparison with the oligotrophic and mesotrophic stations, frontal zone nanoflagellates were less abundant, thereby increasing the bacteria:nanoflagellate ratios.

polycarbonate filters using the Nikon TE2000-U microscope (Student's *t*-test, $P = 0.265$), and were therefore deemed appropriate for calculating virus:bacteria ratios. The highest virus:bacteria ratio of 23:1 was observed at the surface of the front, decreasing to 17:1 and then to 10:1 $<$20 m (Supplementary data, Fig. S3B).

Nano- and microflagellate abundance

Nanoflagellate abundances were evenly distributed from the surface to 40 m both south and north of the front. At the front, abundances were on the order of 4×10^5–1×10^6 L^{-1}, or ∼20–50% of those at the northern and southern adjacent stations (Supplementary data, Table S1). Bacteria:nanoflagellate ratios increased along the transect, 3- to 4-fold at the surface of the station 5 frontal zone and at 15 m in the northernmost station (Fig. 3). Microflagellate abundances generally increased from south (∼10^3 cells L^{-1}) to north (∼8×10^3 cells L^{-1}) and showed maxima at the mesotrophic stations from the surface to 30 m (Supplementary data, Table S1). Unlike nanoflagellates, microflagellate abundance did not decrease markedly at the front, but was more evenly distributed throughout the sampled water column.

Organic and inorganic nutrients

The TOC and POC concentrations were poorly correlated, and subsequent analyses and discussion are based on the premise that the TOC reflects the distribution of the DOC. Slightly higher TOC values at the front coincided with locations of highest BCP and chl *a* (Figs 1B and 2B). Maximal mean depth-integrated concentrations occurred at station 3, with depth-specific maxima from 0 to 20 m (Table II and Supplementary data, Fig. S4A). Station 8 had the highest mean depth-integrated and depth-specific TON, with high values also present at stations 3–6 throughout the water column. Depth-specific POC and PON were elevated at the front and highest at station 2. Mean depth-integrated values did not follow this trend and displayed highest values at station 2 (POC) and 6 (PON). Overall, the profiles were similar to *chl a*, indicating that these measurements reflected depth distribution of biomass concentrations. The DIN, POC/PON and TOC/TON data (Table II and Supplementary data, Table S2) are discussed below as they pertain to microbial activity.

Transparent particles

TEP and FFP differed in concentration and size along the transect (Supplementary data, Fig. S5 and Table S2). The maximal TEP concentration centered $<$40 m and south of the front. Concentrations of TEP at the front were enhanced relative to northern waters while FFP concentrations were highest at the surface in the oligotrophic and northernmost stations. Average areas of each particle size class were also distributed differently with depth, but showed some agreement at the surface of the front where FFP average areas decreased from ∼1000 to 200 μm^2 $<$20 m while maintaining high values northward into the mesotrophic waters.

DISCUSSION

We hypothesized that elevated nutrient fluxes associated with the A-Front (Li *et al.*, 2012) would elicit strong metabolic responses and enhanced primary production, and result in elevated heterotrophic activities, thus affecting carbon cycling at the meso- to submesoscale. The characteristics and responses of primary producers and heterotrophic bacteria highlighted the active and dynamic nature of this frontal zone. Depending on the magnitude of along isopycnal and frontal jet transport of these microbial communities and their biogeochemical influence on inorganic and organic nutrients, such sites may play an important role in nutrient cycling on larger spatial scales.

Bacterial responses at the front

A striking observation was the enhanced rate of depth-integrated and depth-specific BCP at the front (Table I and Fig. 2B). Maximal BCP of ∼13 μg C L^{-1} day^{-1} at 15 m indicated increased bioavailability of DOM and essential nutrients. The range of BCP estimates at the A-Front was within the range of previous measurements in the Southern California Bight region of the CCE (0.28–14 μg C L^{-1} day^{-1}; Fuhrman *et al.*, 1985, assuming 20 fg C cell^{-1} and 1.18×10^{18} cells mol^{-1} TdR;

Table II: Mean depth integrated values of organic carbon, organic nitrogen and ratios along the A-Front transect

Station	Latitude (°N)	Longitude (°W)	Depth of integration (m)	Mean integrated TOC (mg m^{-2})	Mean integrated TON (mg m^{-2})	Mean integrated POC (mg m^{-2})	Mean integrated PON (mg m^{-2})	Mean integrated TOC:TON	Mean integrated POC:PON
1	32.6667	120.7098	41	7900	530	798	120	14.9	6.64
2	32.7018	120.7085	39	7430	502	1530	239	14.8	6.43
3	32.7247	120.7075	44	9160	617	975	148	14.9	6.61
4	32.7498	120.7088	40	7920	628	1360	241	12.6	5.65
5	32.7762	120.7077	35	6820	607	1050	254	11.2	4.14
6	32.8027	120.7097	35	6370	605	1210	270	10.5	4.48
7	32.8263	120.7097	35	6050	577	1290	266	10.5	4.84
8	32.8515	120.7105	40	7490	763	1120	238	9.81	4.72
9	32.8965	120.7082	35	5790	541	961	188	10.7	5.12

TOC, total organic carbon; TON, total organic nitrogen; POC, particulate organic carbon; PON, particulate organic nitrogen.

Simon *et al.*, 1990, assuming 3.1 kg C mol^{-1} Leu), and within the range of seasonally estimated rates in the Arabian Sea (0.50–15.0 μg C L^{-1} day^{-1}; Ducklow *et al.*, 2001, assuming 3.1 kg C mol^{-1} Leu). They were greater than those measured in the Santa Monica Basin (~2.0 μg C L^{-1} day^{-1}; Cho and Azam, 1988, assuming 20 fg C cell^{-1} and 1.18×10^{18} cells mol^{-1} TdR), and the North Atlantic (0.50–10.0 μg C L^{-1} day^{-1}; Hoppe *et al.*, 2002, assuming 3.1 kg C mol^{-1} Leu), yet lower than peak values in the South Atlantic Ocean (0.94–16.6 μg C L^{-1} day^{-1}; Hoppe *et al.*, 2002, assuming 3.1 kg C mol^{-1} Leu).

The enhanced depth-integrated bacterial growth rates, high FDC, high chl *a* concentration and the significant correlation between BCP and chl *a* ($R^2 = 0.622$, $P < 0.0001$) at the front suggest that this oceanographic feature supported enhanced bacterial growth. These results are in agreement with previous work noting the positive correlation between chl *a* (and/or primary production) and heterotrophic bacterial activity and growth rates in aquatic systems (Cole *et al.*, 1988). Bacteria–phytoplankton interactions are facilitated by the release of labile DOM from phytoplankton (Mague *et al.*, 1980). Heterotrophic bacteria rapidly metabolize labile organic matter (Kirchman *et al.*, 1991), causing nutrient remineralization, as we saw at station 5 (frontal) at 100 m where BCP was 1.4–2.6 times greater than either the oligotrophic and mesotrophic stations at 100 m. Thus, microbial activity within the frontal zone likely exerted substantial influence on elemental cycling within and below the euphotic zone of the CCE.

POC and PON were highest at the front (Supplementary data, Fig. S4C and D). These measurements reflected localized high phytoplankton biomass and underscored the uniqueness of the A-Front as a region within the CCE where bloom conditions were closely flanked by less productive waters. However, TOC was, in fact, lower at the A-Front relative to adjacent oligotrophic waters (Table II and Supplementary data, Fig. S4A). Thermal stratification can lead to the accumulation of semi-labile and refractory DOM with reduced influx of inorganic nutrients, which limits bacterial processing of DOC in warm, oligotrophic waters (Hansell and Waterhouse, 1997). The TOC was negatively correlated with density ($R^2 = 0.832$) in our study region. However, at the lowest densities, TOC concentrations were higher than predicted by simple physical mixing. This observation is consistent with greater accumulation of semi-labile TOC in warm surface water south of the front. Additionally, reduced DOC consumption by heterotrophic bacteria due to grazing or insufficient nutrients can result in an accumulation of DOC (Thingstad *et al.*, 1997). Enhanced carbon-rich POM at the southern stations, seen as high POC/PON signatures (>6.6: Supplementary data, Table S2) (Redfield *et al.*, 1963), suggests preferential degradation of nitrogenous organic matter in the oligotrophic system (Kähler and Koeve, 2001).

We note that the TOC/TON was in agreement with other values for the North Pacific Ocean—between 13 and 20 (Supplementary data, Table S2) (Hansell and Waterhouse, 1997; Libby and Wheeler, 1997; Ogawa and Tanoue, 2003). The marginal differences were confined to each water mass, i.e. the southern oligotrophic (stations 1–3), the front and adjacent depths (stations 4–6) and the northern mesotrophic (stations 7–9). The lower TOC/TON and POC/PON at the front and adjacent stations suggested inputs of organic nitrogen while high TOC/TON in the northern and southern stations pointed to the removal of organic nitrogen (including PON), possibly through microbial regeneration and/or metazoan grazing (Table II) (Hansell and Waterhouse, 1997; Ogawa *et al.*, 1999).

Microbial loop dynamics in relation to hydrographic and biotic factors

High bacterial activity at the front is consistent with a heterotrophic community actively influencing carbon and nitrogen cycles and may involve complex interplay between hydrography of the frontal zone and top-down population controls of viral lysis and protist grazing pressure (Hagström *et al.*, 1988; Bratbak *et al.*, 1990). The observation of larger bacteria at the front could be explained by a higher abundance of bacterial phylotype(s) of a larger size (Morán and Calvo-Díaz, 2009; McCarren *et al.*, 2010). However, this observation could also be due to abundant viral particles within the cells and/or to rapid uptake and incorporation of labile viral lysate into the biomass (Parada *et al.*, 2006; Malits and Weinbauer, 2009). Virus:bacteria ratios were high in surface samples at the front and the oligotrophic station, but lower at the depth in the mesotrophic station and with depth in the front. Positive deviations from the canonical 10:1 ratio suggest enhanced viral-mediated bacterial mortality in the bulk seawater and/or at the micrometer scale (Seymour *et al.*, 2006; Suttle, 2007; Yang *et al.*, 2010).

Nano- and microflagellate abundance patterns also varied between the different water masses. Low abundance and high cell-specific BC observed at the front may reflect grazing by protists (Andersson *et al.*, 1986). Direct interception feeding by heterotrophic nanoflagellates is size-selective and can disproportionately remove larger bacteria (Monger and Landry, 1991, 1992). The high relative abundance of large bacteria at the front may therefore suggest a different balance between bacterial growth and removal processes. As noted above, A-Front was characterized by elevated organic matter, bacterial growth rates and bacterial biomass production. Low heterotrophic nanoflagellate abundance at the front is consistent with large, fast-growing bacterial cells within the front likely experiencing a low grazing impact. Compared with typical bacteria:nanoflagellate ratios of 1000:1 (Sanders *et al.*, 1992), higher ratios (~2000) at the surface of the front and at mesotrophic stations further support a reduced nanoflagellate grazing impact on bacteria (Fig. 3). As a major predator of nanoflagellates, microflagellates may have been responsible for maintaining reduced nanoflagellate abundance as our data show maximal heterotrophic nanoflagellate abundance coinciding with the lowest microflagellate abundance in mesotrophic waters (Supplementary data, Table S1). Greater mesozooplankton and copepod nauplii biomass at the front may have been an additional source of nanoflagellate mortality (Ohman *et al.*, 2012).

To compensate for the absence of grazing rate measurements and to test the above predictions, $\log_{10}$ transformed nanoflagellate abundance versus $\log_{10}$ transformed bacterial abundance was plotted and analyzed using the framework of maximum attainable abundance (MAA) and mean realized abundance (MRA) of nanoflagellates (Gasol, 1994) (Figs 4). Data points that lie near or above the MAA line suggest bottom-up control of nanoflagellate populations (in this case by bacterial prey) while points on or below the MRA line suggest top-down

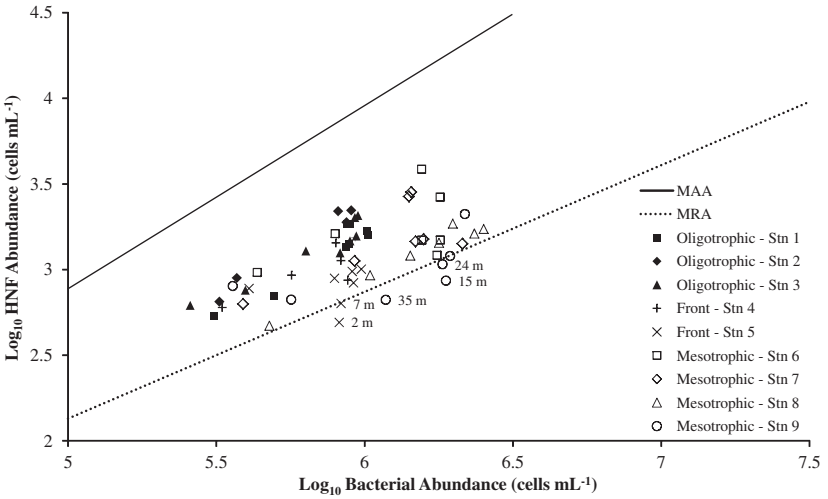

Fig. 4. $\log_{10}$ transformed heterotrophic nanoflagellate (HNF) versus $\log_{10}$ transformed bacterial abundance for all stations and depths. The solid line is the maximum attainable abundance (MAA) and the dotted line is the mean realized abundance (MRA).

forcing by nanoflagellate predators (such as microflagellates). Bottom-up control of nanoflagellates by bacterial availability was not significant. However, top-down control was apparent for the frontal and mesotrophic stations. While surface data for stations 6 and 7 were on the MRA line, stations 5 and 9 with depths of 2 and 7 m and 15, 24 and 35 m, respectively, were below the MRA line and thus likely exhibited significant predation of nanoflagellates. Collectively, these observations support the proposed mechanism at the front whereby increased grazing by microflagellates upon nanoflagellate bacteriovores led to a bacterial population comprised of fast-growing, larger cells predominantly regulated by viral lysis. Through viral lysis, bacterial cell abundance is decreased while the cell lysates could fuel elevated bacterial production through rapid and tightly coupled cycling of labile organic matter (Fuhrman, 1999).

Potential role of transparent particles

We considered the patterns of transparent particles and their capacity as microenvironments to identify their contribution to nutrient cycling and carbon export to the mesopelagic. The size and concentration profiles suggest potential roles of the microbial communities in particle formation and degradation. The maxima of TEP and FFP concentrations were not accompanied by average particle size maxima at any depth (Supplementary data, Fig. S5). This was unexpected, particularly at the front, where FFP concentrations were among the lowest measured while TEP concentration was elevated in comparison with the mesotrophic stations (Supplementary data, Fig. S5A and C). Interestingly, the depth at the front that exhibited maximal FFP average area and slightly elevated TEP average area also had the largest bacterial cell sizes (Supplementary data, Fig. S5B and D). We did not constrain the mechanisms underlying these observations, but they may include varied POM-colloid-DOM transformations involving viral, bacterial and abiotic processes.

Potential influences of frontal hydrodynamics on biogeochemistry in the CCE

The spatial stability of the A-Front was demonstrated by several transects with a moving vessel profiler that showed enhanced chl *a* concentrations and particulate biovolume at the frontal zone east of the transect (Ohman *et al.*, 2012) as well as satellite data depicting the frontal stability of the SST and chl *a* for 3 weeks prior to the transect (Kahru *et al.*, 2012). The eastward velocity along the frontal jet approached $0.3\ m\ s^{-1}$ (Li *et al.*, 2012), and was thus capable of rapidly advecting plankton tens of kilometers within a few days. As a result, enhanced biological production along the frontal zone likely had biogeochemical consequences for adjacent regions within the CCE despite being spatially confined. The timescales of transport are also relevant for constraining and characterizing the growth responses of the microbial community and the formation and removal of non-living carbon (DOM, POM and transparent particles). Front-induced enhancement of the autochthonous biomass and particles was also evident in the higher photosynthetic potential of phytoplankton (Chekalyuk *et al.*, 2012) mediated by elevated diapycnal nitrate fluxes (Li *et al.*, 2012). If the present observations can be extrapolated to other frontal zones in the CCE, these features may be important environments where physically driven nutrient inputs upshift trophic interactions and biogeochemical cycling.

Formed at the interface of oligotrophic and mesotrophic water masses in the CCE, the A-Front was an enhanced microhabitat of high photosynthetic biomass, dynamic formation and removal of dissolved and particulate organic matter, elevated substrate processing and uptake activity by heterotrophic bacteria, and atypical relative abundances of viral, flagellate and zooplankton mortality agents. Although the scales of physical perturbations in the frontal zones are relatively small, such microbially mediated responses may, in the aggregate, affect carbon cycling and export processes on larger scales.

SUPPLEMENTARY DATA

Supplementary data can be found online at http://plankt.oxfordjournals.org.

ACKNOWLEDGEMENTS

We thank the participants of the CCE-LTER and the captain and the crew of the RV Melville. The questions, insights and suggestions of two anonymous reviewers also contributed significantly to the manuscript and the authors are very appreciative of their careful observations and feedback.

FUNDING

This work was supported by U.S. National Science Foundation grants OCE 04–17616 and 10-26607 for

the CCE-LTER Program; OCE-0548275 to L.I.A.; and by a grant from the Gordon and Betty Moore Foundation Marine Microbiology Initiative to F.A.

REFERENCES

Alldredge, A. L., Passow, U. and Logan, B. E. (1993) The abundance and significance of a class of large, transparent organic particles in the ocean. *Deep-Sea Res. I*, **40**, 1131–1140.

Aluwihare, L. I. and Repeta, D. J. (1999) A comparison of the chemical characteristics of oceanic DOM and extracellular DOM produced by marine algae. *Mar. Ecol. Prog. Ser.*, **186**, 105–117.

Andersson, A., Larsson, U. and Hagström, Å. (1986) Size-selective grazing by a microflagellate on pelagic bacteria. *Mar. Ecol. Prog Ser.*, **33**, 51–57.

Azam, F., Fenchel, T., Field, J. G. *et al.* (1983) The ecological role of water-column microbes in the sea. *Mar. Ecol. Prog Ser.*, **10**, 257–263.

Azam, F. and Malfatti, F. (2007) Microbial structuring of marine ecosystems. *Nat. Rev. Microbiol.*, **5**, 782–791.

Bratbak, G. (1985) Bacterial biovolume and biomass estimations. *Appl. Environ. Microbiol.*, **49**, 1488–1493.

Bratbak, G., Heldal, M., Norland, S. *et al.* (1990) Viruses as partners in spring bloom microbial trophodynamics. *Appl. Environ. Microbiol.*, **56**, 1400–1405.

Bray, N. A., Keyes, A. and Morawitz, W. M. L. (1999) The california current system in the southern California bight and the Santa Barbara Channel. *J. Geophys. Res.*, **104**, 7695–7714.

Brussaard, C. P. D. (2004) Optimization of procedures for counting viruses by flow cytometry. *Appl. Environ. Microbiol.*, **70**, 1506–1513.

Chekalyuk, A., Landry, M. R., Goericke, R. *et al.* (2012) Laser fluorescence analysis of phytoplankton across a frontal zone in the California Current ecosystem. *J. Plank. Res.*, **34**, 761–777.

Cho, B. C. and Azam, F. (1988) Major role of bacteria in biogeochemical fluxes in the oceans interior. *Nature*, **332**, 441–443.

Claustre, H., Kerhervé, P., Marty, J. C. *et al.* (1994) Phytoplankton dynamics associated with a geostrophic front: ecological and biogeochemical implications. *J. Mar. Res.*, **52**, 711–742.

Cole, J. J., Findlay, S. and Pace, M. L. (1988) Bacterial production in fresh and saltwater ecosystems: a cross-system overview. *Mar. Ecol. Prog Ser.*, **43**, 1–10.

Del Giorgio, P. A. and Cole, J. J. (1998) Bacterial growth efficiency in natural aquatic systems. *Annu. Rev. Ecol. Syst.*, **29**, 503–541.

Ducklow, H. W. (2000) Bacterial production and biomass in the oceans. In Kirchman, D. L. (ed.), *Microbial Ecology of the Oceans*. 1st edn. Wiley-Blackwell, Hoboken, New Jersey, USA, pp. 85–120.

Ducklow, H. W. and Hill, S. M. (1985) Tritiated-thymidine incorporation and the growth of heterotrophic bacteria in warm core rings. *Limnol. Oceanogr.*, **30**, 260–272.

Ducklow, H. W., Smith, D. C., Campbell, L. *et al.* (2001) Heterotrophic bacterioplankton in the Arabian Sea: Basinwide response to yearround high primary productivity. *Deep-Sea Res. II*, **48**, 1303–1323.

Ewart, C. S., Meyers, M. K., Wallner, E. R. *et al.* (2008) Microbial dynamics in cyclonic and anticyclonic mode-water eddies in the northwestern Sargasso Sea. *Deep-Sea Res. II*, **55**, 1334–1347.

Falkowski, P. G., Ziemann, D., Kolber, Z. *et al.* (1991) Role of eddy pumping in enhancing primary production in the ocean. *Nature*, **352**, 55–58.

Fernández, M., Bianchi, M. and Vanwambeke, F. (1994) Bacterial biomass, heterotrophic production and utilization of dissolved organic matter photosynthetically produced in the Almeria-Oran front. *J. Mar. Syst.*, **5**, 313–325.

Fiala, M., Sournia, A., Claustre, H. *et al.* (1994) Gradients of phytoplankton abundance, composition and photosynthetic pigments across the Almeria-Oran front (SW Mediterranean Sea). *J. Mar. Syst.*, **5**, 223–233.

Franks, P. J. S. (1992) Sink or swim: accumulation of biomass at fronts. *Mar. Ecol. Prog Ser.*, **82**, 1–12.

Fuhrman, J. A. (1999) Marine viruses and their biogeochemical and ecological effects. *Nature*, **399**, 541–548.

Fuhrman, J. A., Eppley, R. W., Hagstrom, A. *et al.* (1985) Diel variations in bacterioplankton, phytoplankton, and related parameters in the Southern California Bight. *Mar. Ecol. Prog Ser.*, **27**, 9–20.

Gasol, J. M. (1994) A framework for the assessment of top-down vs bottom-up control of heterotrophic nanoflagellate abundance. *Mar. Ecol. Prog Ser.*, **113**, 291–300.

Goericke, R. (2002) Top-down control of phytoplankton biomass and community structure in the monsoonal Arabian Sea. *Limnol. Oceanogr.*, **47**, 1307–1323.

Hagström, Å., Ammerman, J. W., Henrichs, S. *et al.* (1984) Bacterioplankton growth in seawater: 2. Organic matter utilization during steady-state growth in seawater cultures. *Mar. Ecol. Prog Ser.*, **18**, 41–48.

Hagström, Å., Azam, F., Andersson, A. *et al.* (1988) Microbial loop in an oligotrophic pelagic marine ecosystem: possible roles of cyanobacteria and nanoflagellates in the organic fluxes. *Mar. Ecol. Prog Ser.*, **49**, 171–178.

Hagström, Å., Larsson, U., H?rstedt, P. *et al.* (1979) Frequency of dividing cells, a new approach to the determination of bacterial growth rates in aquatic environments. *Appl. Environ. Microbiol.*, **37**, 805–812.

Hansell, D. A. and Waterhouse, T. Y. (1997) Controls on the distributions of organic carbon and nitrogen in the eastern Pacific Ocean. *Deep-Sea Res. I*, **44**, 843–857.

Heinänen, A., Kononen, K., Kuosa, H. *et al.* (1995) Bacterioplankton growth associated with physical fronts during a cyanobacterial bloom. *Mar. Ecol. Prog Ser.*, **116**, 233–245.

Hoppe, H. G., Gocke, K., Koppe, R. *et al.* (2002) Bacterial growth and primary production along a north-south transect of the Atlantic Ocean. *Nature*, **416**, 168–171.

Kähler, P. and Koeve, W. (2001) Marine dissolved organic matter: can its C : N ratio explain carbon overconsumption? *Deep-Sea Res. I*, **48**, 49–62.

Kahru, M., Di Lorenzo, E., Manzano-Sarabia, M. *et al.* (2012) Spatial and temporal statistics of surface temperature and chlorophyll fronts in the California Current. *J. Plank. Res.*, **34**, 749–760.

Karl, D. M., Hebel, D. V., Bjorkman, K. *et al.* (1998) The role of dissolved organic matter release in the productivity of the oligotrophic North Pacific Ocean. *Limnol. Oceanogr.*, **43**, 1270–1286.

Kirchman, D., K'nees, E. and Hodson, R. (1985) Leucine incorporation and its potential as a measure of protein synthesis by bacteria in natural aquatic systems. *Appl. Environ. Microbiol.*, **49**, 599–607.

Kirchman, D. L., Suzuki, Y., Garside, C. *et al.* (1991) High turnover rates of dissolved organic carbon during a spring phytoplankton bloom. *Nature*, **352**, 612–614.

Landry, M. R., Ohman, M. D., Goericke, R. *et al.* (2012) Pelagic community responses to a deep-water front in the California Current Ecosystem: overview of the A-Front Study. *J. Plank. Res.*, **34**, 739–748.

Li, Q. P., Franks, P. J. S., Ohman, M. D. *et al.* (2012) Enhanced nitrate fluxes and biological processes at a frontal zone in the Southern California Current System. *J. Plank. Res.*, **34**, 790–801.

Libby, P. S. and Wheeler, P. A. (1997) Particulate and dissolved organic nitrogen in the central and eastern equatorial Pacific. *Deep-Sea Res. I*, **44**, 345–361.

Mague, T. H., Friberg, E., Hughes, D. J. *et al.* (1980) Extracellular release of carbon by marine phytoplankton; a physiological approach. *Limnol. Oceanogr.*, **25**, 262–279.

Malfatti, F., Samo, T. J. and Azam, F. (2010) High-resolution imaging of pelagic bacteria by Atomic Force Microscopy and implications for carbon cycling. *ISME J.*, **4**, 427–439.

Malits, A. and Weinbauer, M. G. (2009) Effect of turbulence and viruses on prokaryotic cell size, production and diversity. *Aquat. Microb. Ecol.*, **54**, 243–254.

Martin, J. H., Coale, K. H., Johnson, K. S. *et al.* (1994) Testing the iron hypothesis in ecosystems of the equatorial Pacific Ocean. *Nature*, **371**, 123–129.

Mccarren, J., Becker, J. W., Repeta, D. J. *et al.* (2010) Microbial community transcriptomes reveal microbes and metabolic pathways associated with dissolved organic matter turnover in the sea. *Proc. Natl. Acad. Sci. U. S. A.*, **107**, 16420–16427.

Monger, B. C. and Landry, M. R. (1991) Prey-size dependency of grazing by free-living marine flagellates. *Mar. Ecol. Prog Ser.*, **74**, 239–248.

Monger, B. C. and Landry, M. R. (1992) Size-selective grazing by heterotrophic nanoflagellates: an analysis using live-stained bacteria and dual-beam flow cytometry. *Adv. Limnol.*, **37**, 173–185.

Monger, B. C. and Landry, M. R. (1993) Flow cytometric analysis of marine bacteria with Hoechst 33342. *Appl. Environ. Microbiol.*, **59**, 905–911.

Morán, X. A. G. and Calvo-Díaz, A. (2009) Single-cell vs. bulk activity properties of coastal bacterioplankton over an annual cycle in a temperate ecosystem. *FEMS Microbiol. Ecol.*, **67**, 43–56.

Morán, X. A. G., Taupier-Letage, I., Vázquez-Domínguez, E. *et al.* (2001) Physical-biological coupling in the Algerian Basin (SW Mediterranean): influence of mesoscale instabilities on the biomass and production of phytoplankton and bacterioplankton. *Deep-Sea Res. I*, **48**, 405–437.

Ogawa, H., Fukuda, R. and Koike, I. (1999) Vertical distributions of dissolved organic carbon and nitrogen in the Southern Ocean. *Deep-Sea Res. I*, **46**, 1809–1826.

Ogawa, H. and Tanoue, E. (2003) Dissolved organic matter in oceanic waters. *J. Oceanogr.*, **59**, 129–147.

Ohman, M. D., Powell, J., Picheral, M. *et al.* (2012) Mesozooplankton and particulate matter responses to a deep-water frontal system in the southern California Current System. *J. Plank. Res.*, **34**, 815–827.

Pallàs-Sanz, E., Johnston, T. M. S. and Rudnick, D. L. (2010) Frontal dynamics in a California Current system shallow front: 1. Frontal processes and tracer structure. *J. Geophys. Res.*, **115**, 14.

Parada, V., Herndl, G. J. and Weinbauer, M. G. (2006) Viral burst size of heterotrophic prokaryotes in aquatic systems. *J. Mar. Biol. Assoc. U.K.*, **86**, 613–621.

Patel, A., Noble, R. T., Steele, J. A. *et al.* (2007) Virus and prokaryote enumeration from planktonic aquatic environments by epifluorescence microscopy with SYBR Green I. *Nat. Protoc.*, **2**, 269–276.

Peinert, R. and Miquel, J. C. (1994) The significance of frontal processes for vertical particle fluxes: a case study in the Alboran Sea (SW Mediterranean Sea). *J. Mar. Syst.*, **5**, 377–389.

Prieur, L. and Sournia, A. (1994) Almofront-1 (April-May 1991): an interdisciplinary study of the Almeria-Oran geostrophic front, SW Mediterranean Sea. *J. Mar. Syst.*, **5**, 187–203.

Raven, J. A. and Falkowski, P. G. (1999) Oceanic sinks for atmospheric CO_2. *Plant Cell Environ.*, **22**, 741–755.

Redfield, A. C., Ketchum, B. H. and Richards, F. A. (1963) The influence of organisms on the composition of seawater. In Hill, M. N. (ed.), *The Sea.* Vol. 2. Wiley, New York, pp. 26–77.

Riemann, L., Nielsen, T. G., Kragh, T. *et al.* (2011) Distribution and production of plankton communities in the subtropical convergence zone of the Sargasso Sea. I. Phytoplankton and bacterioplankton. *Mar. Ecol. Prog Ser.*, **426**, 57–70.

Rykaczewski, R. R. and Checkley, D. M. (2008) Influence of ocean winds on the pelagic ecosystem in, upwelling regions. *Proc. Natl. Acad. Sci. U. S. A.*, **105**, 1965–1970.

Samo, T. J., Malfatti, F. and Azam, F. (2008) A new class of transparent organic particles in seawater visualized by a novel fluorescence approach. *Aquat. Microb. Ecol.*, **53**, 307–321.

Sanders, R. W., Caron, D. A. and Berninger, U. G. (1992) Relationships between bacteria and heterotrophic nanoplankton in marine and fresh waters: an inter-ecosystem comparison. *Mar. Ecol. Prog Ser.*, **86**, 1–14.

Schlitzer, R. (2008) Ocean Data View, version 4.5.0. http://odv.awi.de/.

Sempéré, R., Dafner, E., Van Wambeke, F. *et al.* (2003) Distribution and cycling of total organic carbon across the Almeria-Oran Front in the Mediterranean Sea: Implications for carbon cycling in the western basin. *J. Geophys. Res.*, **108**, 11.

Seymour, J. R., Seuront, L., Doubell, M. *et al.* (2006) Microscale patchiness of virioplankton. *J. Mar. Biol. Assoc. U.K.*, **86**, 551–561.

Simon, M., Alldredge, A. L. and Azam, F. (1990) Bacterial carbon dynamics on marine snow. *Mar. Ecol. Prog Ser.*, **65**, 205–211.

Simon, M. and Azam, F. (1989) Protein content and protein synthesis rates of planktonic marine bacteria. *Mar. Ecol. Prog Ser.*, **51**, 201–213.

Smith, D. C. and Azam, F. (1992) A simple, economical method for measuring bacterial protein synthesis rates in seawater using 3H-leucine. *Mar. Microb. Food Webs*, **6**, 107–114.

Suttle, C. A. (2007) Marine viruses: major players in the global ecosystem. *Nat. Rev. Microbiol.*, **5**, 801–812.

Taylor, A. G., Goericke, R., Landry, M. R. *et al.* (2012) Sharp gradients in phytoplankton community structure across a frontal zone in the California Current Ecosystem. *J. Plank. Res.*, **34**, 778–789.

Thingstad, T. F., Hagstrom, A. and Rassoulzadegan, F. (1997) Accumulation of degradable DOC in surface waters: is it caused by a malfunctioning microbial loop? *Limnol. Oceanogr.*, **42**, 398–404.

Van Wambeke, F., Lefèvre, D., Prieur, L. *et al.* (2004) Distribution of microbial biomass, production, respiration, dissolved organic

carbon and factors controlling bacterial production across a geostrophic front (Almeria-Oran, SW Mediterranean Sea). *Mar. Ecol.-Prog. Ser.*, **269**, 1–15.

Videau, C., Sournia, A., Prieur, L. *et al.* (1994) Phytoplankton and primary production characteristics at selected sites in the geostrophic Almeria-Oran front system (SW Mediterranean Sea). *J. Mar. Syst.*, **5**, 235–250.

Yang, Y. H., Motegi, C., Yokokawa, T. *et al.* (2010) Large-scale distribution patterns of virioplankton in the upper ocean. *Aquat. Microb. Ecol.*, **60**, 233–246.

CHAPTER 4

Rates of single-cell growth, protein, and carbon production rates in natural marine bacterial populations using the methionine analog homopropargylglycine

Rates of single-cell growth, protein, and carbon production rates in natural marine bacterial populations using the methionine analog homopropargylglycine

Ty J. Samo, Steven P. Smriga, Francesca Malfatti, Farooq Azam

Scripps Institution of Oceanography, University of California San Diego, 9500 Gilman Dr., La Jolla, CA 92093-0202

Abstract

The application of copper(I)-catalyzed cycloaddition, or "click", chemistry to biological and biochemical research has recently become a simple and powerful method for probing the synthesis and turnover of macromolecules in model metazoans and *Escherichia coli*. This technique was applied to natural and laboratory samples of heterotrophic marine bacteria in order to microscopically observe active cells and subsequently measure and compare single cell protein synthesis and growth rates. Following incubation with the methionine bioortholog homopropargylglycine (HPG), click processing revealed labeled cells exhibiting wide ranging signal intensities. Comparisons of these labeled cells to microautoradiography using ^{35}S-methionine showed nearly identical labeling percentages, which were corroborated by competitive inhibition of ^{35}S-methionine in natural seawater by HPG. Seawater samples collected at Scripps Pier from November 2009 – October 2011 showed labeling percentages of 15 – 100%, demonstrating the sensitivity of the protocol. A conversion factor enabled the estimation of protein synthesis rates from the signal intensity of each cell, and provided average values of ~1.5 – 12 fg cell^{-1} d^{-1}. The average rates of the top 10% and bottom 90% of cells ranged from ~8.5 – 51 fg cell^{-1} d^{-1} and ~0.78 – 9.0 fg cell^{-1} d^{-1}, respectively,

and represented the contribution of the most active and less active members of the community. Frequency distribution plots of activities arranged in 0.05 fg bins followed power law functions, and were subsequently used as comparative metabolic signatures for each of the sampling dates. This method and its application reveal a previously unknown range of production rates in a substantial fraction of slow growing natural marine bacterial populations previously considered inactive, and represents an approach to quantitatively and more adequately address questions on growth regulation and biogeochemical contributions of these consortia. Overall, click chemistry will be useful in studying the mechanistic responses of heterotrophic bacteria to an assortment of physical, chemical, and biological variables.

Introduction

Marine bacteria and archaea communities significantly affect global ocean biogeochemical cycles through their metabolism and growth reflecting their adaptive biology and response to ecosystem conditions and perturbations in their (micro-) environments. It has now been well established that the pelagic environment offers variety of microhabitats within an organic matter continuum to a bacterium. Seawater contains a great variety and abundance of gels and particles that create a dynamic architecture and surfaces presumably varying in their chemical and physical attributes. Adaptive response (particularly growth) of individual bacteria to these microhabitats will help understand the environmental regulation of bacteria on biogeochemical activities. It should also help test hypotheses on the significance of microscale heterogeneity for the maintenance of bacterial diversity in the ocean.

Previous studies have shown microscale variation in bacterial community composition and activity (Long & Azam 2001b, Barbara & Mitchell 2003, Seymour et al. 2005). The challenge is to now develop highly sensitive and quantitative methods for individual based biogeochemistry. The eventual goal is "see" bacterial activity in its 3D microenvironment. This is currently not feasible due to technical constraints. Individual cell growth is currently studied by ^{3}H-based microautoradiography (Fuhrman & Azam 1982) and the use of a non-radioisotopic, fluorescence-based method using the thymidine analog bromodeoxyuridine (BrdU; Hamasaki et al. 2004). Microautoradiography is a powerful technique and has been extensively used for decades. However, it is difficult to quantify the incorporation. Also, it is a slow and tedious process. Further, it is desirable not to have to use radioisotopes for health and regulatory considerations. The BrdU method overcomes some of the difficulties of ^{3}H-thymidine microautoradiography method, and has been adapted and used for individual cell growth measurements (Tada et al. 2010).

We have now taken advantage of an exciting recent development of the potential of copper catalyzed azide-alkyne cycloaddition ("click") chemistry (Best 2009; below) for measuring protein synthesis rates of individual bacteria. It is a fluorescence-based method that is highly sensitive and easy to use, and may help address hypotheses on marine bacterial ecology not previously accessible. An additional advantage is that the method uses fluorophores bound to a small molecule (compared with the BrdU method that uses a BrdU monoclonal antibody), so it is not necessary to permeabilize the cells.

The reaction is simply a conjugation of an azide to an alkyne group in the presence of copper (I) via the formation of a stable triazole (Rostovtsev et al. 2002,

Tornoe et al. 2002). The target organism(s) is incubated with azide- or alkyne-functionalized analogs. These bioorthogonal molecules are structurally similar to various organic monomers such as thymidine or, in this paper, methionine. Following appropriate washing and fixation, the sample is incubated with copper (II), an appropriate ligand, a reducing agent, a buffer, and a fluorophore (linked to either an alkyne to react with the azide of the incorporated analog, or vice versa) to fluorescently label the analog (Beatty et al. 2005, Salic & Mitchison 2008). The technique allows rapid sample processing. Labeled cell fluorescence intensity can be quantified using an epifluorescence microscope and a CCD camera, enabling the photon flux from the fluorophore covalently bound to the analog to be measured. The spectrum of 1000s of individual cell activities can then be compared within a sample as well as among samples, and provides observations on the distribution of metabolisms within a natural community or in response to experimental perturbations.

We have employed click chemistry to measure protein synthesis in natural microbial assemblages. Of immediate interest is visualizing and quantifying HPG incorporation for single-cell based estimates of protein synthesis rates in marine bacteria. This technique complements our recent study of nucleic acid incorporation quantified via click reactions (Smriga et al., in preparation) and may allow simultaneous interrogations of per cell DNA and protein synthesis. Importantly, with this method it is possible to visualize cell-cell and cell-organic matter interactions and quantify the importance of cell sizes, lifestyles, microhabitats and associations. By measuring cell volume-based carbon content and signal intensity-based carbon production, individual cell growth rates can be

measured. It has the potential to yield bulk bacterial production as well. Further development of the method may assist studies of carbon flow in the microbial loop.

Materials & methods

Field locations and collection

Seawater was collected from a variety of sites representing bacteria from different ocean ecosystems. Preliminary experiments were conducted with water obtained off Scripps Pier (32° 52.02' N, 117° 15.43' W). As part of the Southern California Coastal Ocean Observing System (SCCOOS; www.sccoos.org), temperature, salinity, as well as fluorometry-based and extracted chlorophyll measurements are routinely measured.

Incubation and sample processing

Working solutions of the methionine analog L-homopropargylglycine (HPG; Fig. 1) were prepared in DMSO at 20 – 2000 μM final concentration. Incubations were performed with 1, 2, 10, 20, or 2000 nM HPG for 15 min to 7 h. Field samples were incubated at *in situ* temperature and protected from light. Experiments with bacterial isolates were performed at room temperature under conditions employed during cultivation.

Following incubation, samples were fixed with 0.2 μm-filtered formaldehyde (2% minimum) and filtered onto white 0.2 μm pore size polycarbonate membrane filters (Nuclepore track-etch, GE Whatman, Piscataway, NJ). Click chemistry processing of samples was completed using the Click-iT® reagent kit (Invitrogen, Carlsbad, CA) using the mixture detailed in Table 1. Each filter was cut into ~1/8 – 1/6 slices using a sterile

razor blade or surgical scissors and placed onto a glass microscope slide. The remaining filter was stored (dark, -20°C). The processing steps were completed in darkened conditions to minimize fluorophore photobleaching and reduce azide group decomposition (Abbenante et al. 2007). Staining of bacterial cells was achieved per Glöckner et al (1996), and used antifade mounting media to maintain signal intensities (Patel et al. 2007). The protocol is described in Figure 2. To reduce background signal the filter-transfer-freeze (FTF) technique was also applied (Hewes & Holm-Hansen 1983). This approach was applied to all samples filtered on 0.22 μm filters.

Microscopy and acquisition settings

Slides were visualized on a Nikon TE2000-U inverted microscope using a Plan Apochromat VC 100x, 1.4 numerical aperture oil immersion objective with illumination from an Exfo Xcite series 120 mercury lamp (Lumen Dynamics Group, Mississauga, Ontario, Canada). Images were acquired and analyzed using NIS-Elements (Nikon Instruments Inc., Melville, NY). Each image consisted of three channels with specific excitation and emission filters: 350/50 nm excitation with 457/50 nm emission for DAPI-stained cells, 490/20 nm excitation with 528/38 nm emission for the Alexa Fluor 488® signal from incorporated HPG, and 555/28 nm excitation with 617/73 nm emission for chlorophyll autofluorescence of cyanobacteria and eukaryotic microalgae. Ten to twenty fields were captured, with exposure times from tens of milliseconds to a few seconds. After optimizing the exposure time for each channel to ensure maximal, unsaturated pixel intensities, these settings were maintained throughout the acquisition of the sample set. The lookup tables (LUTs) for each of the three image channels were

adjusted to facilitate easy observation, and the binary editor was used to manually include cells with signal intensities slightly higher to that of the background.

Controls and incorporation specificity

Several killed and experimental controls were completed to assess non-specific binding of HPG or Alexa Fluor® 488, identify false positives from background signals, and confirm the specificity of HPG as a methionine analog. Although it has been demonstrated that methionyl-tRNA synthetase can bind to and incorporate HPG into protein (Wang et al. 2008), we asked if this observation could be expanded to natural marine microbial communities, and questioned the ability of other amino acids to reduce labeling by influencing uptake, incorporation, or cleavage of post-translated HPG.

Killed controls. The purpose was to identify false positive labeling. Two controls were made during several experiments. 1) Samples were fixed with 2% formaldehyde before adding HPG. 2) No HPG was added before incubation.

HPG-methionine competition. These experiments tested the competitive ability of methionine to reduce or eliminate HPG uptake. Methionine was added at 0 (HPG only), 1 μM or 20 μM plus 20 nM HPG to seawater and incubated 0.5, 1, 4, and 6 h. Samples were processed as above and visualized to determine possible inhibition of incorporation of HPG.

Chloromphenicol inhibition of HPG incorporation. Because chloramphenicol inhibits peptidyl transferase activity of sensitive bacterial ribosomes, we reasoned it may inhibit HPG incorporation into protein while testing method specificity. Chloramphenicol

was added at 50 μg ml^{-1} and incubated with 20 nM HPG for 1 and 6 h. The samples were then processed on filters compared to no-chloramphenicol controls.

HPG inhibition of methionine uptake. Bulk incorporation experiments using ^{35}S-methionine were conducted to ascertain the ability of HPG to reduce methionine incorporation. Four treatments were employed, using whole Scripps Pier seawater incubated for one hour with 2 nM ^{35}S-methionine, 2 nM ^{35}S-methionine + 20 nM HPG, 2 nM ^{35}S-methionine + 200 nM HPG, and 2 nM ^{35}S-methionine + 2 μM HPG. Samples were prepared and processed using the centrifugation method (Smith & Azam 1992).

Further bulk incorporation experiments were conducted with ^{35}S-methionine to identify HPG as a competitive, noncompetitive, or mixed inhibitor of methionine. Five concentrations of ^{35}S-methionine + cold methionine were incubated with unfiltered Scripps Pier seawater in the presence of three HPG concentrations as noted in Table 2. The specific activity of the radioactive methionine was adjusted proportionately to the concentration of cold methionine added. Triplicate measurements and duplicate blanks were used to generate a Michaelis-Menten plot from which K_m, V_{max}, and K_i values were calculated based on non-linear regressions calculated in GraphPad Prism software (Michaelis & Menten 1913). These numbers were then used to assess the uptake kinetics, substrate preferences, and competition between ^{35}S-methionine and HPG in natural seawater bacterial communities. We assumed that all replicates had similar permease and other cellular transport enzyme concentrations.

Microautoradiographic and bulk uptake evaluation. Parallel incubation experiments were designed to compare microautoradiographic labeling percentages

between bacterial communities amended with HPG versus those pulsed with ^{35}S-methionine.

In the first parallel incubation experiment, seawater was incubated with 1 or 20 nM HPG alongside a separate incubation of 2 nM ^{35}S-methionine + 18 nM methionine and incubated for 1 hour in the dark. Inoculation, incubation parameters, and processing steps for HPG were identical to those described above. Following incubation with radiolabeled amino acid, samples were fixed at 2% final concentration formaldehyde for at least 15 minutes. Killed controls were prepared by adding each sample to a mixture of radiolabeled amino acid and formaldehyde. After incubating, the samples were then filtered onto 0.2 μm pore size polycarbonate filters backed with 0.45 μm pore size mixed cellulose ester filters (Isopore membrane filters & MF membrane filters, Millipore, Billerica, MA). Each well and filter was rinsed with 0.2 μm filtered 1x PBS or Milli-Q water. The filters were then dried on absorbent tissue and stored at –20°C until processing.

The aim of the second parallel incubation experiment was to confirm the results of the first while also observing the reduction in labeling percentages by HPG or methionine in microautoradiographic or Click-processed samples, respectively. The first setup consisted of bulk measurements of ^{35}S-methionine uptake performed in triplicate with duplicate 5% TCA-killed controls with the following concentrations: 1) 2 nM ^{35}S-methionine + 18 nM methionine, 2) 2 nM ^{35}S-methionine + 18 nM methionine + 200 nM HPG, 3) 2 nM ^{35}S-methionine + 18 nM methionine + 2 μM HPG. The samples were processed via the centrifugation method. The second microautoradiography setup was completed with duplicate experimental and duplicate controls with the identical 3 groups

of concentrations as the bulk measurements. The third and final setup for HPG and Click processing was performed in duplicate using these concentrations: 1) 20 nM HPG, 2) 20 nM HPG + 2 μM methionine, 3) 20 nM HPG + 2% formaldehyde, 4) 200 nM HPG, 5) 200 nM HPG + 2 μM methionine, 6) 200 nM HPG + 2% formaldehyde.

For the filters containing ^{35}S-methionine-labeled microbes, each membrane filter was cut into a 1/8 – 1/4 piece under normal light conditions. Preparations for microautoradiography were performed under darkroom conditions using a Kodak GBX-2 safelight with a 15 W bulb placed approximately 5 meters away and pointed toward the work area. This extremely faint light ensured low background signal, but necessitated the use of night vision monocular goggles (D-112MG; Night Optics USA, Inc., Huntington Beach, CA). We developed an emulsion coating and cell transferring protocol based on those from previous publications (Teira et al. 2004, Longnecker et al. 2010). Ammersham LM-1 emulsion was melted at 43°C for 15 minutes to 1 hour. Slides were dipped in emulsion for 5 seconds, allowed to drip for 5 seconds, wiped to remove emulsion on the back of the slide, and immediately placed onto a flat sheet of aluminum foil on ice. After 5 – 10 minutes, a filter slice was placed cell side down onto the emulsion and the slide was returned to the ice-cold foil. When this was completed for all of the filters, each slide was then placed in a slide box with desiccant. The slide box was sealed with black tape, wrapped in foil, placed in a cardboard box, left at room temperature for 1 hour, and then transferred to 4°C for 24 - 72 hour exposure.

Processing of the slides was completed using Kodak D19 developer and fixer. In 50 ml tubes, 1.6 g of developer was mixed with 40 ml of milli-Q and dissolved at 43°C for 15 minutes. Nine grams of fixer was mixed with 40 ml milli-Q at room temperature

until fully dissolved. Four slide mailers corresponding to the developer, developer wash, fixer, and fixer wash were filled with 20 ml of appropriate liquid. Under darkroom conditions, the slides were removed from the darkened box, and the filters on each slide were then removed gently with forceps, thereby transferring the cells and exposing the emulsion to the processing chemicals.

Slides were dipped in developer for 4 minutes, washed for 10 seconds, then dipped in fixer for 5 minutes, washed again for 5 minutes, and then allowed to dry on a kimwipe. Once the slide was dry, 50 – 100 µl of 1 µg ml^{-1} DAPI was added to the location of the cells and incubated for 10 minutes. The slide was then washed in autoclaved and filtered milli-Q and dried again. A coverslip with #1.5 thickness was mounted to the slide with 15 - 20 µl of the antifade mounting media.

Visualization was performed using the Nikon TE2000-U inverted microscope with 350/50 nm excitation and 457/50 emission to observe DAPI-stained bacteria. Transmitted light was used to observe the presence or absence of exposed emulsion grains. Images were acquired with approximately 2-second exposure times to document each experiment and permit analyses at a later date. Percent labeling was calculated as the number of DAPI-labeled cells located within exposed emulsion divided by the total number of DAPI-labeled cells in each field of view. These values were arcsine transformed, averaged, and then back transformed.

Signal quantification of individual bacterial cells

Labeling percentages. The percentage of labeled cells imaged on polycarbonate filters was calculated using the following equation:

$$[(\#\ \text{HPG+ cells}) - (\#\ \text{TRITC+ cells})] \div (\#\ \text{DAPI+ cells})$$

This equation was based on the observation that control samples not amended with HPG displayed bright green cells in the FITC channel. These were presumably cyanobacteria and/or picoeukaryotes with autofluorescence emission that carried over into the FITC channel. Autofluorescent cells were therefore excluded due to the observed carryover and reduce the possibility of false positives.

Labeled cells imaged on slides via the FTF technique were selected in the software to analyze the fluorescence intensity information (described in the following section). This data was comprised of a minimum of 10 fields containing at least 20 cells. After background subtraction, the sum intensity (S.I. = total amount of fluorescence emitted from the cell) values greater than zero from all of the images combined were used to calculate percentage of labeled cells:

$$(\#\ \text{of cells with FITC sum intensity} > 0) \div (\text{total}\ \#\ \text{of cells imaged})$$

Single-cell signal measurements. Most of the filters from experiments and pier samples were re-processed and transferred to coverslips using FTF. The binary thresholding feature in the Nikon Elements software was used to select individual cells in the DAPI channel in order to quantify both labeled and unlabeled cells in an unbiased fashion. Cyanobacteria and other sources of red fluorescence that appeared to crossover into the green emission channel were manually removed. Once the selections were

completed, data for cell area, width, and length were exported to Microsoft Excel. Signal intensities in the FITC channel were exported as two separate parameters: sum intensity and mean intensity, equivalent to the sum intensity divided by the numbers of pixels. The number of pixels of each cell was calculated by dividing the area of the cell (μm^2) by the $(\#\ pixels/\mu m)^2$.

To accurately quantify signal intensities from individual cells and the whole community, a stringent subtraction of background and blanks was employed. Formaldehyde-fixed control samples revealed that HPG and/or Alexa Fluor 488® were adsorbing onto bacterial cell surfaces and creating faint signals. It was concluded that the background of the glass slide did not contribute to background signals because in some cases the background mean intensity was greater than the mean intensity of a control cell. Therefore, the mean FITC channel intensities of all cells from 5 different fields in the HPG + 2% formaldehyde controls (>200 cells, red autofluorescing cells removed) were averaged. This average background was subtracted from the HPG+ samples by multiplying this value by the pixel area of each cell and then subtracting this number from the sum intensity of the cell.

A conversion factor was applied to transform the sum intensities into a carbon production and growth rate for each cell (method, results, and discussion below). The values were then averaged, including averages for the top 10% and bottom 90% of cells.

Signal intensity validation. To confirm constant illumination by the mercury bulb and to ensure the linearity of fluorescence intensity vs. exposure time, an InSpeck Green Microscope Image Intensity Calibration Kit was used (Life Technologies, Grand Island, NY). The 0.3% relative intensity beads were imaged on three separate dates at 2, 10, 25,

100, and 200 ms exposure times. Additionally, the 0, 0.3, 1, 3, 10, 30, and 100% relative intensity beads were imaged at a constant 30 ms exposure time.

Signal intensity conversion to single cell carbon production and growth rate

The bacterial isolates AS1 and ALT199 (*Alternomonas* sp.) were acclimated to and maintained in GF/F filtered and autoclaved seawater to simulate natural seawater conditions and eliminate potential responses to high organic nutrient load in ZoBell media (Pedler et al., *in prep*). Each isolate was inoculated into 3 flasks containing 100 ml of GF/F filtered and autoclaved seawater at a starting concentration of 10^2 cells ml^{-1} from exponentially growing cultures. All six flasks were incubated at room temperature for 16 hours, at which point concentrations were expected to be ~10^3 cell ml^{-1} following 4 doublings as confirmed via DAPI staining. HPG was added to one flask of each isolate at 0 nM, 2 nM, and 20 nM concentrations, and 20 ml samples were formaldehyde fixed (2%) and filtered after 24 and 48 hours. Cell counts and click chemistry processing was performed on each sample and imaged on the Nikon microscope. Images for the FITC channel were acquired with 200 ms acquisition because the cells were very brightly labeled. Cell volumes (V) were calculated according to (Bratbak 1985) by measuring the lengths and widths of each cell. Cellular protein content (P) in fg was estimated using $P = 88.6 \times V^{0.59}$ and converted to carbon (C) by multiplying by 0.86 (Simon & Azam 1989, Malfatti et al. 2010). After background subtraction, sum intensity data points for each isolate in 2 nM and 20 nM HPG were divided by volume-based cell carbon to obtain a conversion factor of S.I./fg carbon. This value was multiplied by 5 to apply the 200 ms exposure to images acquired from the standard 1 s exposure ($1 \div 0.2 = 5$). After sorting

in ascending fashion, the average values of the top 10% for 2 nM and 20 nM HPG conditions were deemed appropriate conversion factors and later applied to HPG sum intensities acquired from natural samples and other experiments to obtain single-cell protein or carbon production (scBPP, scBCP), generation times (g), and growth rates (μ) using the following equations:

$$g = P \div scBPP$$

$$\mu = LN(2) \div g$$

Activity upshift experiment

Confirmation that enhanced cell growth resulted in elevated HPG signal intensity was performed by comparing 0.6 μm filtered seawater amended with and without glucose and ammonium chloride. 300 ml of the filtrate was divided into two-500 ml glass bottles, and 1 μM of both glucose and ammonium chloride was added to one bottle. Duplicate 2 ml samples were taken from each bottle for bacterial abundance and 1 hour incubations with 20 nM HPG at 0, 4, 8, 12, and 24 hours, including duplicate formaldehyde controls. Images were acquired as above, and processed for activity measurements as described below.

Scripps Pier monitoring experiment

To monitor dynamics of HPG uptake at the pier, samples were taken at 12pm, 4pm and 8-9pm for 3 consecutive days using the standard incubation parameters with 2 ml volumes. Images were acquired as described above, and processed for activity measurements as described below. Automated measurements of chlorophyll, temperature,

and salinity and production and growth rates were analyzed using Spearman rank correlations.

HPG uptake by particle-attached bacteria

The incorporation and visualization of HPG within particle-associated bacterial cells was tested to determine if the method could detect elevated cell production and labeling intensity in comparison to other particles and unattached cells. Whole seawater (40 ml) was added to glass culture vials. In duplicate, three sets of vials were treated as follows: 1) 20 nM HPG, 2) 20 nM HPG + 2% formaldehyde (final conc.), 3) 2 μM HPG, 4) 2 μM HPG + 2% formaldehyde, 5) No addition. The three sets of these manipulations corresponded to incubation times of 1 hr., 48 hrs., and 8 d. At each time point, 2 and 30 ml was removed from each vial, fixed with 2% formaldehyde, and filtered respectively on 0.22 μm or 8 μm white polycarbonate filters. All filters were Click processed normally, but the FTF technique was not applied to the 8 μm filters to minimize damage to particles and phytoplankton and maintain the positions and orientations of attached bacteria. Ten image fields were acquired for the 2 ml samples while 10 particles greater than 10 μm in diameter and containing at least 20 cells were imaged on the 8 μm filters. Values were $\log_{10}$-transformed to ensure normality for statistical tests.

HPG-based activity structure

Comparison of HPG-based protein production profiles among all the sampling dates was achieved by graphically representing the frequency distribution of cell-specific production in $\log_{10}$-$\log_{10}$ charts of percentage of cells vs. fg cell^{-1} hr^{-1}. Using 0.05 fg cell^{-1}

hr^{-1} bins, the percentage of cells within each bin was plotted. A power function was fit to each series of points, and the resulting equation was used to generate a continuous line. Ranges of the axes were adjusted after applying the log_{10} scale to enable fine or coarse observation of the community production structures in relation to each other.

Results & Discussion

Controls and incorporation specificity

Killed controls. Non-specific labeling did not occur in any samples. However, autofluorescence of cyanobacteria was seen to carry over into the FITC channel in HPG- samples. This necessitated their removal from signal intensity measurements.

HPG-methionine competition. Methionine addition partially or completely eliminated HPG signals, supporting the method's basic premise that HPG competitively replaces methionine in protein **(**Fig. 3**)**.

Chloromphenicol inhibition of HPG incorporation. Chloramphenicol reduced the percentage of HPG labeled cells by 10-fold (15.1% to 1.4%) and 44-fold (28.4% to 0.6%) in the 1 and 6 hour incubations, respectively. These results support HPG being actively incorporated into protein by bacterial ribosomes.

HPG inhibition of methionine uptake. The subsequent set of bulk incorporation experiments further explored the mechanism of methionine-HPG inhibition and identified the inhibitory constant, K_i. The results showed that HPG is a competitive analog for methionine in natural marine systems; increasing inhibitor (HPG) concentration had no effect on V_{max} (Fig. 4). These values provided an average K_i for the three HPG

concentrations. Because the inhibition constant (also known as the dissociation constant, K_d, for the inhibitor and enzyme) is equivalent to the concentration at which half of HPG is free and half is bound to the enzyme, and since the velocity of enzyme reactions is proportional to the concentration of the enzyme-substrate (or enzyme-inhibitor) complex, then $K_i = K_m$ for HPG, which was calculated to be 372.8 nM. The much smaller K_m for methionine (~30 nM) confirms that while HPG substitutes for methionine it has ~ 100-fold lower affinity for incorporation in natural marine prokaryotic communities. This suggests that our protocol employing 20 nM HPG is sufficient to minimize extracellular competition since methionine concentrations typically found in seawater are 100x less (200 pM)

Microautoradiographic and bulk uptake evaluation. Bulk seawater experiments showed that adding equimolar methionine or HPG as competitors of ^{35}S-methionine showed that HPG caused much lower inhibition than methionine **(**Fig. 5**)**. Thus, uptake of methionine is kinetically preferred over HPG.

Parallel incubations of Scripps Pier seawater with ^{35}S-methionine or HPG revealed similar percentages of labeled cells following microautoradiographic or click protocol. However, this result depended on whether HPG samples were observed on filters or using FTF protocol (Table 3). The filters method yielded percentages comparable to microautoradiography while percentages from FTF (lower background) were ~ 1.5 – 3-fold higher (Fig. 3). Importantly, this indicated that the click protocol has a higher sensitivity for detecting active cells than microautoradiography.

General observations

Labeling percentages and the importance of sample processing. The percentage of HPG positive cells from Scripps Pier ranged 9% - 47% on filters. Some labeled cells were easily detectable on filters due to strong signal intensity despite high background. The Nikon software was particularly helpful in the manual selection of cells required when faint DAPI-stained cells were unable to be adequately separated from background signal or associated cells were measured as single loci. The filter-transfer-freeze technique reduced background by ~5-fold and increased the percent-labeled estimates to 15% - 100% (Fig. 6**)**; presumably background reduction enabled visualization of faintly labeled cells (Fig. 7). However, the transfer efficiency was 69% to 200%, making cell concentration calculations unreliable. This wide range of transfer efficiency is likely due to the incomplete transfer of cells to coverslip and accumulation of transferred cells to areas where the remaining condensation pooled. Assuming equal transfer efficiency of both labeled and unlabeled cells, variable incomplete and variable transfer efficiency should not affect the percentages. Indeed, large differences in labeled cell percentages were not seen between duplicates in which transfer efficiencies were very different.

Cell labeling characteristics. Labeled cells frequently had a larger signal area than DAPI labeling. This suggests distribution of HPG labeled protein to both intra- and cell surface compartments; alternatively, the nucleoid labeling seen with DAPI may underestimate cell volume **(FIG 8)**(Fig. 8; Straza et al. 2009). We also note that many other HPG-positive cells did not exhibit this characteristic. The cause of these differences were not investigated, but they may signify sub-cellular incorporation patterns in different physiological conditions. Additionally, we often saw dividing cells with label evenly distributed between two cells. Occasionally only one of the daughter cells was

HPG positive (Fig. 9). Our protocol was not designed to distinguish mother and daughter cell, or to explain why only one cell would be labeled. Perhaps, one of these cells was senescent.

Utility in other fields of microbial ecology. The HPG method in natural marine environments may be useful to quantify protozoan grazing and/or viral infection, lysis, and burst size in marine prokaryotic communities. We noticed in our samples some heterotrophic nanoflagellates (HNF) with bright green signals over the whole cell or within concentrated sections of their cytoplasm. This suggests that these grazers were consuming HPG labeled cells and then incorporating HPG into biomass, yet we cannot rule out that some nanoflagellates directly incorporate HPG into protein. The scenario was not explored in detail and may be due to ingestion of cyanobacteria that, as mentioned earlier, exhibit strong green emissions naturally and in the absence of HPG. Further study should clarify whether HPG labeled bacteria can be used to identify and quantify bactivorous grazing.

Signal intensity conversion to single cell carbon production and growth rate

The average conversion factor from the top 10% values for both ALT199 and AS1 was set at 122,775.0827 S.I. units fg^{-1} protein. We concluded that this approach reduced the influence of anomalously high intensity measurements, and provided an asymptotic value that most closely represented an accurate conversion factor. Because the overall approach was based on bacterial isolates that grew well in seawater without nutrients, the conversion factor is likely a realistic figure that was not based on growth traits influenced by excess organic matter.

This experiment provided a straightforward calculation of biogeochemically relevant rates based on cell fluorescence that, when applied to the sum intensities of other HPG datasets, provided realistic single-cell values that were in agreement with past studies of cell specific carbon production estimation. Minimum and maximum rates of 1 and 100 amol Leu cell^{-1} d^{-1} were reported by Sintes and Herndl (2006), which is equivalent to 0.13 and 13 fg C cell^{-1} hr^{-1} assuming 3.1 kg C per mole of leucine incorporated (Simon & Azam 1989). The method afforded the detection of very low values with a minimum of ~ 10^{-6} fg C cell^{-1} hr^{-1} while the maximum rate was 5.5 fg C cell^{-1} hr^{-1}. However, the accuracy of the lowest values is has a lower limit set by the fluorescence of the control cells. Due to the fact that the faint fluorescence of the control cells converts to an average carbon production value of 0.05 fg C cell^{-1} hr^{-1}, this represents the base of detection of HPG-based scBCP.

We calculated average scBCP for each of the 21 dates that HPG incubation experiments were performed (Table 4). The average values provided a snapshot of the single cell community production and ranged from ~ 0.1 – 0.5 fg C cell^{-1} hr^{-1}. The average scBCP of the top 10% and bottom 90% was examined to identify the contribution of the most active versus remaining members of the community. These values ranged from ~ 0.4 – 2.1 fg C cell^{-1} hr^{-1} and ~ 0.04 – 0.4 fg C cell^{-1} hr^{-1} for the top 10% and bottom 90%, respectively. The 10% to 90% ratios permitted comparison among all of the dates, and showed that the most active cells were approximately 5 to 16 times more so than the remaining active cells.

The sums of scBCP and ratios for the top 10% and bottom 90% enabled comparisons among the dates to determine the relative influence on carbon cycling by the

partitioning of activities in the bacterial community (Table 5). Ratios greater than 1 highlight dates when the cumulative scBPP of the top 10% of active bacteria was greater than the cumulative scBPP of the rest of the active cells. Ratios less than 1 denote when the bottom 90% of the community contributed more to carbon production. Overall, the ratios were evenly distributed above and below 1 (ratios > 1 in 11/21 dates).

A summary of μ calculated for each date is organized in Table 6. The broad distribution of growth rates combined with many low values resulted in averages ranging from ~ 0.09 – 0.35 d^{-1}. Meanwhile, averages of the top 10% showed that cells double approximately once per one to four days. Maximum growth rates approached 2.5 d^{-1}. Because these cells represented approximately $1/1000^{th}$ of the community containing ~ 3 x 10^6 cells ml^{-1}, it is possible that 3 x 10^3 cells ml^{-1} were rapidly growing and disproportionately assimilating carbon in that particular water parcel on that date. The eventual fate and contribution to microbial community structure of these cells remains a topic for future research.

The quantitative nature of the method has afforded a novel view of the single-cell growth and carbon cycling, and may represent an attractive approach to address unanswered questions in marine microbial ecology and elemental cycling. For example, what are the factors explaining how and why the most active portion of the community is growing or incorporating carbon at a rate that is more, less, or similarly than the remaining community? Or, conversely, what influences the bottom 90% community to be more, less, or as active as the top 10%? Experiments combining HPG incubations with measurements identifying top-down control by viruses and/or protists may help to elucidate some of these dynamics. Applying HPG-based activity quantification alongside

analyses of the quantity and quality of organic matter available for bacterial incorporation into biomass may assist in characterizing the bottom-up dynamics influencing bacterial growth and carbon cycling.

Surprisingly, the method did not agree with previous observations noting the positive relationship between cell size and activity (Gasol et al. 1995, Lebaron et al. 2002), as regressions of sum intensities and mean intensities vs. biovolume were not significant (data not shown). Given the diversity of metabolic characteristics within marine bacterial communities, this result is not unexpected. The propensity for certain members of the community to exhibit highly specific metabolic traits has been discussed (del Giorgio & Gasol 2008), and highlight how complementary measurements provided by HPG incorporation expand our knowledge on the physiological states and rates that partially govern individual bacterial subsistence. Moreover, quantifying this survival with HPG in concert with other approaches may highlight the resulting influences over the cycling of carbon, nitrogen, phosphorous, and other marine elements (Smith & del Giorgio 2003).

Activity upshift experiment

Seawater cultures amended with 1 μM glucose and 1 μM NH_4Cl displayed significant, linearly increasing cell-specific production over time in comparison to control samples (Fig. 10). These results supported the utility of HPG incorporation as a reliable detector of growth enhancement in single cells.

Scripps Pier monitoring experiment

The goal of this three-day/night observation of HPG incorporation was to detect temporal variability patterns (e.g. diel) in bacterial activity at a fixed location and characterize relationships with chlorophyll, temperature, and salinity. Sharp changes in bacterial abundance were observed alongside strong dynamics in cell activities (Fig. 11a). Day 1 was characterized by stable abundances throughout the day, and exhibited a significantly elevated average cell-specific protein production and growth rate at 12pm. The abundance and activity data from day 2 were elevated compared to day 1, and a striking observation was the greatly enhanced abundance, protein production, and growth rate at 4pm. The cell abundance-based growth rate of the community between 12pm and 4pm on day 2 (~5 d^{-1}) was not similar to average HPG-based growth rate measurement nor the average top 10% growth rate (0.23 and 1.19 d^{-1}, Fig. 11b & c). However, these values were significantly elevated relative to the previous and following timepoints. Potential explanations for this major shift include the transport of water masses containing high abundance communities by currents, sediment resuspension and mixing of high-density benthic bacterial communities, a surge in growth that tapered before or during sampling, or bacterial consortia for which the conversion factor was incorrect. Day 3 exhibited a different pattern of abundance, production, and growth rate compared to both days 1 and 2. An extremely high abundance at 12pm decreased 3-fold by 4pm and then 2-fold by 9pm. This trend agreed with stepwise decreases in the protein production and growth rate, but the rates of change were different. It appears that on relatively short timescales, the carbon cycling dynamics of heterotrophic bacterial communities rapidly shifted in tempo.

Significantly positive Spearman's rho values ($p > 0$ .05) were found between chlorophyll and the 10% to 90% ratios of the average and sum production and growth rate, with one significantly negative correlation between chlorophyll and average production of the bottom 90%. A confluence of events likely explains these dynamics of HPG-based physiology. The decreasing abundance and production trends on day 2 between 4pm and 8pm and day 3 between 12pm and 4pm are consistent with grazers consuming the most active prey (del Giorgio et al. 1996). However, the ratios of the top 10% and bottom 90% active cells for cell-specific growth rate and protein production increased (Fig. 11d), indicating the elevated abundance of more active cells and/or the removal of less active cells. Lytic viruses may be an additional mortality agent responsible for these observations, and in fact may induce similar enhancements in growth, but with focused effects on certain members of the community, potentially mildly active cells in this case (Noble et al. 1999, Weinbauer 2004). These biotic forcings combined with the productivity (chlorophyll) and physical parameters (salinity and temperature) at the pier may influence bacterial growth, with potential feedbacks on trophic webs, phylogenetic structure, and elemental cycling dynamics. Yet additional structuring mechanisms include high substrate concentration exposure and inducement of slow growth or death (Koch 1997), lack of and/or competition for inorganic nutrients (Thingstad et al. 1997), and sunlight and UV damage (Alonso-Sáez et al. 2006). Overall, the HPG-based activities from this experiment provide constraints on the ecological and biogeochemical effects arising from dynamics in cell-specific heterotrophic bacterial growth and physiology.

HPG uptake by particle-attached bacteria

This investigation tested the hypothesis that heterotrophic bacterial cells attached to particles exhibit enhanced growth performance, and identified the potential for HPG incorporation to characterize abiotic and biotic interactions at such microenvironments. Because methionine outcompetes and eliminates HPG incorporation, the monomerization of proteins to amino acids (and specifically methionine) by bacteria attached to marine organic particles would possibly reduce HPG uptake, resulting in diminished cell signal intensity. The signal intensities of the 4 manipulations at each timepoint (unattached + 20 nM, unattached + 2 μM, particle-attached + 20 nM, particle-attached + 2 μM) were significantly different from one another (student's t-test, $p < 0.05$), except for the 48 hour unattached + 20 nM and the particle-attached + 2 μM. Not surprisingly, the mean signal intensities from the 2 μM HPG samples were always higher than the 20 nM, and, in the case of the particle-attached bacteria, suggested that high HPG concentration enabled increased incorporation in an environment of potentially high exogenous methionine (Fig. 12). It is possible, however, that 2 μM was not sufficient to completely and competitively overwhelm cell permease systems as the signal intensities for unattached + 20 nM and unattached + 2 μM in the 1 hour and 48 hour samples were significantly higher than the those of particle-attached cells. Not until 8 days later did the signal intensities from the 2 μM HPG samples exhibit significant and elevated differences from the 20 nM counterparts, and was presumably caused by the reduced concentration of methionine and other amino acids within the particles.

These results agree with previous studies of bacterial carbon cycling and consumption on particles. Simon et al (1990) observed low carbon production of bacteria

attached to marine snow. As with Cho & Azam (1988), the authors concluded that the depth dissipation of particulate organic carbon (POC) was due to the carbon demand of unattached bacteria. Greater contribution of unattached cells to particle dissolution and turnover supports our findings of higher mean sum intensities for the unattached cells at the 1 and 48 hr. timepoints. Nevertheless, the issue of competitive inhibition remains. We concluded that both the HPG concentration and incubation time affect the labeling characteristics of these unattached and particle-attached bacteria, and that short incubation times may not adequately resolve bacterial activity on particles. Either determining the amino acid composition of the particles to confirm the absence of methionine, or using other analogs whose natural counterpart is absent from the particle may address this. However, several other circumstances may explain these observations.

The unique microenvironment of a nutrient rich marine organic particle likely elicits strong competition among bacteria attempting to maintain space and a stable food source to support cell growth and progeny release. We would therefore expect particle-attached cells to inhibit the growth of one another if in direct competition for a particular resource, and our observations support the potential for such antagonistic interactions (Long & Azam 2001a). As with most natural phenomena, dynamics in cell intensities/growth are likely indicative of several mechanisms acting in concert to structure the composition and metabolism of the microbial community. High substrate concentrations and antagonism-mediated reduction in cell growth on particles serve to partially explain the dynamics observed here. Further research on this topic is needed to clarify the relative contributions of theses mechanisms and identify the role of spatiotemporal variability in this important component of the microbial food web.

HPG-based activity structure

The binning approach enabled visual comparison and contrast of the community activity structure of unattached cells sampled from Scripps Pier. Lines that are closely parallel or identical indicate heterotrophic communities with similar carbon production profiles (Fig. 13). Presenting data in this fashion is one approach to simultaneously observe the broad scale and cellular scale growth responses of marine bacteria. Exploring additional statistical techniques to organize and model the data should augment interpretations of ecological and geochemical functions leveraged by individual heterotrophic bacterial activities. The distribution of activity as a power function is a noteworthy result since nearly all evaluations of microbial activity assume Gaussian or normal distributions within the natural community. Such a fundamental observation on the ecology of marine bacteria may be an important insight for future assessments of growth and prevalence of certain phylotypes. Ideally, these quantitative discernments will inform numerical models to characterize and predict bacteria population trajectories and their ecosystem and geochemical consequences.

Single cell growth heterogeneity of clonal bacterial isolates and implications for marine carbon cycling by natural bacterial populations

The broad range of S.I. values measured in growing cultures of ALT199 and AS1 demonstrated the sensitivity of the method and suggested that S.I. heterogeneity is a reflection of heterogeneous growth in each of the clonal populations. While one hundred percent of the cells were positive for HPG at each time point, the intensity values varied

by an order of magnitude among all of the cells in both cultures. This observation may reflect several mechanisms enabling marine bacteria to adapt and succeed in a variety of environments.

As mentioned earlier, asymmetrical growth in prokaryotes is likely to have important consequences for carbon cycling and population dynamics of marine prokaryotic communities. Observing the wide range of intensities in clonal laboratory cultures supports recent work on the adaptive strategy of bacterial aging in *E. coli* (Rang et al. 2011). The large difference between the least and greatest signal intensities may indicate the repeated accumulation of oxidative damage to one daughter cell (lower intensity cells) that serves to rejuvenate the other daughter cell (higher intensity cells). If these characteristics of clonal bacterial populations in laboratory cultures are representative of natural marine communities, this diversity of growth rates is an adaptive feature. Different taxa may experience different microniches at any given time, and the mechanism of creating progeny of varying age and growth response will diversity the metabolic portfolio to increase the likelihood of succeeding within that niche.

Conclusions

The main objective of this work was to develop a method to sensitively observe and quantify growth of individual heterotrophic marine bacteria. Our analyses focused on the dynamics of single cell carbon production and growth rates, and in doing so, we obtained selectivity to characterize the silent majority of less active cells and those that exhibit rapid growth. The spectrum of responses confirm the heterogeneous nature of marine microbial ecosystems, and provide a powerful means to characterize the

functional contribution of heterotrophic bacterial metabolisms to marine carbon cycling. As of yet, HPG incorporation has not been utilized to measure single-cell production rates in bacteria. The protocol described here allows the sensitive, relative, and absolute measurement of cell-specific protein synthesis. Future work should focus on the manipulation of this method to enable bulk production estimates that can be studied alongside the single cell data. Additionally, the application of complementary cell visualization protocols will supplement current studies on marine microbial identities, functions, and growth efficiencies to better predict their climatic and oceanic importance on relevant spatiotemporal scales. For example, integrating the method with fluorescent in situ hybridization (FISH) is a tractable manner to assign and rank the biogeochemical influence of bacterial phylotypes on marine ecosystems as a function of low versus high molecular weight organic matter (Cottrell & Kirchman 2000). Further, linking HPG incorporation to measurements of cellular respiration using 5-Cyano-2,3-ditolyl tetrazolium chloride (CTC; Sherr et al. 1999), or other redox dyes, may enable reliable estimations of single cell bacterial growth efficiency (BGE; del Giorgio & Cole 1998). New information on the growth responses and requirements of marine bacteria may be obtained from the use of additional bioorthogonal compounds. Analogs for carbohydrates and fatty acids are available and may augment the suite of single-cell activity quantification approaches in microbial ecology. The resulting evidence may shed light on the heterotrophic control of organic matter transformation into biomass and constrain values of CO_2 production to better inform models on the fluxes of the greenhouse gas and microbial contributions to climate change. This method adds to the ability of microbial ecologists and oceanographers to decipher the growth, responses, and potential

biogeochemical influences of single bacterial cells in the natural marine environment. The continued development and application of such tools represents an exciting avenue of research, and may contribute important details of microbial influence on the world ocean.

Chapter 4, in part, is prepared for submission to the International Society for Microbial Ecology Journal. The dissertation author was the primary investigator and author of this paper.

References

Abbenante G, Le GT, Fairlie DP (2007) Unexpected photolytic decomposition of alkyl azides under mild conditions. Chem Commun 43:4501-4503

Alonso-Sáez L, Gasol JM, Lefort T, Hofer J, Sommaruga R (2006) Effect of natural sunlight on bacterial activity and differential sensitivity of natural bacterioplankton groups in northwestern Mediterranean coastal waters. Applied and Environmental Microbiology 72:5806-5813

Barbara GM, Mitchell JG (2003) Marine bacterial organisation around point-like sources of amino acids. FEMS Microbiology Ecology 43:99-109

Beatty KE, Xie F, Wang Q, Tirrell DA (2005) Selective Dye-Labeling of Newly Synthesized Proteins in Bacterial Cells. J Am Chem Soc 127:14150-14151

Best MD (2009) Click Chemistry and Bioorthogonal Reactions: Unprecedented Selectivity in the Labeling of Biological Molecules. Biochemistry 48:6571-6584

Bratbak G (1985) Bacterial biovolume and biomass estimations. Applied and Environmental Microbiology 49:1488-1493

Cho BC, Azam F (1988) Major Role of Bacteria in Biogeochemical Fluxes in the Oceans Interior. Nature 332:441-443

Cottrell MT, Kirchman DL (2000) Natural assemblages of marine proteobacteria and members of the Cytophaga-Flavobacter cluster consuming low- and high-

molecular-weight dissolved organic matter. Applied and Environmental Microbiology 66:1692-1697

del Giorgio PA, Cole JJ (1998) Bacterial growth efficiency in natural aquatic systems. Annual Review of Ecology and Systematics 29:503-541

del Giorgio PA, Gasol JM (2008) Physiological Structure and Single-Cell Activity in Marine Bacterioplankton. In: Kirchman DL (ed) Microbial Ecology of the Oceans. John Wiley & Sons, Inc., Hoboken, N.J.

del Giorgio PA, Gasol JM, Vaqué D, Mura P, Agustí S, Duarte CM (1996) Bacterioplankton community structure: Protists control net production and the proportion of active bacteria in a coastal marine community. Limnology and Oceanography 41:1169-1179

Fuhrman JA, Azam F (1982) Thymidine Incorporation as a Measure of Heterotrophic Bacterioplankton Production in Marine Surface Waters - Evaluation and Field Results. Marine Biology 66:109-120

Gasol JM, delGiorgio PA, Massana R, Duarte CM (1995) Active versus inactive bacteria: Size-dependence in a coastal marine plankton community. Marine Ecology-Progress Series 128:91-97

Glöckner FO, Amann R, Alfreider A, Pernthaler J, Psenner R, Trebesius K, Schleifer KH (1996) An in situ hybridization protocol for detection and identification of planktonic bacteria. Systematic and Applied Microbiology 19

Hamasaki K, Long RA, Azam F (2004) Individual cell growth rates of marine bacteria, measured by bromodeoxyuridine incorporation. Aquatic Microbial Ecology 35

Hewes CD, Holm-Hansen O (1983) A Method for Recovering Nanoplankton from Filters for Identification with the Microscope: The Filter-Transfer-Freeze (FTF) Technique. Limnol Oceanogr 28:389-394

Koch AL (1997) Microbial physiology and ecology of slow growth. Microbiology and Molecular Biology Reviews 61:305-&

Lebaron P, Servais P, Baudoux AC, Bourrain M, Courties C, Parthuisot N (2002) Variations of bacterial-specific activity with cell size and nucleic acid content assessed by flow cytometry. Aquatic Microbial Ecology 28:131-140

Long RA, Azam F (2001a) Antagonistic interactions among marine pelagic bacteria. Applied and Environmental Microbiology 67:4975-4983

Long RA, Azam F (2001b) Microscale patchiness of bacterioplankton assemblage richness in seawater. Aquatic Microbial Ecology 26:103-113

Longnecker K, Wilson MJ, Sherr EB, Sherr BF (2010) Effect of top-down control on cell-specific activity and diversity of active marine bacterioplankton. Aquat Microb Ecol 58:153-165

Malfatti F, Samo TJ, Azam F (2010) High-resolution imaging of pelagic bacteria by Atomic Force Microscopy and implications for carbon cycling. ISME Journal 4:427-439

Michaelis L, Menten ML (1913) The kinetics of invertase action. Biochemische Zeitschrift 49:333-369

Noble RT, Middelboe M, Fuhrman JA (1999) Effects of viral enrichment on the mortality and growth of heterotrophic bacterioplankton. Aquatic Microbial Ecology 18:1-13

Patel A, Noble RT, Steele JA, Schwalbach MS, Hewson I, Fuhrman JA (2007) Virus and prokaryote enumeration from planktonic aquatic environments by epifluorescence microscopy with SYBR Green I. Nature Protocols 2:269-276

Rang CU, Peng AY, Chao L (2011) Temporal Dynamics of Bacterial Aging and Rejuvenation. Current Biology:1-4

Rostovtsev VV, Green LG, Fokin VV, Sharpless KB (2002) A stepwise Huisgen cycloaddition process: Copper(I)-catalyzed regioselective "ligation" of azides and terminal alkynes. Angew Chem Int Ed 41:2596-2599

Salic A, Mitchison TJ (2008) A chemical method for fast and sensitive detection of DNA synthesis in vivo. Proceedings of the National Academy of Sciences 105:2415-2420

Seymour JR, Seuront L, Mitchell JG (2005) Microscale and small-scale temporal dynamics of a coastal planktonic microbial community. Marine Ecology-Progress Series 300

Sherr BF, del Giorgio P, Sherr EB (1999) Estimating abundance and single-cell characteristics of respiring bacteria via the redox dye CTC. Aquatic Microbial Ecology 18:117-131

Simon M, Alldredge AL, Azam F (1990) Bacterial carbon dynamics on marine snow. Marine Ecology-Progress Series 65:205-211

Simon M, Azam F (1989) Protein content and protein synthesis rates of planktonic marine bacteria. Marine Ecology Progress Series 51:201-213

Sintes E, Herndl GJ (2006) Quantifying substrate uptake by individual cells of marine bacterioplankton by catalyzed reporter deposition fluorescence in situ hybridization combined with micro autoradiography. Applied and Environmental Microbiology 72:7022-7028

Smith DC, Azam F (1992) A simple, economical method for measuring bacterial protein synthesis rates in seawater using 3H-leucine. Mar Microb Food Webs 6:107-114

Smith EM, del Giorgio PA (2003) Low fractions of active bacteria in natural aquatic communities? Aquatic Microbial Ecology 31:203-208

Straza TRA, Cottrell MT, Ducklow HW, Kirchman DL (2009) Geographic and Phylogenetic Variation in Bacterial Biovolume as Revealed by Protein and Nucleic Acid Staining. Applied and Environmental Microbiology 75:4028-4034

Tada Y, Taniguchi A, Hamasaki K (2010) Phylotype-specific growth rates of marine bacteria measured by bromodeoxyuridine immunocytochemistry and fluorescence in situ hybridization. Aquatic Microbial Ecology 59

Teira E, Reinthaler T, Pernthaler A, Pernthaler J, Herndl GJ (2004) Combining catalyzed reporter deposition-fluorescence in situ hybridization and microautoradiography to detect substrate utilization by bacteria and archaea in the deep ocean. Appl Environ Microbiol 70:4411-4414

Thingstad TF, Hagstrom A, Rassoulzadegan F (1997) Accumulation of degradable DOC in surface waters: Is it caused by a malfunctioning microbial loop? Limnology and Oceanography 42:398-404

Tornoe CW, Christensen C, Meldal M (2002) Peptidotriazoles on solid phase: [1,2,3]-triazoles by regiospecific copper(I)-catalyzed 1,3-dipolar cycloadditions of terminal alkynes to azides. J Org Chem 67:3057-3064

Wang A, Nairn NW, Johnson RS, Tirrell DA, Grabstein K (2008) Processing of N-terminal unnatural amino acids in recombinant human interferon-beta in Escherichia coli. Chembiochem 9:324-330

Weinbauer MG (2004) Ecology of prokaryotic viruses. Fems Microbiology Reviews 28:127-181

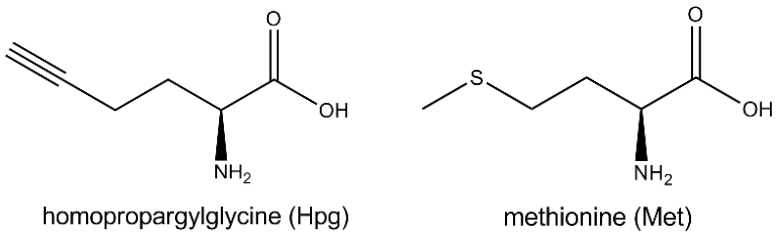

homopropargylglycine (Hpg) methionine (Met)

Figure 4.1. Chemical structures of methionine (m.w. 149.21) and homopropargylglycine (m.w. 127.14).

Table 4.1. Appropriate mixture of reagents needed to conjugate alkyne-containing HPG to azide functionalized Alexa Fluor® 488.

Reagent	**Volume (*μ*l)**
Milli-Q water	155
Reaction buffer	20
Copper (I) sulfate	4
Buffer additive	20
Alexa Fluor® 488	1
Total	200

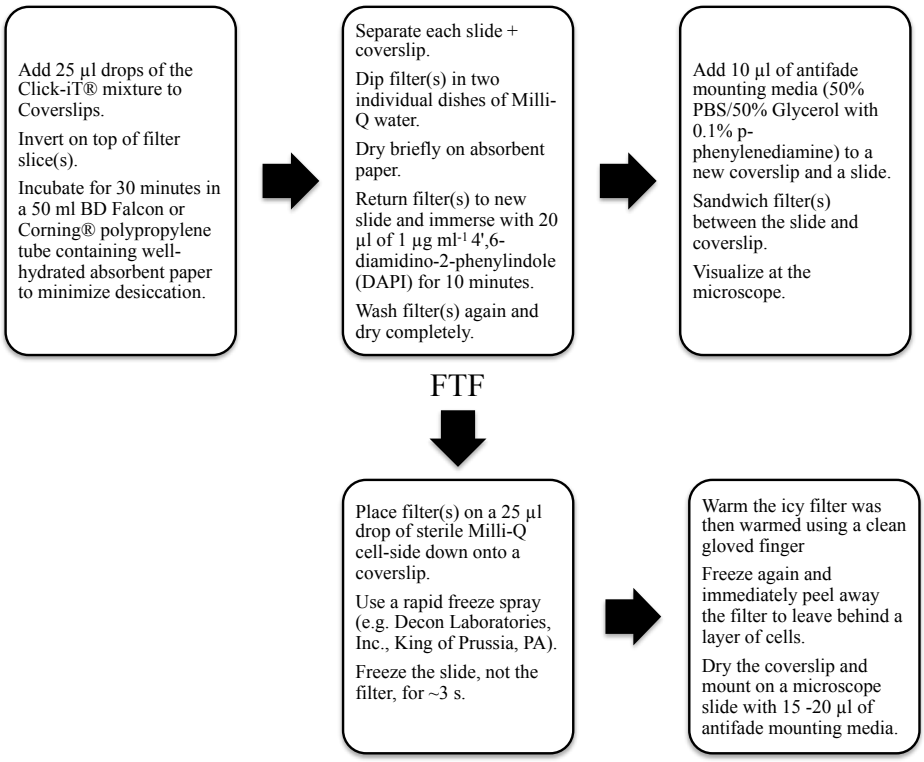

Figure 4.2. Flow chart of protocols to covalently bond alkyne-containing HPG to azide functionalized Alexa Fluor® 488.

Table 4.2. Setup of 35S-methionine incubations conducted in the presence of homopropargylglycine.

HPG concentration (nM)	Final 35S-methionine concentration (nM)	35S-methionine concentration (nM)	Methionine concentration (nM)
0	2	2	0
30			
100			
1000			
0	5	2	3
30			
100			
1000			
0	10	2	8
30			
100			
1000			
0	30	2	28
30			
100			
1000			
0	100	2	98
30			
100			
1000			

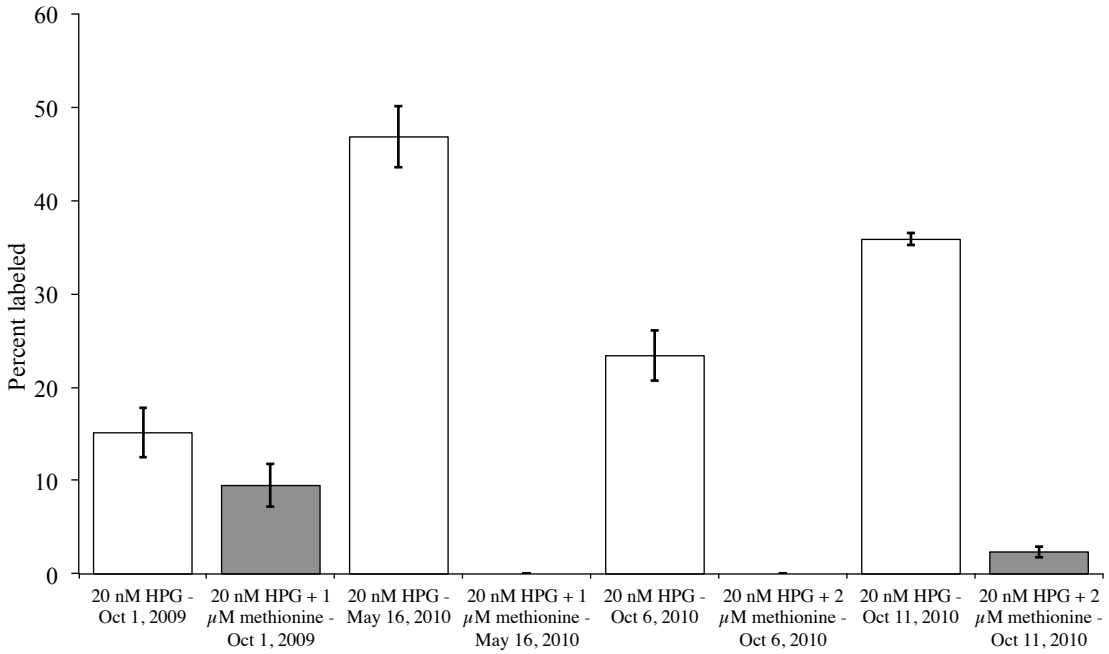

Figure 4.3. Percentages of HPG-labeled prokaryotic assemblages from Scripps Pier comparing incubations with the analog and with the analog plus methionine. Bars represent standard error.

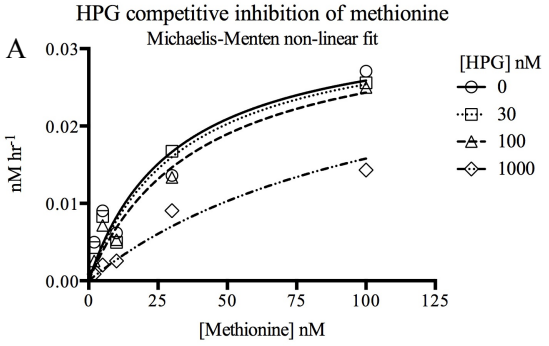

B

		Standard error
K_m of methionine	31.19	8.120
K_i of HPG	372.8	142.6
V_{max}	0.03395	0.003447
Shared R^2 of fits	0.9228	

Figure 4.4. Michaelis-Menten enzyme kinetics chart displaying HPG competitive inhibition of methionine (A). Summary values of fitted values calculated from each dataset (B).

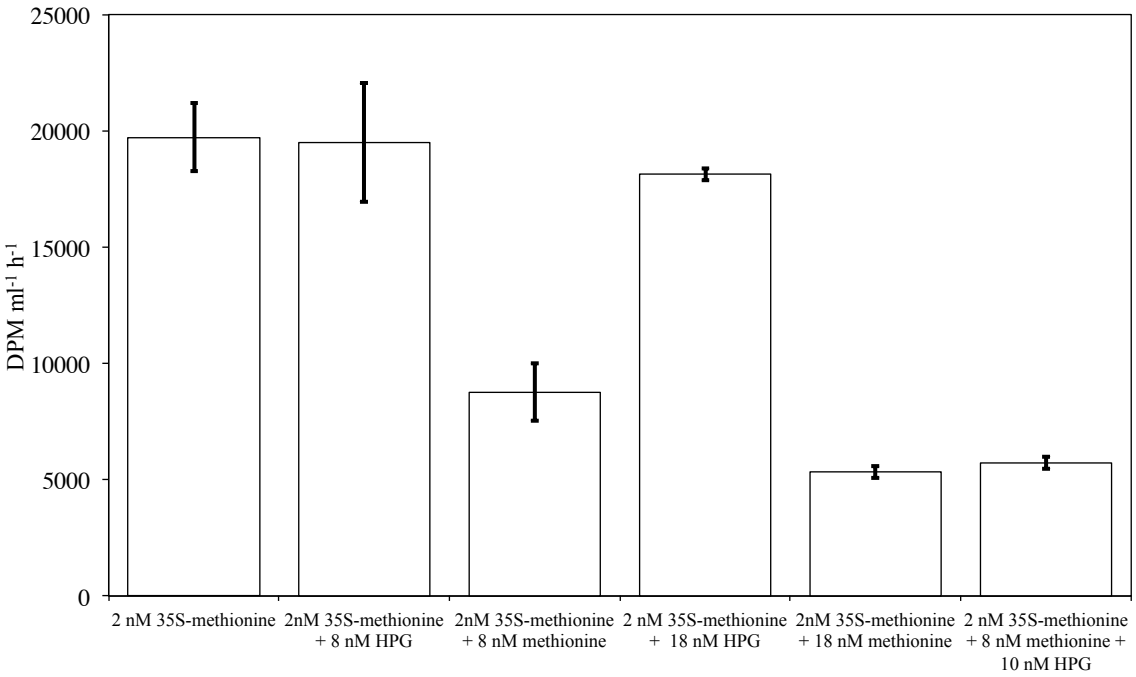

Figure 4.5. Measurements of disintegrations per minute in whole seawater samples incubated with ^{35}S-methionine alone and with varying concentrations of cold methionine and HPG.

Table 4.3. Comparisons of labeled bacteria percentages cells in seawater incubated with 20 nM homopropargylglycine for 1 hour.

Sample	^{35}S-methionine labeling (%)	HPG labeling on filter (%)	HPG labeling with FTF (%)
17-Aug-2010	16.1	12.8	94.8
10-Oct-2010	17.20	14.3	70.2

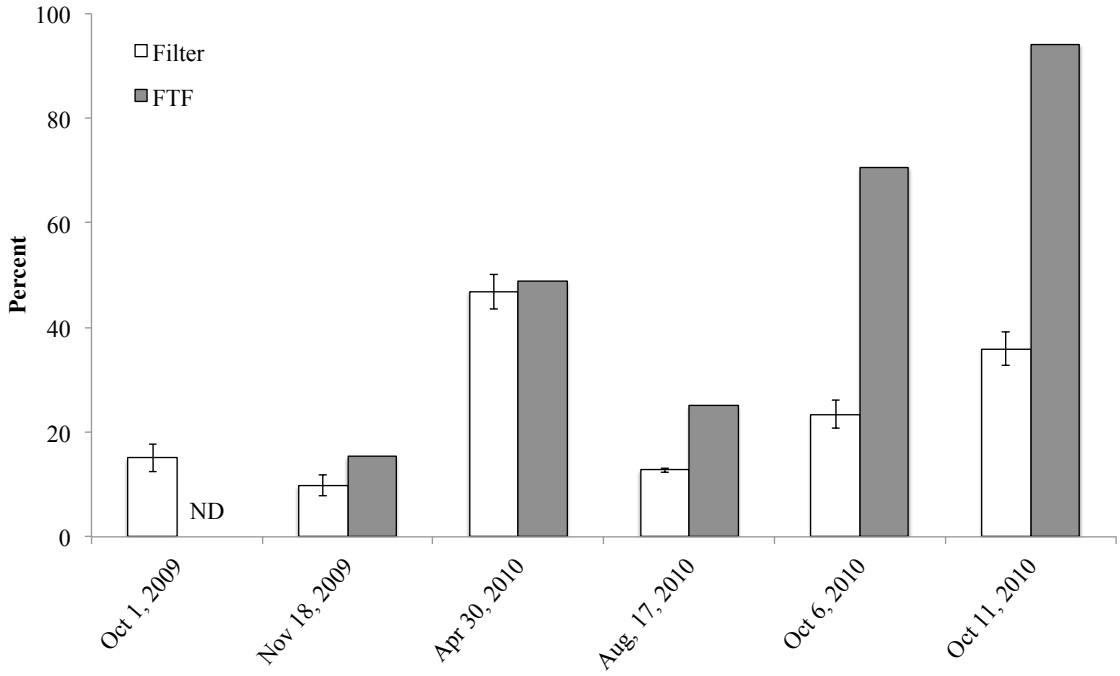

Figure 4.6. Percentages of labeled bacterial cells in seawater incubated with 20 nM homopropargylglycine for 1 hour. Cells were visualized directly (filter) or after transferring to slides (FTF). Bars represent standard errors.

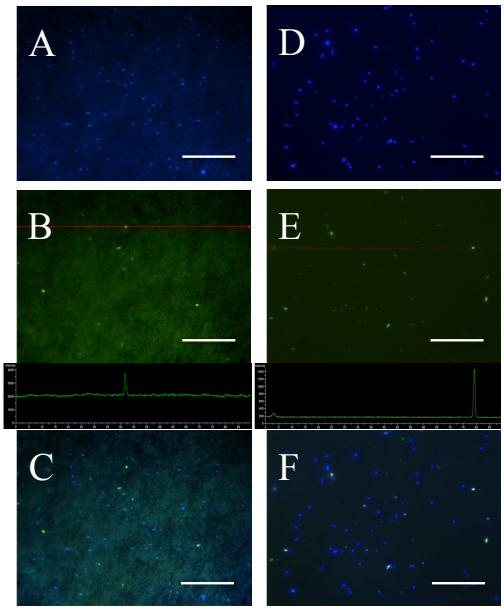

Figure 4.7. A representative scene of HPG-labeled bacteria observed on polycarbonate filters and split into DAPI, FITC, and DAPI+FITC channels (A-C). The filter-transfer-freeze technique reduced the background and enabled observation of both faintly and brightly labeled cells (D-F). The green lines in panels B and E correspond to the signal intensity histogram measured across the image and further illustrate the reduction of background using FTF. Scale bars = 20 µm.

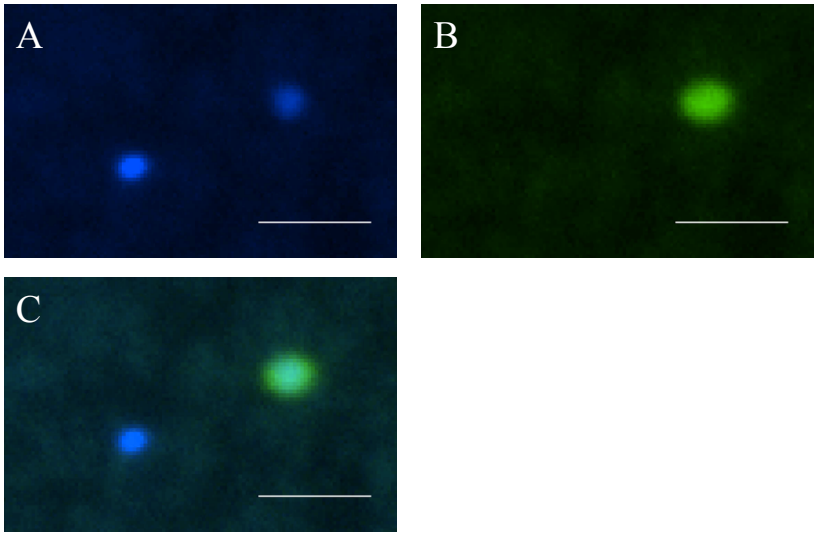

Figure 4.8. Magnified image of bacteria from Scripps Pier stained with the nucleic acid stain DAPI (A) next to the same field showing the green AlexaFluor 488® emission of an HPG-positive cell (B). Panel C depicts the DAPI + FITC composite view. The HPG signals appear as a greater portion of the cell than what is stained with DAPI (C). Scale bars = 2 µm.

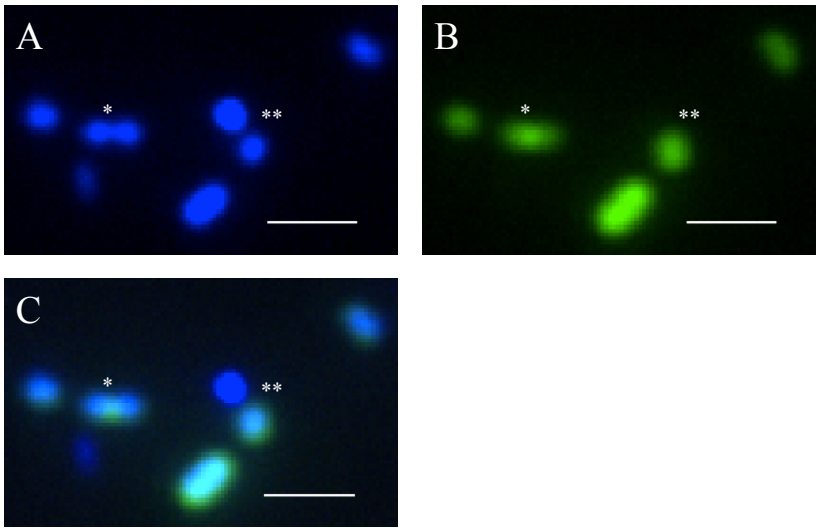

Figure 4.9. Dividing cells observed in the DAPI channel (A) displayed a variety of HPG labeling characteristics as seen in the FITC and DAPI + FITC channels (B & C). Both cells may be labeled (*) or one cell is labeled and the other is not (**). Scale bar = 5 µm.

Table 4.4. Cell concentrations, percentages of HPG positive cells, averages, and ratios of scBCP for 21 dates at Scripps Pier (± standard error of the mean).

Sample	Concentration (cells ml^{-1} x 10^6)	Percent labeled	Avg scBCP (fg $cell^{-1}$ hr^{-1})	Avg scBCP of top 10% (fg $cell^{-1}$ hr^{-1})	Avg C prod. of bottom 90% (fg $cell^{-1}$ hr^{-1})	10% to 90% ratio	Max scBCP (fg $cell^{-1}$ hr^{-1})	Min scBCP (fg $cell^{-1}$ hr^{-1})
11/18/09 10:00 AM	1.21	15.29	0.3744 ± 0.076	1.8942 ± 0.287	0.2144 ± 0.038	8.84	2.8879	0.0023
4/30/10 10:00 AM	2.38	48.87	0.2360 ± 0.013	0.9193 ± 0.081	0.1604 ± 0.005	5.73	5.5063	0.0003
8/17/10 4:00 PM	2.41	25.00	0.2451 ± 0.019	1.1501 ± 0.076	0.1454 ± 0.009	7.91	2.6392	0.0001
10/6/10 10:00 AM	3.25	70.53	0.2731 ± 0.012	1.2438 ± 0.045	0.1655 ± 0.006	7.52	3.4081	0.0000
10/11/10 2:00 PM	2.87	94.08	0.1035 ± 0.007	0.6727 ± 0.050	0.0400 ± 0.002	16.81	5.5335	0.0001
10/20/10 2:00 PM	1.62	43.40	0.2087 ± 0.014	0.9731 ± 0.048	0.1244 ± 0.007	7.82	1.8221	0.0002
12/15/10 10:00 AM	1.18	17.29	0.5146 ± 0.068	1.7612 ± 0.275	0.3739 ± 0.042	4.71	3.3852	0.0004
3/30/11 12:00 PM	0.82	62.55	0.3391 ± 0.018	1.5953 ± 0.071	0.1993 ± 0.009	8.00	3.7576	0.0082
3/30/11 4:00 PM	0.74	81.73	0.1464 ± 0.010	0.8692 ± 0.049	0.0658 ± 0.003	13.20	2.8545	0.0000
3/30/11 9:00 PM	0.56	97.89	0.1891 ± 0.011	0.9279 ± 0.058	0.1074 ± 0.003	8.64	2.8686	0.0113
3/31/11 12:00 PM	1.20	72.63	0.2771 ± 0.019	1.4462 ± 0.092	0.1465 ± 0.008	9.87	4.1849	0.0001
3/31/11 4:00 PM	2.71	62.61	0.3879 ± 0.030	2.1199 ± 0.089	0.1938 ± 0.014	10.94	3.9513	0.0000
3/31/11 8:00 PM	0.78	63.21	0.2325 ± 0.013	1.3118 ± 0.059	0.1124 ± 0.005	11.67	5.3128	0.0000
4/1/11 12:00 PM	3.82	44.50	0.1346 ± 0.009	0.6993 ± 0.036	0.0715 ± 0.004	9.78	2.0772	0.0000
4/1/11 4:00 PM	1.24	86.28	0.1069 ± 0.006	0.6090 ± 0.028	0.0509 ± 0.002	11.96	1.9099	0.0001
4/1/11 9:00 PM	0.70	66.83	0.0837 ± 0.007	0.4697 ± 0.031	0.0406 ± 0.002	11.56	1.2883	0.0000
4/12/11 9:00 AM	3.55	14.73	0.1985 ± 0.029	0.8883 ± 0.108	0.1173 ± 0.014	7.57	1.6526	0.0024
9/30/11 9:00 AM	2.24	63.00	0.0651 ± 0.006	0.3560 ± 0.029	0.0325 ± 0.002	10.96	0.9245	0.0000
10/3/11 9:00 AM	3.52	70.78	0.3420 ± 0.030	1.8799 ± 0.101	0.1698 ± 0.013	11.07	3.2370	0.0001
12/9/11 2:30 PM	1.70	75.21	0.1250 ± 0.024	0.9650 ± 0.212	0.0309 ± 0.001	31.21	7.2288	0.0002
4/16/12 4:30 PM	0.67	100.00	0.2092 ± 0.027	1.5428 ± 0.143	1.4738 ± 0.005	25.12	4.4395	0.0012

Table 4.5. Sum and ratio values of scBCP for each of the 21 dates. Green cells denote greater contributions of the top 10% of active cells to the cumulative BCP. Red cells denote greater contributions from the bottom 90%.

Sample	Concentration (cells ml^{-1} x 10^6)	Percent labeled	Sum scBCP of top 10% (fg hr^{-1})	Sum scBCP of bottom 90% (fg hr^{-1})	10% to 90% ratio
11/18/09 10:00 AM	1.21	15.29	11.36	12.22	0.93
4/30/10 10:00 AM	2.38	48.87	63.43	99.91	0.63
8/17/10 4:00 PM	2.41	25.00	42.55	48.85	0.87
10/6/10 10:00 AM	3.25	70.53	146.77	176.05	0.83
10/11/10 2:00 PM	2.87	94.08	95.52	50.93	1.88
10/20/10 2:00 PM	1.62	43.40	47.68	55.22	0.86
12/15/10 10:00 AM	1.18	17.29	12.33	23.18	0.53
3/30/11 12:00 PM	0.82	62.55	122.84	137.91	0.89
3/30/11 4:00 PM	0.74	81.73	82.57	56.09	1.47
3/30/11 9:00 PM	0.56	97.89	74.23	77.78	0.95
3/31/11 12:00 PM	1.20	72.63	94.00	85.27	1.10
3/31/11 4:00 PM	2.71	62.61	108.11	88.16	1.23
3/31/11 8:00 PM	0.78	63.21	156.10	120.14	1.30
4/1/11 12:00 PM	3.82	44.50	51.05	46.68	1.09
4/1/11 4:00 PM	1.24	86.28	87.08	65.39	1.33
4/1/11 9:00 PM	0.70	66.83	23.49	18.21	1.29
4/12/11 9:00 AM	3.55	14.73	8.88	9.97	0.89
9/30/11 9:00 AM	2.24	63.00	14.60	11.89	1.23
10/3/11 9:00 AM	3.52	70.78	77.08	62.13	1.24
12/9/11 2:30 PM	1.70	75.21	53.07	15.18	3.50
4/16/12 4:30 PM	0.67	100.00	60.17	21.62	2.78

Table 4.6. Averages and ratios for growth rates estimated for the 21 dates (± standard error of the mean).

Sample	Concentration (cells ml^{-1} x 10^6)	Percent labeled	Avg. growth rate (d^{-1})	Avg growth rate of top 10% (d^{-1})	Avg growth rate of bottom 90% (d^{-1})	10% to 90% ratio	Max growth rate (d^{-1})	Min. growth rate (d^{-1})
11/18/09 10:00 AM	1.21	15.29	0.1952 ± 0.035	0.9074 ± 0.132	0.1203 ± 0.018	7.54	1.4492	0.0008
4/30/10 10:00 AM	2.38	48.87	0.1657 ± 0.007	0.5649 ± 0.021	0.1215 ± 0.004	4.65	1.2291	0.0004
8/17/10 4:00 PM	2.41	25.00	0.1916 ± 0.014	0.8735 ± 0.059	0.1165 ± 0.007	7.50	1.8720	0.0001
10/6/10 10:00 AM	3.25	70.53	0.1626 ± 0.006	0.6746 ± 0.020	0.1059 ± 0.003	6.37	1.3628	< 0.0001
10/11/10 2:00 PM	2.87	94.08	0.0477 ± 0.003	0.2803 ± 0.019	0.0218 ± 0.001	12.88	2.2446	< 0.0001
10/20/10 2:00 PM	1.62	43.40	0.1463 ± 0.009	0.6352 ± 0.027	0.0923 ± 0.005	6.88	1.1575	0.0001
12/15/10 10:00 AM	1.18	17.29	0.3587 ± 0.044	1.1707 ± 0.113	0.2670 ± 0.030	4.39	1.7561	0.0002
3/30/11 12:00 PM	0.82	62.55	0.1827 ± 0.009	0.8364 ± 0.028	0.1099 ± 0.005	7.61	1.6505	0.0058
3/30/11 4:00 PM	0.74	81.73	0.0887 ± 0.005	0.5003 ± 0.020	0.0428 ± 0.002	11.69	1.2319	< 0.0001
3/30/11 9:00 PM	0.56	97.89	0.1137 ± 0.006	0.5256 ± 0.027	0.0682 ± 0.002	7.71	1.6126	0.0178
3/31/11 12:00 PM	1.20	72.63	0.1396 ± 0.008	0.6514 ± 0.026	0.0825 ± 0.004	7.90	1.3293	0.0001
3/31/11 4:00 PM	2.71	62.61	0.2296 ± 0.017	1.1939 ± 0.051	0.1215 ± 0.008	9.83	2.0066	< 0.0001
3/31/11 8:00 PM	0.78	63.21	0.1599 ± 0.008	0.8509 ± 0.026	0.0830 ± 0.004	10.25	1.8596	< 0.0001
4/1/11 12:00 PM	3.82	44.50	0.0877 ± 0.005	0.4134 ± 0.011	0.0513 ± 0.003	8.06	0.7875	< 0.0001
4/1/11 4:00 PM	1.24	86.28	0.0663 ± 0.003	0.3571 ± 0.010	0.0339 ± 0.001	10.52	0.8242	0.0001
4/1/11 9:00 PM	0.70	66.83	0.0469 ± 0.004	0.2527 ± 0.017	0.0239 ± 0.001	10.58	0.6454	< 0.0001
4/12/11 9:00 AM	3.55	14.73	0.1310 ± 0.018	0.5718 ± 0.048	0.0791 ± 0.009	7.23	0.8628	0.0015
9/30/11 9:00 AM	2.24	63.00	0.0435 ± 0.004	0.2286 ± 0.014	0.0228 ± 0.002	10.03	0.5427	< 0.0001
10/3/11 9:00 AM	3.52	70.78	0.1862 ± 0.015	0.9433 ± 0.046	0.1014 ± 0.008	9.30	1.6719	0.0001
12/9/11 2:30 PM	1.70	75.21	0.0616 ± 0.009	0.4314 ± 0.076	0.0202 ± 0.001	21.41	1.9455	0.0002
4/16/12 4:30 PM	0.67	100.00	0.1124 ± 0.014	0.7799 ± 0.071	0.0384 ± 0.003	20.2918	1.8686	0.0011

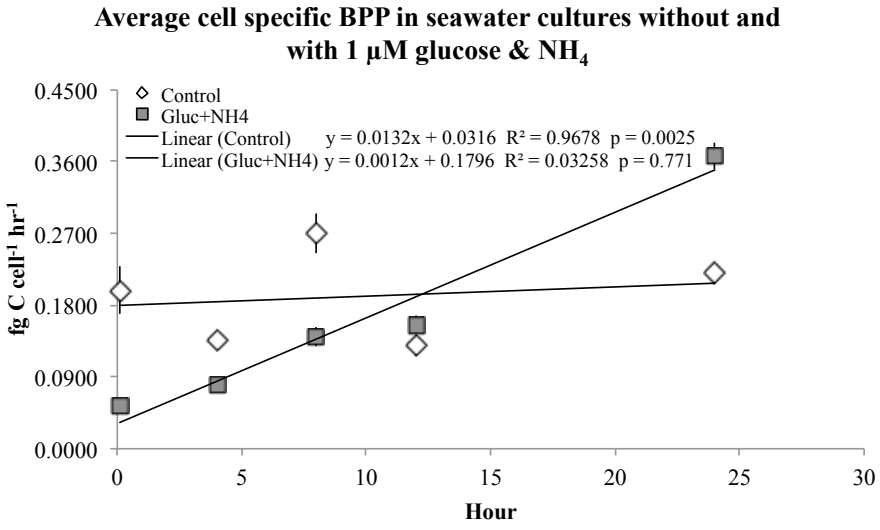

Figure 4.10. XY plot of HPG-based cell-specific BPP measured over 24 hours in the presence or absence of 1µM glucose and ammonium chloride.

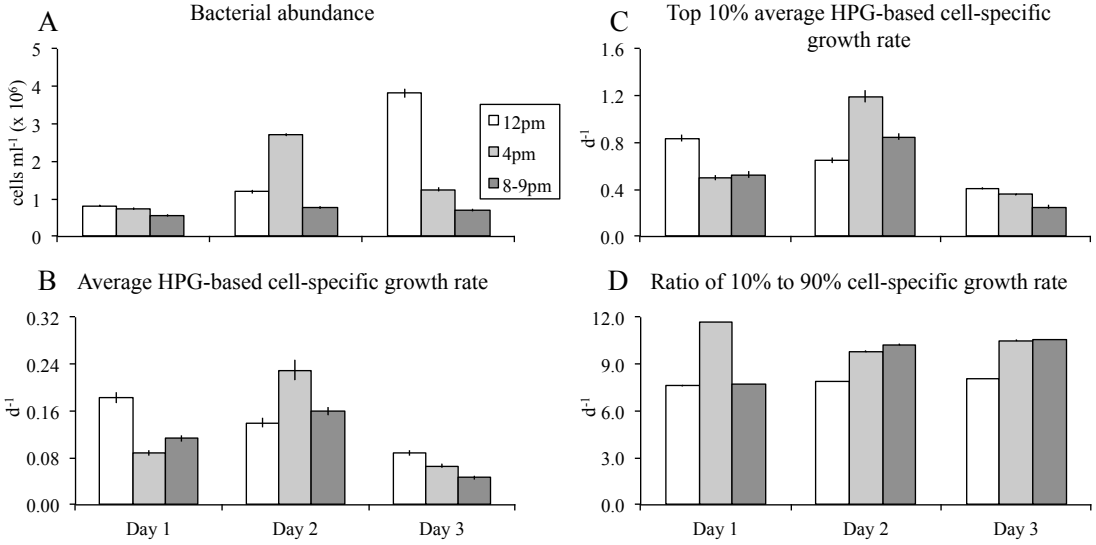

Figure 4.11. Bacterial parameters measured for the Scripps Pier monitoring experiment.

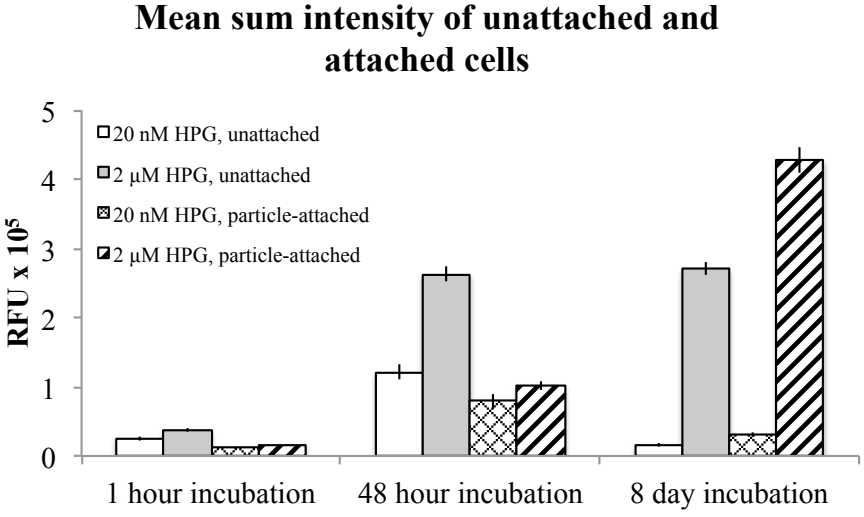

Figure 4.12. Mean sum intensity values of single bacterial cells incubated in 20 nM or 2 µM HPG and existing in unattached or particle-attached. Bars represent standard errors.

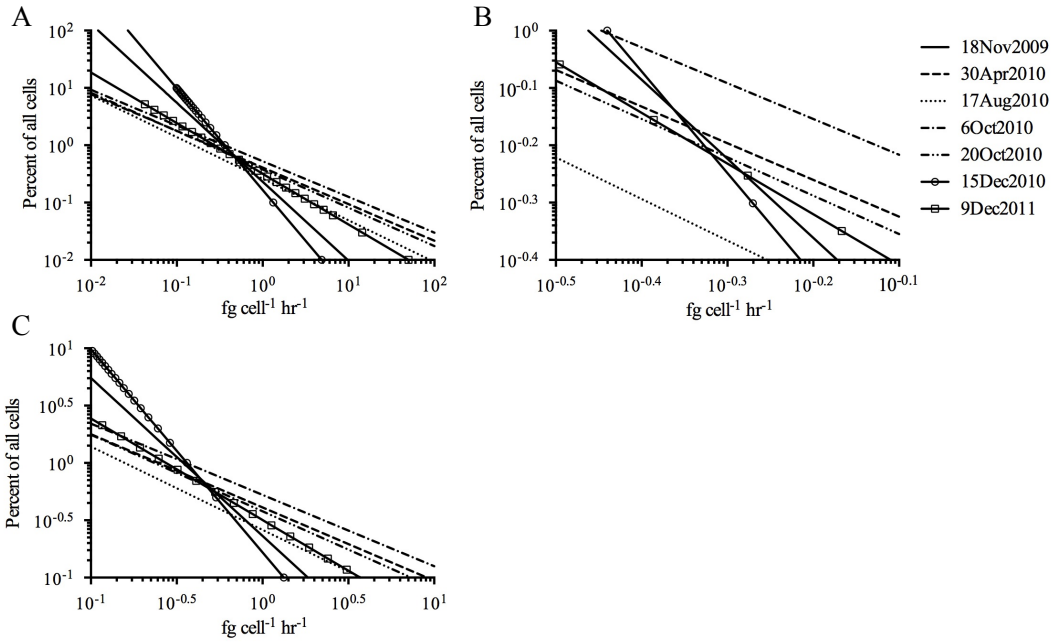

Figure 4.13. Plots of protein production physiological structure derived from single-cell measurements on seven sampling dates at Scripps Pier. XY ranges set for (A) provide a broad view comparison of metabolisms. The more focused ranges of (B) and (C) display the similarities and differences of slopes among the dates.

CHAPTER 5

Conclusions & Outlook

This dissertation has assessed and developed useful techniques and approaches to better quantify and understand microbial control over marine carbon cycling. It is apparent that the scales of interaction among microbes and their physicochemical environments must be understood before we can hope to portend responses and consequences to these connections (Brussaard et al. 2008, Stocker et al. 2008, Malfatti & Azam 2009, Lidstrom & Konopka 2010). The experiments discussed in the preceding pages represent potentially useful techniques that will, when applied to a variety of oceanic environments, contribute insights on marine elemental cycles, microbial oceanography, and ecology.

In general, it is difficult to fully characterize organisms and their environments without direct observation. As a consequence of this limitation, one cannot fully determine how the environment affects the physiology of the organisms, and vice versa. Extending this concept to marine microbial communities, a major challenge lies in obtaining meaningful observational data that provides ecological and/or biogeochemical information. In an early example, direct counts of bacteria using the nucleic acid stain Acridine Orange revealed bacterial abundances that were 3 orders of magnitude greater than previously believed (Hobbie et al. 1977). This major finding, based on the application of a novel method, revolutionized the field of aquatic microbial ecology and spurred the advancement of protocols to view and quantify microbes. An immediate paradigm shift resulted as well, detailing the extent to which phytoplankton and bacterial production coupling influences the dynamics of nutrient remineralization and uptake in

addition to the fate of the photosynthetically-derived organic carbon (Cole 1982, Vaqué et al. 1989).

Since then, the importance of elemental cycling dynamics between bacterioplankton and phytoplankton communities (mediated by viral lysis and protozoan grazing mortality) has become a central tenet in marine microbial oceanography and ecology. As the field continues to develop and grow, so does the need to observe the *in situ* and *in vivo* activity of microorganisms in their native state. One recent method discarded fluorescent stains to minimize non-specific binding to inorganic surfaces and applied deep-UV lasers to excite the natural fluorescence of basalt-attached bacterial cells for *in situ* abundance and biomass quantification (Bhartia et al. 2010). While such an approach is unlikely to be usable for determining single-cell activity, this trajectory of imaging technology will likely usher in new ways to see microbial processes at meaningful ecological scales. The development and deployment of an underwater imaging flow cytometer (FlowCytobot) is a specific example of how the combination of engineering and biology principles has enabled unprecedented views of marine phytoplankton dynamics in real time (Olson & Sosik 2007). It is plausible that the next step is a true *in situ* and *in vivo* instrument. Conceptually, this could be accomplished with an incubation chamber and sampler that enables addition of probes or dyes for incubation, followed by processing and signal quantification. The ongoing development and application of the environmental sample processor (ESP) has resulted in a sophisticated device capable of temporal sampling and quantitative molecular assaying of RNA-targeted organisms (Greenfield et al. 2006). A useful endeavor, then, may be to

modify these pieces of equipment to observe single-cell activity (via HPG incorporation) at high temporal and spatial resolution.

In light of this current state of the science, the best approach to more fully characterize and predict microbial contributions to ecological and biogeochemical dynamics is to assess microbial, geochemical, and physical properties at several scales. For example, this observational scheme was utilized to better understand the microbial food web during a *Phaeocystis globosa* bloom in the Eastern English Channel (Seymour et al. 2008). The authors found that mean differences in biological measurements (chl *a*, bacterial and viral abundances) at the mesoscale were met with significantly different values calculated from microscale (< 5 cm) samplings. They state that the combination of tidal fronts (mesoscale physics) results in nutrient enrichment (mesoscale geochemistry) to elicit a mesoscale bloom. Contemporaneously, microscale patches of *P. globosa* form due to the variable stickiness properties of the cells and secreted organic material. Bacteria cluster differentially at the microscale to consume these point sources of energy and potentially influence nutrient cycling dynamics at this scale as well. In the coastal and open ocean regions of the CCE (or other marine systems), a similar hypothesis could be posited; physical oceanographic structure maintains distinct mesoscale and microscale responses in marine microbial communities by influencing marine chemistry at the same scales. To address this, one could sample within and across distinct zones (tidal fronts and/or internal waves, Omand et al. 2011, temperature-salinity fronts, Landry et al. 2012) for transparent particles and HPG-based activity measurements of unattached and particle-attached bacteria along with bulk measurements of chl *a* and bacterial abundance.

This would provide information on the mesoscale and microscale dynamics of bacterial activity, and the physical characteristics generating larger scale patterns of phytoplankton blooms and particle creation brought about by upward nutrient fluxes (Li et al. 2012). This work would be well informed by continued work on marine fluid dynamics since, as plankton, all microbes are ultimately transported at the whim of water mass and current movements. Furthermore, physical dynamics play a role in particle formation, maintenance, and degradation via microscale eddies and motions that enhance DOM collisions (Passow 2002).

One of the most recent frontiers in microscopy and digital imaging has been super-resolution visualization, or nanoscopy. In achieving resolution below the theoretical limit of diffraction (i.e. < 200 nm), various techniques have enabled researchers to observe and quantify cellular dynamics otherwise unobservable with traditional methods and microscopes (Hell 2009). Furthermore, the list of fluorophores compatible with these methodologies has expanded, allowing some of the most widely used compounds to be applied, quantified, and observed for a variety of samples (Moneron et al. 2010). These exciting developments have enabled unprecedented views of internal and external architecture of single cells, including cytoskeletal microtubules, protein microdomains, and the bacterial cytoskeletal filament ftsZ (Müller et al. 2012), Integrating these techniques with the sampling and visualization methods described in this dissertation is likely tractable, and would facilitate the molecular characterization of microbial communities at the nanoscale to complement mesoscale and microscale observations. Quantifying and describing the sub-cellular localization of newly

synthesized, HPG-containing proteins and peptides would reveal the activity of single cells and constrain how the cell is spatially partitioning incorporated DOM (using HPG as a tracer) via catabolic and anabolic processes. Live and video rate nanoscopy has also been demonstrated (Hein et al. 2008), and would be an ideal way to achieve high temporal significance in controlled laboratory experiments. Devotion of energy into biomass enhancement versus cell division is an important process in bacteria and one of several bacterially-mediated mechanisms that influence the marine pool of photosynthetically-derived organic matter (Chin-Leo & Kirchman 1988). Traditionally, these measurements were made in bulk samples using radiolabeled thymidine (cell division) and leucine (protein/biomass production) to calculate leucine:thymidine incorporation ratios as an expression of balanced or unbalanced growth (balanced ratio being $1 < \text{Leu:TdR} < 20$; Chin-Leo & Kirchman 1990, Gasol et al. 2009). The recent availability of the thymidine analog 5-ethynyl-2'-deoxyuridine (EdU) has assisted with the probing of DNA replication dynamics in archaeal and bacterial cells (Ferullo et al. 2009, Gristwood et al. 2012). If combined with HPG incorporation and multiplex imaging with different fluorophores, simultaneous EdU uptake could be used to visualize and quantify this ratio to further characterize the growth and biogeochemical implications of balanced versus unbalanced growth in individual cells. Moreover, the application of fluorescent i*n situ* hybridization (Amann et al. 1995) to these protocols would ascribe biogeochemical functions to bacterial phylogeny.

It is an exciting era for microbial oceanography and ecology. Interdisciplinary research has been central to oceanography, but now it has become even more

commonplace and widespread, enabling unique perspectives of microorganisms and their functions in the marine environment. Our ability to extract evocative and quantitative information from these observations has been aided by advances in microscopy and computing while the labeling technologies have benefitted from recent strides in Click chemistry. While this dissertation examined how to quantify single heterotrophic bacterial cells, these strategies have the potential to reveal more about photoautotrophic communities as well. Such innovations along with the continued investigation of molecular mechanisms underpinning microbial activity and diversity may inform other fields of study to permit prognostic insights on microorganism responses to and control over marine biogeochemistry. As interest and knowledge of anthropogenic climate change increases, this prescience will become more and more necessary as marine microbes assume mitigating or exacerbating roles (Joint et al. 2011, Doney et al. 2012). As the lifestyles of marine microorganisms continue to be characterized across several scales of the world ocean, our understanding of microbial influence on the natural world will optimistically contribute to improving the health of the planet and its inhabitants.

References

Amann RI, Ludwig W, Schleifer KH (1995) Phylogenetic identification and in situ detection of individual microbial cells without cultivation. Microbiological Reviews 59:143-169

Bhartia R, Salas EC, Hug WF, Reid RD, Lane AL, Edwards KJ, Nealson KH (2010) Label-Free Bacterial Imaging with Deep-UV-Laser-Induced Native Fluorescence. Applied and Environmental Microbiology 76:7231-7237

Brussaard CPD, Wilhelm SW, Thingstad F, Weinbauer MG, Bratbak G, Heldal M, Kimmance SA, Middelboe M, Nagasaki K, Paul JH, Schroeder DC, Suttle CA, Vaque D, Wommack KE (2008) Global-scale processes with a nanoscale drive: the role of marine viruses. ISME J 2:575-578

Chin-Leo G, Kirchman DL (1988) Estimating Bacterial Production in Marine Waters from the Simultaneous Incorporation of Thymidine and Leucine. Applied and Environmental Microbiology 54:1934-1939

Chin-Leo G, Kirchman DL (1990) Unbalanced growth in natural assemblages of marine bacterioplankton. Marine Ecology-Progress Series 63:1-8

Cole JJ (1982) Interactions between Bacteria and Algae in Aquatic Ecosystems. Annual Review of Ecology and Systematics 13:291-314

Doney SC, Ruckelshaus M, Duffy JE, Barry JP, Chan F, English CA, Galindo HM, Grebmeier JM, Hollowed AB, Knowlton N, Polovina J, Rabalais NN, Sydeman WJ, Talley LD (2012) Climate Change Impacts on Marine Ecosystems. Annual Review of Marine Science, Vol 4 4:11-37

Ferullo DJ, Cooper DL, Moore HR, Lovett ST (2009) Cell cycle synchronization of Escherichia coli using the stringent response, with fluorescence labeling assays for DNA content and replication. Methods 48:8-13

Gasol JM, Alonso-Saez L, Vaque D, Baltar F, Calleja ML, Duarte CM, Aristegui J (2009) Mesopelagic prokaryotic bulk and single-cell heterotrophic activity and community composition in the NW Africa-Canary Islands coastal-transition zone. Progress in Oceanography 83:189-196

Greenfield DI, Marin III R, Jensen S, Massion E, Roman B, Feldman J, Scholin CA (2006) Application of environmental sample processor (ESP) methodology for quantifying Pseudo-nitzschia australis using ribosomal RNA-targeted probes in sandwich and fluorescent in situ hybridization formats. Limnology and Oceanography-Methods 4:426-435

Gristwood T, Duggin IG, Wagner M, Albers SV, Bell SD (2012) The sub-cellular localization of Sulfolobus DNA replication. Nucleic Acids Research 40:5487-5496

Hein B, Willig KI, Hell SW (2008) Stimulated emission depletion (STED) nanoscopy of a fluorescent protein-labeled organelle inside a living cell. Proceedings of the National Academy of Sciences of the United States of America 105:14271-14276

Hell SW (2009) Microscopy and its focal switch. Nature Methods 6:24-32

Hobbie JE, Daley RJ, Jasper S (1977) Use of Nuclepore Filters for Counting Bacteria by Fluorescence Microscopy. Applied and Environmental Microbiology 33:1225-1228

Joint I, Doney SC, Karl DM (2011) Will ocean acidification affect marine microbes? ISME Journal 5:1-7

Landry MR, Ohman MD, Goericke R, Stukel MR, Barbeau KA, Bundy R, Kahru M (2012) Pelagic community responses to a deep-water front in the California Current Ecosystem: overview of the A-Front Study. Journal of Plankton Research

Li QP, Franks PJS, Ohman MD, Landry MR (2012) Enhanced nitrate fluxes and biological processes at a frontal zone in the southern California current system. Journal of Plankton Research

Lidstrom ME, Konopka MC (2010) The role of physiological heterogeneity in microbial population behavior. Nature Chemical Biology 6:705-712

Malfatti F, Azam F (2009) Atomic force microscopy reveals microscale networks and possible symbioses among pelagic marine bacteria. Aquatic Microbial Ecology 58:1-14

Moneron G, Medda R, Hein B, Giske A, Westphal V, Hell SW (2010) Fast STED microscopy with continuous wave fiber lasers. Optics Express 18:1302-1309

Müller T, Schumann C, Kraegeloh A (2012) STED Microscopy and its Applications: New Insights into Cellular Processes on the Nanoscale. Chemphyschem 13:1986-2000

Olson RJ, Sosik HM (2007) A submersible imaging-in-flow instrument to analyze nano- and microplankton: Imaging FlowCytobot. Limnology and Oceanography-Methods 5:195-203

Omand MM, Leichter JJ, Franks PJS, Guza RT, Lucas AJ, Feddersen F (2011) Physical and biological processes underlying the sudden surface appearance of a red tide in the nearshore. Limnology and Oceanography 56:787-801

Passow U (2002) Transparent exopolymer particles (TEP) in aquatic environments. Progress In Oceanography 55:287-333

Seymour JR, Seuront L, Doubell MJ, Mitchell JG (2008) Mesoscale and microscale spatial variability of bacteria and viruses during a Phaeocystis globosa bloom in the Eastern English Channel. Estuarine Coastal and Shelf Science 80:589-597

Stocker R, Seymour JR, Samadani A, Hunt DE, Polz MF (2008) Rapid chemotactic response enables marine bacteria to exploit ephemeral microscale nutrient patches. Proceedings of the National Academy of Sciences 105:4209-4214

Vaqué D, Duarte CM, Marrasé C (1989) Phytoplankton colonization by bacteria: encounter probability as a limiting factor. Marine Ecology-Progress Series 54:137-140